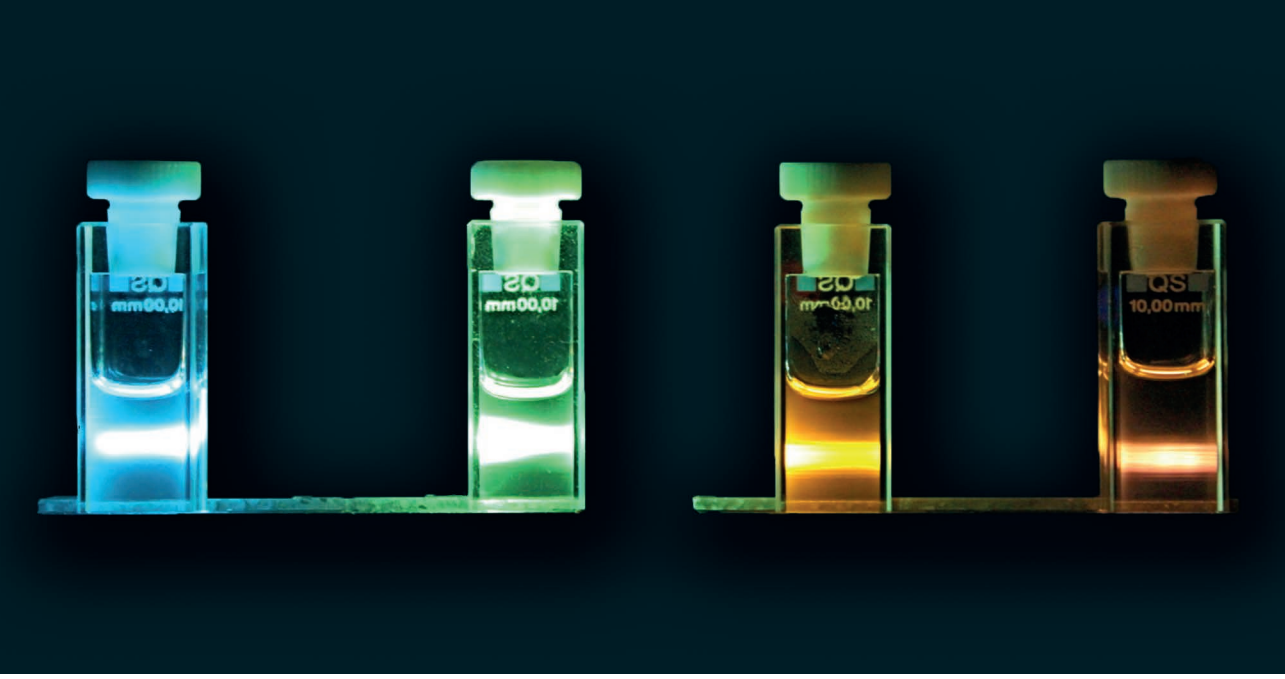

Fabian Plass

Nanostructured Architectures for Solar Energy Conversion

From New Photoactive Compounds to Photocatalytic and Photonmanaging Applications

FAU UNIVERSITY PRESS

Fabian Plass

Nanostructured Architectures for Solar Energy Conversion

From New Photoactive Compounds to Photocatalytic and Photonmanaging Applications

Fabian Plass

Nanostructured Architectures for Solar Energy Conversion

From New Photoactive Compounds to Photocatalytic and Photonmanaging Applications

Erlangen
FAU University Press
2022

Bibliografische Information der Deutschen Nationalbibliothek:
Die Deutsche Nationalbibliothek verzeichnet diese Publikation in der Deutschen Nationalbibliografie; detaillierte bibliografische Daten sind im Internet über http://dnb.d-nb.de abrufbar.

Bitte zitieren als
Plass, Fabian. 2022. *Nanostructured Architectures for Solar Energy Conversion. From New Photoactive Compounds to Photocatalytic and Photonmanaging Applications*. Erlangen: FAU University Press. DOI: 10.25593/978-3-96147-482-0.

Der vollständige Inhalt des Buchs ist als PDF über den OPUS-Server der Friedrich-Alexander-Universität Erlangen-Nürnberg abrufbar:
https://opus4.kobv.de/opus4-fau/home

Umschlagbild: Fabian Plass

Verlag und Auslieferung:
FAU University Press, Universitätsstraße 4, 91054 Erlangen

Druck: docupoint GmbH

ISBN: 978-3-96147-481-3 (Druckausgabe)
eISBN: 978-3-96147-482-0 (Online-Ausgabe)
DOI: 10.25593/978-3-96147-482-0

Nanostructured Architectures for Solar Energy Conversion – From New Photoactive Compounds to Photocatalytic and Photonmanaging Applications

Nanostrukturierte Architekturen für Solare Energieumwandlung – Von Neuen Photoaktiven Materialien zu Photokatalytischen und Photonenverwaltenden Anwendungen

Der Naturwissenschaftlichen Fakultät
der Friedrich-Alexander-Universität
Erlangen-Nürnberg

zur
Erlangung des Doktorgrades Dr. rer. nat.

vorgelegt von

Fabian Plass

aus Lauf a. d. Pegnitz

Als Dissertation genehmigt von der Naturwissenschaftlichen Fakultät der Friedrich-Alexander-Universität Erlangen-Nürnberg

Tag der mündlichen Prüfung: 05.10.2021

Vorsitzender der Promotionskommission: Prof. Dr. Georg Kreimer

Gutachter/in: Prof. Dr. Dr. h.c. Dirk M. Guldi

Prof. Dr. Svetlana B. Tsogoeva

Whether you think you can, or you think you can't – you're right.
— Henry Ford —

Selected publications of the following thesis:

(1) Christina Stangel,* Fabian Plass,* Asterios Charisiadis, Emmanouil Giannoudis, Georgios Charalambidis, Kostas Karikis, Georgios Rotas, Galateia E. Zervaki, Nektarios N. Lathiotakis, Nikos Tagmatarchis, Axel Kahnt, and Athanassios G. Coutsolelos, Interfacing Tetrapyridyl-C_{60} with Porphyrin Dimers via π-Conjugated Bridges: Artificial Photosynthetic Systems with Ultrafast Charge Separation, *Phys. Chem. Chem. Phys.* **2018**, *20*, 21269-21279

(2) Vasilis Nikolaou,* Fabian Plass,* Aurélien Planchat, Asterios Charisiadis, Georgios Charalambidis, Panagiotis A. Angaridis, Axel Kahnt, Fabrice Odobel, and Athanassios G. Coutsolelos, Effect of the Triazole Ring in Zinc Porphyrin-Fullerene Dyads on the Charge Transfer Processes in NiO-Based Devices, *Phys. Chem. Chem. Phys.* **2018**, *20*, 24477-24489

(3) Ning Liu,* Shiva Mohajernia,* Nhat T. Nguyen, Seyedsina Hejazi, Fabian Plass, Axel Kahnt, Tadahiro Yokosawa, Andres Osvet, Erdmann Spiecker, Dirk. M. Guldi, and Patrik Schmuki, Long-Living Holes in Grey Anatase TiO_2 Enable Noble-Metal-Free and Sacrificial-Agent-Free Water Splitting, *ChemSusChem* **2020**, *13*, 4937-4944

(4) Fabian Plass, Daniil A. Lukyanov, Alexander S. Konev, Axel Kahnt, Konstantin Y. Amsharov, Alexander F. Khlebnikov, and Dirk M. Guldi, Controlling the Charge Transfer Mechanism and Efficiency by Means of Different C_{70} Regioisomeric Adducts, *Small Struct.* **2020**, *1*, 2000012

(5) Fabian Plass,* Sebastian Bönisch,* Felix Held,* Tobias Ullrich, Florian E. J. Fischer, Anton Guryev, Andreas Görling, A. Kahnt, and Svetlana B. Tsogoeva, Controlling and Fine-Tuning Charge Transfer Emission in 2,6-Dicyanoaniline Multichromophores Prepared through Domino Reactions: Entry to a Potentially New Class of OLEDs, *J. Org. Chem.* **2021**, *86*, 6111-6125

Acknowledgements

First and foremost I want to express my deep gratitude to my supervisor Prof. Dr. Dr. h.c. Dirk M. Guldi. The dedication and enthusiasm he shows for his research was both motivational and inspiring for me. I want to thank him for enlightening discussions and interesting projects. Both, my professional and personal development greatly benefit from his guidance, encouragement and support during the last years, which I highly appreciate.
Furthermore, I like to thank Dr. Axel Kahnt for his support within my master thesis and also beyond this during my PhD student time. I will never forget the detailed information about climbing knots, Sweden, elks, and hiking tracks in the world.
Prof. Dr. Athanassios G. Coutsolelos, Prof. Dr. Fabrice Odobel, Prof. Dr. Svetlana Tsogoeva, Prof. Dr. Patrik Schmuki, Prof. Dr. Alexander F. Khlebnikov, Prof. Dr. Konstantin Y. Amsharov, Prof. Dr. Alexander S. Konev, Prof. Dr. Andreas Görling, Dr. Tadahiro Yokosawa, Dr. Andres Osvet, Prof. Dr. Erdmann Spiecker, and Dr. Nikos Tagmatarchis and their groups are gratefully acknowledged for enjoyable and prolific collaborations.

I am also thankful to Dr. Guido Sauer, Dr. Karin Mansyreff, and Dr. Christian Ehli. I am also very grateful to all former and current Guldi group members for an always comfortable atmosphere. Thanks to Margit Hartmann, and Beate Maaß for their assistance in all administrative matters. Dirk Harnisch, Gerd Gätzschmann, Angelika Leistner, Manfred Pfennig, and Handa Rudolph are acknowledged for help with technical problems and consumables. Thanks to Sebastian and Friedhold Wölfel and the whole workshop for assistance and cooperation.
A tree is nothing without his leaves, consequently I would like to thank all the members of the Guldi group for the pleasant and often funny moments. Beyond the scientific part, it has been a source of friendship for me, ending in several vacation rides and extended evenings not only on conferences. I really appreciate the time with you. In particular, Alejandro, Zirzl, Max, Schierli, Baui, Jan, Wiebke, Marcel, Kim, Tobi U., Bingzhe, Betti, Michel, Peter, Rubenito, Bianka, Nicole, Michi, Olli, Andi, Anki, Peter S., Anja, Leonie, Raman, Tobi S., Arjun, Beni, and Philipp - and last but not least Domi and Christian H., also thank you for the many philosophic quotes and funny moments on our vacation trips and/or in the Nanoland making nanosecond great again.

Furthermore, to all my friends who have supported me in all this time. Lastly, I would like to thank my whole family for all their love, support, and encouragement during my life. Thank you so much!

List of Abbreviations

A	acceptor
A*	excited acceptor
Å	angstrom
ADP	adenosine diphosphate
AM 1.5(G)	air mass coefficient (1.5 atmosphere thickness; solar zenith angle z = 48.2°)
ATP	adenosine triphosphate
Au	gold (aurum)
a.u.	arbitrary units
B	arbitrary dye B
B*	excited arbitrary dye B
BET	back electron transfer
BHJ	bulk heterojunction
BN	benzonitrile
BODIPY	4,4-difluoro-4-bora-3a,4a-diaza-s-indacene
C_{60}	[60]fullerene
C_{70}	[70]fullerene
C_{78}	[78]fullerene
C_{82}	[82]fullerene
C_{84}	[84]fullerene
CB	conduction band
CCD	charge-coupled device
$(CH_3)_2{}^{\bullet}COH$	isopropyl radical
CL	cathodoluminescence
cm^{-1}	reciprocal centimeter / wavenumber
$Co^{(II/III)}$	cobalt$^{(II/III)}$ couple
CO_2	carbon dioxide
CR	charge recombination
CSS	charge separated state
CT	charge transfer
c(t)	concentration at time point t
cytochrome-b_6f	plastoquinol—plastocyanin reductase
D	donor
D*	excited donor
D-B-A	donor-bridge-acceptor (system)
DBU	1,8-diazabicyclo[5.4.0]undec-7-ene
DDQ	2,3-dichloro-5,6-dicyano-1,4-benzoquinone

DFT	density functional theory
dm^3	cubic decimeter
DSSC	dye-sensitized solar cell
E	energy transfer efficiency
e^-	electron
ε	permittivity
ε_A	molar extinction coefficient of A
EAS	evolution associated spectrum
e.g.	exempli gratia (for the sake of example)
EnT	energy transfer
ET	electron transfer
et. al.	et alii/et aliae
etc.	et cetera
eV	electron volt
f_D	emission of donor D
Fe	iron (ferrum)
f.ex.	for example
φ_D	fluorescence quantum yield of donor D
FF	fill factor
Φ_{Fl}	fluorescence quantum yield
Fig.	Figure
FRET	Förster Resonance Energy Transfer
ΔG^0	change of free reaction enthalpy
ΔG^0_{ET}	change of free reaction enthalpy for the electron transfer
$\Delta G^‡$	change of the driving force of the activation energy
Gy	Gray
η	efficiency
ħ	reduced Planck constant
h^+	hole
H_2	hydrogen
H_2O	water
H_2O_2	hydrogen peroxide
H_2P	5,10,15,20-tetraphenyl-21*H*,23*H* -porphyrin
HOMO	highest occupied molecular orbital
I^-/I_3^-	iodide/triiodide redox couple
I_h	icosahedral symmetry (point) group
i. e.	id est (that is)
In	indium
InGaAs	indium-gallium-arsenide
IR	infrared

J	overlap integral
J(V)	net current
J_{SC}	short-circuit current density
κ	orientation factor
K	Kelvin
K	experimental constant
K	transfer matrix
$K_4Nb_6O_{17}$	potassium hexaniobate
k_B	Boltzmann constant
k_T	energy transfer rate constant
k_x	rate constant of x
L	Bohr radius
λ_R	reorganization energy
LUMO	lowest unoccupied molecular orbital
M	mole per liter
Me-THF	2-methyltetrahydrofuran
Mn	manganese
Mn_4Ca	manganese-calcium cluster (part of the PS II)
ms	millisecond
µs	microsecond
n	refractive index
n	n-component
N_2O	nitrous oxide/ laughing gas
N_A	Avogadro constant
NADPH	nicotinamide adenine dinucleotide phosphate
Nb	niobium
Nd:YAG laser	laser neodymium-doped yttrium aluminum garnet/ $Nd:Y_3Al_5O_{17}$ laser
NDI	1,4,5,8-naphthaldiimides
Ni	nickel
NIC	newly industrialized country
NiO	nickel oxide
nm	nanometer
NOPA	noncollinear OPA
NP	nanoparticle
n-type SC	negatively doped semiconductor
N/S	not specified
ns	nanosecond
O_2	oxygen
OD	optical density
$^{\cdot}OH$	hydroxyl radical

OLED	organic light-emitting diode / organic LED
OPA	optical parametric amplifier
oPPE	oligo(*p*-phenyleneethynylenes)
oPPV	oligo(*p*-phenylenevinylenes)
P	matrix with population/concentration properties
P25 (Degussa)	Degussa P25 titanium dioxide nanopowder (85% rutile/ 15% anatase)
P680	Photosystem II primary donor
P680*	excited Photosystem II primary donor
P700	Photosystem I primary donor
P700*	excited Photosystem I primary donor
$PC_{61}BM$	[6,6]-phenyl-C_{61}-butyric acid methyl ester
$PC_{71}BM$	[6,6]-phenyl-C_{71}-butyric acid methyl ester
PCE	power conversion efficiency
Pd	palladium
PDI	*N*, *N*-bis(2,6-diisopropylphenyl)-perylene-3,4,9,10-bisdicarboximide
PET	photoinduced electron transfer
PHOLED	phosphorescent OLED
P_{in}	power of incident light
P_{max}	maximum power
Ψ_q	multiwavelength dataset / matrix containing spectral and concentration components in time and wavelength
ps	picosecond
Pt	platinum
p-type SC	positively doped semiconductor
R_o	Förster distance
RASI	rotationally accessed spin-state inversion
r_{DA}	distance between donor D and acceptor A
RT	room temperature
Ru	ruthenium
S	matrix containing the spectral components
S_1	first singlet excited state / $^{1*}(X)$
SAS	species associated spectra
SB	symmetry-breaking
SEV	secondary electron amplifier
sp^x	type of hybridization, with x = [1–3]
$Sr_2Ta_2O_7$	strontium tantalate oxides
SVD	singular value decomposition
SV_X	x^{th} singular value

SXRPD	synchrotron x-ray powder diffraction
t	time
τ	lifetime
T_1	first triplet excited state / ^{3*}(X)
Ta	tantalum
Tab.	table
TADF	thermally activated delayed fluorescence
TCO	transparent conducting oxide
TCSPC	time-correlated single photon counting
TD-DFT	time-dependent density functional theory
THF	tetrahydrofuran
Ti	titanium
TiO_2	titania/ titanium dioxide
TPA	triphenylamine
tr	trap state
tr	triazole ring
TRES	time-resolved emission spectroscopy
TTA	triplet-triplet annihilation
TW	tera watt
UV	ultraviolet
v	volume percent
V	electron coupling
V	volt
VB	valence band
Vis	visible
UV	ultraviolet
W	watt
$\hat{x}$	unit vector of x
XBO lamp	xenon discharge lamp
XPS	x-ray photoelectron spectroscopy
Zn(H_2DPA)	1,8-bis[5-(2,8,13,17-tetraethyl-3,7,12,18-tetramethyl-zinc(II)porphyrinyl)]anthracene
Zn(H_2DPB)	1,8-bis[5-(2,8,13,17-tetraethyl-3,7,12,18-tetramethyl-zinc(II)porphyrinyl)]biphenylene
Zn(H_2DPO)	4,6-bis[5-(2,8,13,17-tetraethyl-3,7,12,18-tetramethyl-zinc(II)porphyrinyl)]dibenzofuran
Zn(H_2DPS)	4,6-bis[5-(2,8,13,17-tetraethyl-3,7,12,18-tetramethyl-zinc(II)porphyrinyl)]dibenzothiophene
Zn(H_2DPX)	4,5-bis[5-(2,8,13,17-tetraethyl-3,7,12,18-tetramethyl-zinc(II)porphyrin)]-9,9-dimethylxanthene
ZnO	zinc oxide

ZnP	5,10,15,20-tetraphenylporphyrin-zinc(II)
ZrO_2	zirconium oxide

Abstract

Sustainable solar energy conversion is one of the main tasks of younger human history to be able to herald a successful energy turnaround by using profitable and environmentally friendly energy sources and carriers. Particularly due to the increasing use of fossil fuels, ever worse events are becoming apparent, caused by climate change. The use of nanostructured architectures, such as the implementation of molecular electron donor-acceptor systems in opto-electronic applications, is a promising option. Various strategies can be pursued: On the one hand, the development of novel and promising carbon rich compounds, the fundamental characterization of those plays a major role in this PhD thesis, and, on the other hand, the development and optimization of already existing compounds of molecules and materials, whose enormous potential has perhaps not yet been fully exploited.

From the first project it can be shown that the use of small, but synthetically cheap and fast producible 2,6-dicyanoanilines, in combination with triphenylamines, an extremely interesting molecular electron donor-acceptor system with fascinating charge transfer emission can be generated. The investigation of such promising compounds for opto-electronic devices such as OLEDs is, therefore, of great demand in terms of improved LED technologies, as well as the desire for cost-effective and environmentally friendly alternatives to rare metal based OLEDs. The investigation of this molecule class was carried out with the help of a variety of photophysical, as well as radiation chemical measurement methods, namely pulse radiolysis. The use of transient absorption spectroscopy, also temperature-dependent based, has been instrumental in determining the exact origin of the emissive character of this electron donor-acceptor system.

The further development of such molecular electron donor-acceptor systems on a supramolecular and covalent basis also played an important role in this thesis. Among others, self-assembling systems consisting of a fullerene with oPPE/oPPV bridge and four pyridyl groups together with a zinc porphyrin monomer, as well as a dimer were investigated. Again, for the main task stationary and time-resolved spectroscopy measurements were conducted. In combination with transient absorption spectroscopy, it could be shown that the introduction of multi-bearing pyridyl groups has a beneficial effect on the formation of a charge separated state. This is of particular importance in the use of artificial photosynthetic architectures,

especially with regard to a sustainable solar energy conversion. As a covalently linked example, the next project dealt with the influence of regioisomeric units on a possible charge transfer and its electronic pathways within the molecule. Exactly this effect was determined by investigating two regioisomeric C_{70} derivatives in connection with *meso*-tetraphenyl porphyrin, together with radiation chemical and photophysical methods. Furthermore, and as a first step, the containing building blocks determining the systems have been investigated to gather a more detailed look. Again, in connection with steady-state, as well as time-resolved measurements, as for example transient absorption spectroscopy, it was shown that the use of α- or β-C_{70} derivatives has an interesting impact on their photophysical behavior, like their lifetime, as well as their electronic pathway distribution. Since such influences show clear performance differences in BHJs, the investigation of such regioisomeric systems, especially with regard to solid state materials, takes a decisive role. The last project of the chapter, which covers from the pure fundamentals to the final, improved application, deals with the use of different zinc porphyrin containing fullerene systems with and without triazole groups as spacer on p-type NiO. Those p-type dye-sensitized solar cells have been investigated, besides molecular electron donor-acceptor system in solution, as well as in the solid state using various photophysical techniques, and in particular transient absorption spectroscopy. It could not only be demonstrated that an up to 37 times performance improvement, with respect to $Co^{II/III}$, was achieved, but also a complete photophysical explanation is given. This project, too, is to be seen as a model, since it shows, besides the mere optimization, also a possible improvement potential, the end of which is a significant performance conversion efficiency increase of porphyrin containing systems on NiO.

The third and final topic of this PhD thesis is the photophysical investigation of special "grey" titanium dioxide in terms of an economic water splitting using sunlight. This photonmanaging and photocatalytic material shows particularly remarkable high and efficient conversion rates from pure water to hydrogen as the solar fuel of the future. In combination with transient absorption spectroscopy, the origin of its enormous superiority compared to white titania could be stated and in addition to this, it allows room for further optimization and tuning. Especially the combination of solar fuels such as hydrogen, as well as the use of novel, economical solar cells, but also sustainable OLEDs, will be important elements to protect life as we know it today and will make it worth living for future generations. The climate change, and its consequences, and especially the prevention of it, is THE central challenge of the 21st century.

Kurzzusammenfassung

Nachhaltige solare Energieumwandlung ist eine der Hauptaufgaben der jüngeren Menschheitsgeschichte, um durch die Nutzung rentabler und umweltfreundlicher Energiequellen und -träger eine erfolgreiche Energiewende einleiten zu können. Insbesondere durch die zunehmende Nutzung fossiler Brennstoffe zeichnen sich immer schlimmere Ereignisse ab, die durch den Klimawandel verursacht werden. Der Einsatz nanostrukturierter Architekturen, wie z.B. die Implementierung von molekularen Elektronen Donor-Akzeptor-Systemen in opto-elektronischen Anwendungen, ist eine vielversprechende Option. Es können verschiedene Strategien verfolgt werden: Zum einen die Entwicklung neuartiger und vielversprechender kohlenstoffreicher Verbindungen, deren grundlegende Charakterisierung in dieser Dissertation eine wichtige Rolle spielt, und zum anderen die Weiterentwicklung und Optimierung bereits bestehender Verbindungen von Molekülen und Materialien, deren enormes Potenzial vielleicht noch nicht voll ausgeschöpft ist.

Im ersten Projekt kann gezeigt werden, dass durch den Einsatz von kleinen, aber synthetisch günstigen und schnell herstellbaren 2,6-Dicyanoanilinen in Kombination mit Triphenylaminen ein äußerst interessantes molekulares Elektronen Donor-Akzeptor-System mit faszinierender Ladungstransfer-Emission erzeugt werden kann. Die Untersuchung solch vielversprechender Verbindungen für opto-elektronische Bauelemente wie OLEDs ist daher, sowohl im Hinblick auf verbesserte LED-Technologien, als auch in Anbetracht des Wunsches nach kostengünstigen und umweltfreundlichen Alternativen zu seltenen metall-basierten OLEDs, sehr gefragt. Die Erforschung dieser Molekülklasse wurde mit Hilfe verschiedener photophysikalischer, aber auch strahlungschemischer Messmethoden, nämlich der Pulsradiolyse, durchgeführt. Der Einsatz der Transient-Absorptions-Spektroskopie, zusammen mit temperaturabhängigen Messungen, war bei der Bestimmung des genauen Ursprungs des Emissionscharakters dieses Elektronen Donor-Akzeptor-Systems von entscheidender Bedeutung.

Die Weiterentwicklung solcher molekularer Elektronen Donor-Akzeptor-Systeme auf supramolekularer und kovalenter Basis spielte auch in dieser Arbeit eine wichtige Rolle. Unter anderem wurden selbstorganisierende Systeme untersucht, die aus einem Fulleren mit oPPE/oPPV-Brücke und vier Pyridylgruppen zusammen mit einem Zink-Porphyrin Monomer sowie

einem Dimer bestehen. Auch hier wurden für die Hauptaufgabe stationäre und zeitaufgelöste spektroskopische Messungen durchgeführt. In Kombination mit der Transienten-Absorptions-Spektroskopie konnte gezeigt werden, dass die Einführung von mehrfach tragenden Pyridylgruppen einen günstigen Einfluss auf die Bildung eines ladungsgetrennten Zustandes hat. Dies ist von besonderer Bedeutung bei der Verwendung künstlicher photosynthetischer Architekturen, insbesondere im Hinblick auf eine nachhaltige solare Energieumwandlung. Als ein kovalent verknüpftes Beispiel befasste sich das nächste Projekt mit dem Einfluss von regioisomeren Einheiten auf einen möglichen Ladungstransfer und seine elektronischen Verläufe innerhalb des Moleküls. Genau dieser Effekt wurde durch die Untersuchung von zwei regioisomeren C_{70} Derivaten zusammen mit *meso*-tetraphenyl Porphyrin und strahlenchemischen und photophysikalischen Methoden erforscht. Darüber hinaus wurden in einem ersten Schritt, die in dem System enthaltenen Bausteine untersucht, um einen genaueren Einblick zu erhalten. Wiederum im Zusammenhang mit stationären, wie auch zeitaufgelösten Messungen, wie z.B. der Transienten-Absorptions-Spektroskopie, kann gezeigt werden, dass die Verwendung von α- oder β-C_{70} Derivaten einen interessanten Einfluss auf ihr photophysikalisches Verhalten, wie z.B. ihre Lebensdauer, sowie ihre elektronische Wegverteilung hat. Da solche Regioisomere deutliche Leistungsunterschiede bei BHJs zeigen, kommt der Untersuchung solcher regioisomerer Systeme, insbesondere im Hinblick auf Festkörpermaterialien, eine entscheidende Rolle zu. Das letzte Projekt des Kapitels, das von den reinen Grundlagen bis zur endgültigen, verbesserten Anwendung reicht, beschäftigt sich mit dem Einsatz verschiedener zinkporphyrinhaltiger Fullerensysteme mit und ohne Triazolgruppen als Spacer auf p-Typ NiO. Diese p-Farbstoff-Solarzellen wurden neben dem molekularen Elektronen Donor-Akzeptor-System in Lösung auch im festen Zustand mit verschiedenen photophysikalischen Techniken, insbesondere der Transienten-Absorptions-Spektroskopie, untersucht. Es konnte nicht nur gezeigt werden, dass eine bis zu 37-fache Leistungssteigerung bezüglich $Co^{II/III}$ erzielt wurde, sondern es wird auch eine vollständige photophysikalische Erklärung gegeben. Auch dieses Projekt ist als Modell zu sehen, da es neben der reinen Optimierung auch ein mögliches Verbesserungspotential aufzeigt, an dessen Ende eine signifikante Leistungsumwandlungseffizienzsteigerung Porphyrin-haltiger Systeme auf NiO steht.

Das dritte und letzte Thema dieser Doktorarbeit ist die photophysikalische Untersuchung von speziellem "grauem" Titandioxid im Hinblick auf einen wirtschaftlichen Wasserspaltungsprozess unter Nutzung von Sonnenlicht.

Dieses photonenmanagende und photokatalytische Material zeigt besonders bemerkenswert hohe und effiziente Umwandlungsraten von reinem Wasser zu Wasserstoff als solarem Brennstoff der Zukunft. In Kombination mit der Transienten-Absorptions-Spektroskopie konnte der Ursprung seiner enormen Überlegenheit gegenüber weißem Titandioxid festgestellt werden und lässt darüber hinaus Raum für weitere Optimierungen und Anpassungen. Insbesondere die Kombination von solaren Brennstoffen wie Wasserstoff, sowie der Einsatz neuartiger, wirtschaftlicher Solarzellen, aber auch nachhaltiger OLEDs, werden wichtige Elemente sein, um das Leben, wie wir es heute kennen, zu schützen und für zukünftige Generationen lebenswert zu machen. Der Klimawandel, und seine Folgen, und vor allem seine Verhinderung, ist DIE zentrale Aufgabe des 21. Jahrhunderts.

Table of Contents

1 Introduction

The climate of our planet earth is a highly complex framework. Different elements like atmosphere, oceans, and land interact in numerous ways with each other and are inseparable entangled with living beings including the human race.[1] Over the time, climatic conditions have counterbalanced themselves. Although temporarily strong fluctuations like the Little Ice Age existed, life as we know it today became possible.[2]

The atmosphere plays a crucial role, ensuring a sufficient temperature on earth for the spread of life in abundance and the rise of mankind, which is dependent on the so called natural greenhouse effect caused by trace gases – mainly on water vapor and carbon dioxide (CO_2), as well as methane and nitrous oxide (N_2O). These greenhouse gases retain a certain part of the incoming thermal radiation in the atmosphere. As a result, this withholding of thermal energy leads to an average temperature on earth of about 14°C, instead of resulting in a completely frozen planet.[3]

Since the dawn of industrialization, mankind has released a great extent of greenhouse gases like methane and especially carbon dioxide. Due to the increased use of fossil fuels like coal, oil, and natural gas, their concentration in the atmosphere was greatly enriched. Emissions like carbon dioxide in the atmosphere caused by humans has risen up to 40% since the beginning of the industrialization in the late 18^{th} century and its concentration was never as high as in the last fourteen million years – an age in which a meteorite formed the so called *Nördlinger Ries*.[4][5] Another factor is also the progressive deforestation, like in the Amazon region or in Africa, notwithstanding their property to store and, therefore, lower the CO_2 concentration in the atmosphere. For example, the whole tropical rain forests retain billion tons of carbon dioxide and the rate of deforestation of the Amazon alone contributes up to 17.4% of carbon dioxide emissions to the atmosphere worldwide.[6]

On the basis of a rapid increase of greenhouse gases in the atmosphere, the radiation balance is changing and, therefore, the greenhouse effect will cause higher average temperatures, more extreme weather phenomena like heavy rain, stronger hurricanes, and floods. Furthermore, it triggers an enhanced melting of glaciers in the mountains or the poles, as well as higher land degradation, especially in developing countries in Africa.[1][7][8]

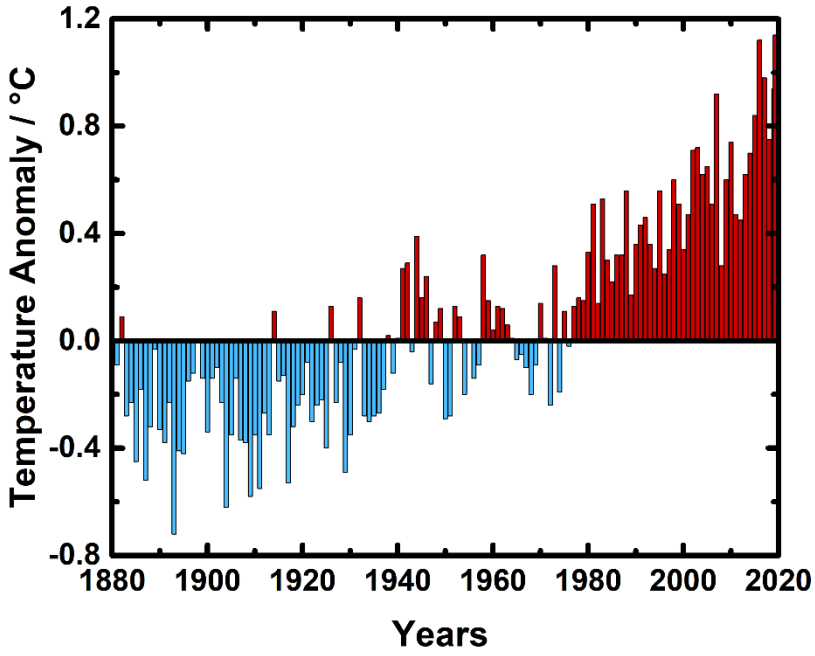

Fig. 1.1.: Diagram of the global temperature anomalies with respect to the 20th century temperature average between the data recording starting at 1880 until 2020. The colored columns show the values below (blue) or above (red) of the defined average temperature. This graph is adapted from reference.[9]

As a result, political and social responsibility of mankind accrue, leading to international cooperations, initiatives, and treaties climaxing in the Paris agreement. On December 12th, 2013 history was made in Paris: The long term goal of limiting the temperature rise of at least 2°C up to 2050 was set out in writing and was signed by 197 and ratified by already 189 different parties.[10] To accomplish this goal, a worldwide reduction of greenhouse gas emissions has to be achieved by at least 50% up to 2050.[11]
In contrast to previous treaties, almost every state on earth has now national defined aims that target the climate change. Another important part of the agreement is the technology, knowledge, and financial transfer from richer to poorer countries assisting them to implement actions on individual defined climate protection goals. To achieve the national climate goal different measures can be taken. Here are the facts: The majority, over seventy-two percent, of the world's greenhouse gas emissions originates from energy-related sources like electricity production, heating, and transportation.[12] Our dependency on fossil fuels is the major culprit to many

environmental problems and the driving force of climate change.[12] Among strategies to tackle climate change, the use of sustainable energy sources like solar and wind power to replace non-renewable energy sources is crucial.[12] The global energy consumption will rise up to 30% from 2017 onwards and is expected to reach up to 25 TW in 2040.[13] Likewise, BP predicted in its outlook for 2019 an enhanced energy demand up to one third from now on until the year 2040, predominantly driven by an increasing prosperity in developing countries.[14] Hence, especially in the newly industrialized countries (NIC) like China and India, the model of energy saving is hardly acceptable. Therefore, it is indispensable to optimize already given energy carries and sources, and to develop new ones. Solar cells have a great potential to save carbon dioxide, which will have an additional impact on climate change. Practical solar energy potential exists of about 600 TW and solar panels with 10% efficiency would already produce 20 TW by only using 0.16% of the land on earth.[15]
The idea of solar energy conversion is not new. More than 100 years ago Giacomo Ciamician published an enticing vision in *Science*:[16]

"*In the desert regions, unadapted to any kind of cultivation, photochemistry will artificially put their solar energy to practical uses. On the arid lands there will spring up industrial colonies without smoke and without smokestacks; forests of glass tubes will extend over the plains and glass buildings will rise everywhere; inside of these will take place the photochemical processes that hitherto have been the guarded secret of the plants, but that will have been mastered by human industry which will know how to make them bear even more abundant fruit than nature, for nature is not in a hurry and mankind is.*"

To make Ciamician's dream of a sustainable energy generation and consumption come true, scientists tried to decipher the "secret of the plants": First of all, three different technical energy conversion strategies are possible: photovoltaics, semiconductor or liquid junctions, and artificial photosynthesis leading to solar electricity and solar fuels.
The principle of a solar cell relies on the photophysical effect discovered 1839 by Alexandre-Edmond Becquerel.[17] However, the first working solar cell was developed by Chapin *et. al.*[18] in the 50's of the last century. The efficiency of 6% was optimized early up to 10% and, in the meantime, a great progress concerning this technology was achieved. Single silicon crystals feature these days an efficiency of about 25%, but are very cost intensive and, therefore, prevent a simple and fast conversion as future energy source.[19][20] But, there is even more development potential: Nowadays,

efficiencies of more than 37.9% are achievable in case of multijunction devices.[21] The great energy potential of solar energy led to a new and very fast growing branch of industry and research. The development of perovskite, plastic, and dye-sensitized solar cells offers multiple application-options for new technologies. However, the production and maintenance of solar cells is still very costly. This is the reason, why more efficient and reasonable solar cell systems are still researched.

2 Objectives

However, the development of novel and sustainable DSSCs requires fundamental mechanistic research, some of which has not yet been adequately carried out. Porphyrin based DSSCs on TiO_2 show acceptable results regarding their PCE (power current efficiency) values, but disappointingly inefficient ones on NiO. Therefore, research on that topic by investigating the effect of a covalent electron donor-acceptor system based on zinc porphyrin and C_{60} fullerene in combination with triazole rings on NiO has been conducted. The aim was to increase the performance of the system on NiO, to understand its precise mechanism, and to investigate the influence of triazoles as the connecting unit to the system (see subsection **4.2.3**). Especially the knowledge for or against the use of a certain unit in solar cells is an important step to advance further development. However, this precisely tailored development also requires basic knowledge. The photophysical and radiation chemical research of novel carbon rich, supramolecular, and covalent based electron donor-acceptor systems (see section **4.1** and **4.2**), especially on porphyrin and fullerene basis in solution, plays an important role in this work, as it provides the basic building block for possible use in opto-electronic devices like solar cells or organic light emitting diodes (OLEDs). The latter is still a very unexplored area, however molecular electron donor-acceptor systems exhibit novel and outstanding photophysical properties (see subsection **4.1.1**). A further and complementary possibility to transform solar energy into usable energy carriers is the use and research of solar fuels such as hydrogen. Thus, the development of fuel cell based means of transportation like trains and cars, especially for Japanese car manufacturers such as Honda and Toyota, like the *Mirai*, is a remarkable alternative not only to well-known combustion engines, which are the best solution to the problems caused by man-made climate change, but also as a replacement for electric cars. Despite the immense progress of the sustainable hydrogen economy, the production of hydrogen by water splitting without the use of noble metals or sacrificial-agents is a difficult undertaking, since, in addition to the development of economically friendly systems, their precise photophysical mechanics are in many cases a great mystery. In the course of this, revealing the exact photophysical and mechanistic origins of a noble-metal and sacrificial-agent free Ni-decorated Grey Anatase TiO_2 system with respect to black anatase and anatase (see section **4.3**) has been researched.

As a consequence, this PhD thesis is divided into three experimental main sections dealing with the fundamental characterization of new carbon rich materials (section **4.1**), new supramolecular and covalent architectures for solar energy conversion (section **4.2**), and finally a solar fuel generating grey anatase system for an enhanced nobel- and sacrificial-agent-free water splitting by also shedding new light on the mechanistic origin of such systems (section **4.3**).
This in combination has the ultimate goal to disclose fundamental processes of known and newly developed nanostructured architecture for solar energy conversion based systems, as well as the evolution of new photoactive compounds in photocatalytic and photonmanaging applications.

3 Theoretical Considerations

3.1 Basic Considerations

Besides the usage of photovoltaic cells, fully integrated molecular artificial photosynthetic systems are promising candidates. The idea: Splitting water into molecular hydrogen and oxygen at separate catalytic sites resulting in subsequent hydrogen storage. The general mechanism of these artificial photosynthetic devices is shown below:

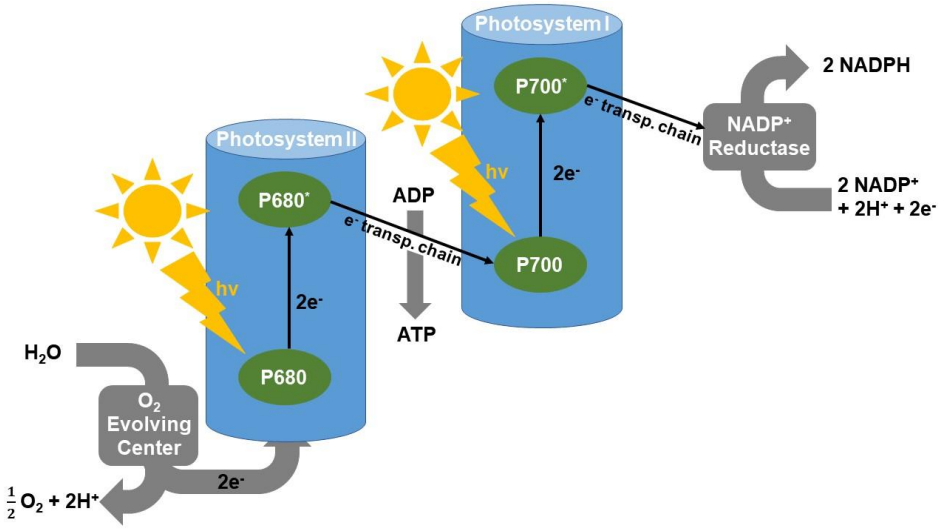

Fig. 3.1.: Simplified Z-Scheme of the light reaction of photosynthesis. This scheme is adapted from reference.[22]

The solar energy is harvested by the light antenna and transferred to the photosensitizer, which is acting as electron donor or acceptor and, hence, starting the charge separation. Shifting the charges to the corresponding electron donor and acceptor, respectively, results in long-distance and long-lived charge separated states and promotes preventing unwanted charge recombination. The oxidation or reduction of water occurs after the transport of charges to their catalytic sites. Inserting membranes in between the catalysts may have a positive impact such as preventing short cuts.[23] Research nowadays frequently emphasizes on the single and customized processes within artificial photosynthetic systems. The main focus relies especially on the choice of the catalyst: Since the beginning of the

idea to split water with light, numerous studies on those transition metal based complexes have been conducted mimicking the natural photosynthetic processes in order to efficiently store solar energy.[24][25]
Nowadays, research focuses more on the preparation of more abundant transition metals like Co,[26] Mn, and Fe,[24] instead of more rare ones like Ru, In, Nb or Ta – doped and undoped – complexes and oxides.[24][27][28]
Scientists find inspiration in nature: Like the oxygen evolving Mn_4Ca complex in the Photosystem II of plants, algae and cyanobacteria play an important role – the so called light reaction.[22] As a result, in Photosystem II (PS II), P680, consisting of chlorins and other porphyrinic members (see also subsection **3.5**), the so called chlorophylls, is excited at 680 nm by sunlight to P680*.[29] From there on, an electron is transferred via an electron transfer chain involving porphyrinoids like pheophytin or the cytochrome-b_6f complex.[22] The resulting energy at the end of this electron transport leads to the conversion of adenosine diphosphate (ADP) to adenosine triphosphate (ATP) and the oxidation from the electron donating pheophytin to the reductant P680 species enabling to split water within the oxygen evolving complex. In a second step, after excitation, P700 in Photosystem I (PS I)[29] acts as electron donor to start a second electron transport chain reaction giving an electron through a ferredoxin and iron sulfur bound membrane.[22] Hence, this results in the reduction of nicotinamide adenine dinucleotide phosphate ($NADP^+$) to NADPH. Besides ATP, NADPH is a major condition to transform carbon dioxide to carbohydrates like sugar.[22]
The overall electron requirement for a complete water splitting process contains eight electrons – four for each Photosystem.[29] Notwithstanding an almost complete light harvesting management of most plants, algae and bacteria, the overall energy efficiency of natural photosynthesis does hardly overcome 2%,[30] mainly originating from the required energy for water splitting and carbon dioxide reduction.[22][31]
To conclude, the development of new or improved materials for solar energy conversion is primarily a challenge, since it is necessary to understand and control the fundamental processes directing the conversion of photons into electric energy.

3.2 Photoinduced Electron Transfer

The aim of artificial photosynthesis is the generation of long-lived charge separated states promoting catalytic centers like in artificial photosynthetic systems and ultimately in the production of solar fuels. Mimicking electron transfer reactions occurring in natural photosynthesis is the key step in solar energy conversion.[32][33] Thus, understanding the aspects of the natural photosynthesis requires insights into its fundamental process – the photoinduced electron transfer (PET). Since photoinduced electron transfer plays a crucial role, much effort has been expended to understand its principles with the ultimate goal of achieving cost-effective natural light-harvesting systems.[34]

PET can be regarded as a process in which absorbed light energy is transferred into chemical energy. The subsequent event, after photoexcitation, is the actual transfer of electrons. This step is crucial for the successful generation of intermediate charge transfer (CT) species in such processes as photosynthesis. The property of some excited states to act as strong electron donor and/or acceptor depends on thermodynamic factors.[34]

The photoexcitation of an electron donor leads to a transfer of an electron, first into an excited state of the donor molecule and further into the HOMO-orbital of the electron acceptor.[35] This electron transfer process leads automatically to the formation of a radical ion pair $D^{\bullet+}$ and $A^{\bullet-}$, which is stabilized or destabilized by solvent molecules due to intermolecular interactions based on Coulomb forces.[36] In 1952, Libby suggested that the electron exchange reaction can be accommodated by the Franck-Condon principle to receive a reasonable explanation for the low reaction rate constants of certain electron exchanges. Additional to that, Libby postulated that different solvation energies (dielectric reorganization energies) for different complexes exist. He concluded, that the smaller the radius of an ion is, the stronger the electrostatic interaction. Reorientation requires therefore more energy.[37][38] According to the Marcus Theory, developed by Rudolph A. Marcus who was, therefore, awarded with the Nobel Prize, it is acknowledged that energy and momentum must be centered. The system gains energy from thermal collisions with surrounding molecules until the energy barrier of the transition state is reached. The energy is transferred from the thermal environment to the vibrational modes if the reactants undergo saturated distortions, which is described by parabolic free energy curves shifted relative to each other as a function of the driving force of the electron transfer ΔG^{o} (see **Figure 3.2**).[34][39] Thereby, λ_R describes the reorganization energy, which refers to the effects of the oriented changes in the

solvent molecules surrounding the reactants during the electron transfer[34] and ΔG^{o} the reaction enthalpy of the electron transfer process.[35] Marcus postulated the driving force of the activation energy by:

$$\Delta G^{\ddagger} = \frac{\lambda_R}{4}\left(1 + \frac{\Delta G^{0}_{ET}}{\lambda_R}\right)^2 \tag{3.1}$$

Mathematically, equation (3.1) describes a quadratic relationship between the driving force and the activation free energy. If the driving force of each one of these electron transfers is plotted vs. the measured rate constants then, according to (3.1), the following trends should be observed:

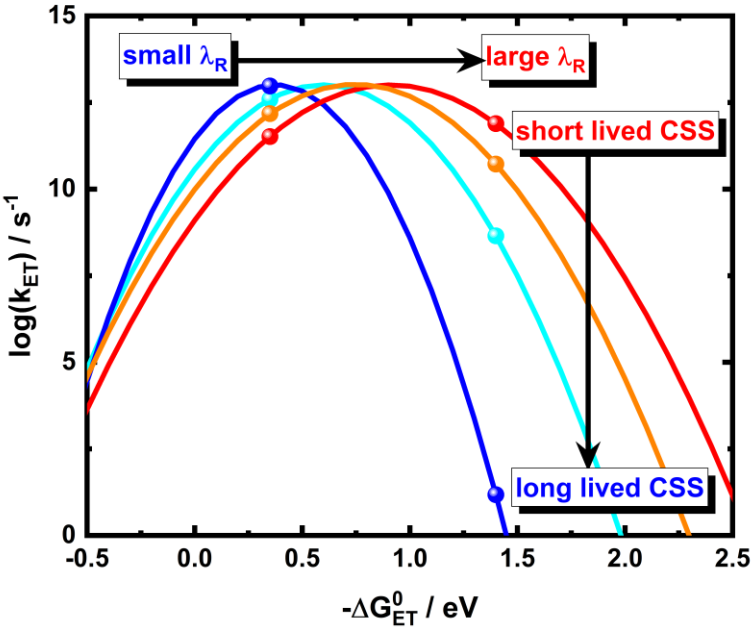

Fig. 3.2.: Driving force dependence of the electron rate constant k_{ET} with respect to different λ_R values (blue line: 0.4 eV, light blue line: 0.6 eV, orange line: 0.8 eV and red line: 1.0 eV) based on Marcus theory equation (3.2). This graph is adapted from reference.[40]

Initially, the rate will increase with an increase in driving force, but level off at some value of ΔG_{ET}, where the rate minimizes with further increases in the driving force, the rate should progressively decrease again (see **Figure 3.3**).

Therefore, and due to collision theory, the reaction rate constant of the electron transfer is given by:

$$k_{ET} = \left(\frac{\pi^2}{\hbar^2 \lambda_R k_B T}\right)^{1/2} V^2 \exp\left(-\frac{\left(\Delta G_{ET}^0 + \lambda_R\right)^2}{4\lambda_R k_B T}\right) \qquad (3.2)$$

One of the following three kinetic regions are encountered depending on the driving force:

1. The normal region: $-\Delta G^o < \lambda_R$
2. The top region: $-\Delta G^o = \lambda_R$
3. The inverted region: $-\Delta G^o > \lambda_R$

In the normal region, the driving forces are lower than the reorganization energy. An increase of the thermodynamic driving force leads to an increase of reaction rate constant for the electron transfer. When $-\Delta G^o$ equals the reorganization energy (λ_R), the maximum rate constant for the electron transfer reaction is reached and basically controlled by the electronic coupling (V) between the electron donor and acceptor moiety (equation 3.2).[41] When the driving force $-\Delta G^o$ becomes lower than the reorganization energy, the rate constant for the electron transfer decreases again – the so called inverted region.
According to equation (3.2), the logarithm of the intramolecular electron transfer rate constant ($\log(k_{ET})$) can be related to the driving force of the electron transfer ($-\Delta G^o$) between an electron donor and an acceptor, as well as the reorganization energy (λ_R) (see **Figure 3.3**). Even though (3.2) predicts a parabolic behavior for the inverted region, which was experimentally confirmed by Miller *et. al.*[42] in 1984 after investigating a series of bifunctional 4-biphenylyl steroids,[34] in the most cases a more linear shape of the curve is observed due to several effects like the solvent polarity, as well as the temperature, distances, and geometry dependences.[42] In the inverse region, an increase of the driving force leads to a decline of the reaction rate constant, due to a smaller vibrational overlap of the combined and the single wave functions.[35] In this case, the magnitude of the reorganization energy can be considered as the major parameter to control.[43]

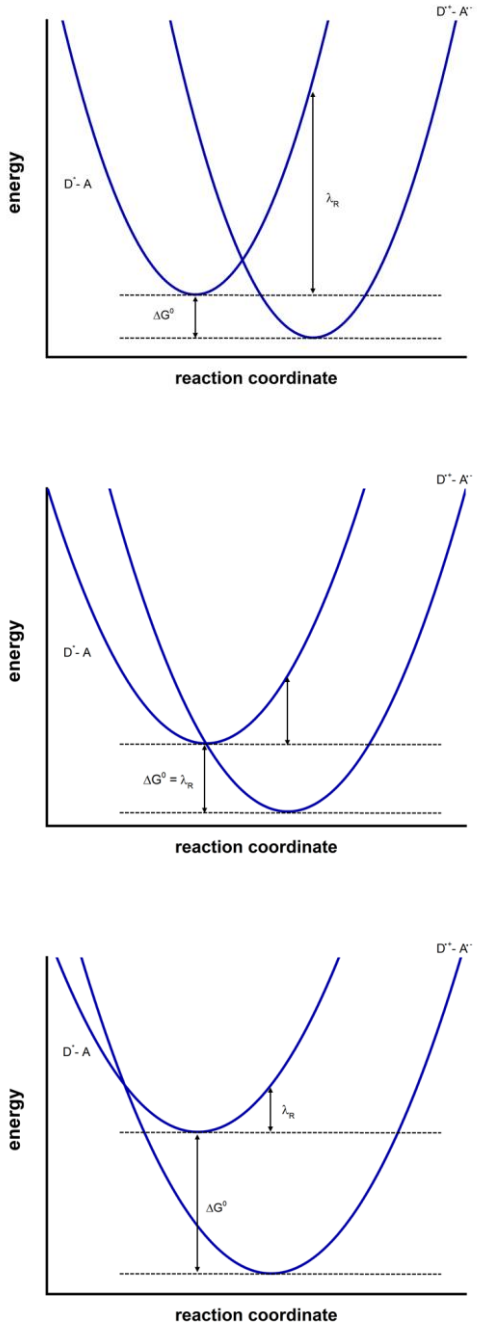

Fig. 3.3.: The different regions in the Marcus theory of electron transfer, together with the representations of the Gibbs free energy change ΔG^0 and the reorganization energy λ_R.

Considering the use of electron transfer systems for solar devices, ideally, charge separation should occur at the top region and the charge recombination process in the inverted region of the Marcus parabola. This would make charge separation very fast and efficient, whereas the charge recombination is slowed down.

3.3 Energy Transfer

Additional to electron transfer processes, another important non-radiative deactivation mechanism exists playing a fundamental significance in modern solar energy conversion research – energy transfer.
Already in 1946, Theodor Förster described this additional deactivation mechanism of electronically excited molecules.[44] In general, energy transfer is defined as a process between an energy donor (D) and an acceptor (A), at which upon photoexcitation the corresponding energy of the excited state of the donor is transformed to the acceptor.[45] In fact, two reaction mechanisms are distinguishable and are illustrated more thorough – the Förster Resonance Energy Transfer and the Dexter or exchange mechanism: In the beginning of the early 40's of the last century, several scientists among them inter alia, Emerson and Arnold, observed in "Chlorella" algae saturation effects in case of the assimilation of carbonic acid upon photoexcitation. In their experiment an enhanced turnover rate for this assimilation process could not be achieved despite increased intensity.[46] Förster inferred that in several biological systems the obtained energy after photoabsorption through an energy donor D seems to be transferred to a distant acceptor A. Due to this energy transfer mechanism the fluorescence of the donor is consequently quenched and enhanced vice versa for the acceptor.[44] This fluorescence quenching matched very well the results of future Nobel Prize winner Jean Baptiste Perrin and his son Francis Perrin in the mid twenty's and thirty's. In their experiments they described intermolecular energy transfer reactions in dye solutions leading to fluorescence quenching of the used dyes through depolarization.[47][48]
As a result, the Förster Energy Transfer mechanism is considering the following key features:

1. Energy donor and acceptor require a strong electronic transition through dipole-dipole interactions in the spectrum of light or in the IR region.

2. The fluorescence quantum yield of the corresponding energy donor has to be high enough.
3. The distance between energy donor and acceptor requires a value of about 2 nm at least.
4. The orientation factor κ^2, also in term of dot products between $\hat{d}$, $\hat{a}$ (the unit vector of the dipole of D and A) and $\hat{r}$ (the unit vector of the distance between D and A). Consequently, $\hat{d} \cdot \hat{r} = \cos(\varphi_D)$, $\hat{a} \cdot \hat{r} = \cos(\varphi_A)$ and $\hat{d} \cdot \hat{a} = \cos(\varphi_T)$ leading to the following equation of kappa: $\kappa = \hat{d} \cdot \hat{a} - 3(\hat{d} \cdot \hat{r})(\hat{r} \cdot \hat{a}) = \cos(\varphi_T) - 3\cos(\varphi_D)\cos(\varphi_A)$

In the following, the resulting three equations and resulting key values of the Förster Theory are shown, while a derivation in detail is forwent, as it would go beyond of the scope of this doctoral thesis:[49]

$$E = \frac{k_T}{k_T + 1 / \tau_D} = \frac{R_0^6}{R_0^6 + r_{DA}^6} \tag{3.3}$$

$$k_T = {}^1/_{\tau_D}\left(\frac{R_0^6}{r_{DA}^6}\right) \tag{3.4}$$

$$R_0^6 = \frac{9(\ln 10)k^2\varphi_D J}{128\pi^5 n^4 N_A} \tag{3.5}$$

k_T = the energy transfer rate
τ_D = the lifetime of the excited state of the energy donor D
r_{DA}= the distance between D and A
R_o = the Förster distance, at which $k_T = 1/\tau$ is valid. This is the distance, at which the probability of deactivation through fluorescence and an energy transfer to the energy acceptor from the excited state of the donor is equal.
E = the energy transfer efficiency
J = The overlap integral, that extends over the region comprising the line shapes of the donor emission f_D and the acceptor absorption band and, consequently, the molar extinction coefficient ε_A.
It is valid: $J = \int f_D(\lambda)\varepsilon_A(\lambda)\lambda^4 \, dt$
κ^2 = the orientation factor
φ_D= the fluorescence quantum yield of the donor molecule
n = the refractive index of the medium

As it can be noticed from equation (3.3), the efficiency rate for the Förster mechanism is strongly distance-dependent. Practically, in case of several nanometers space between energy donor and acceptor FRET is preferred in singlet-singlet energy transfer reaction systems, whereas in cases of smaller distances a totally different mechanism occurs – the Dexter or exchange mechanism.

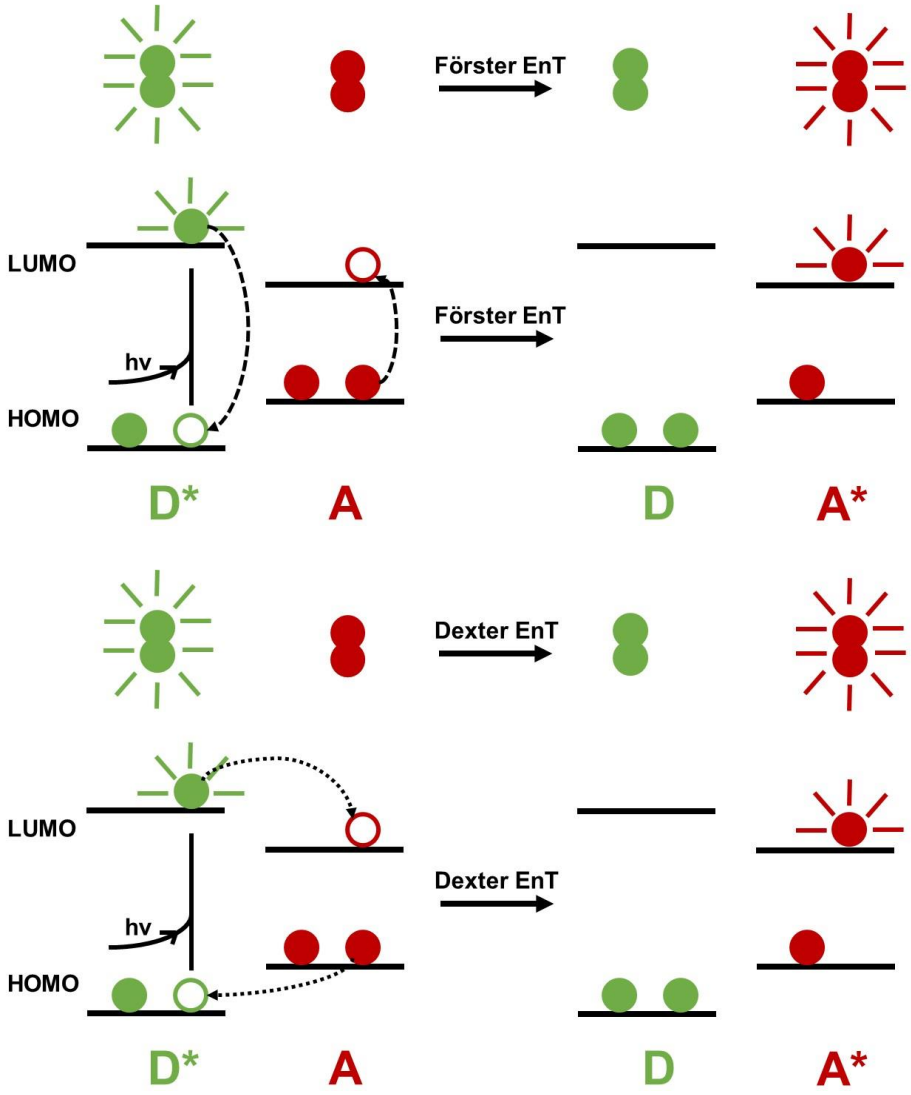

Fig. 3.4.: Molecular orbital schematic representation of dipole-dipole (Förster) and electron exchange (Dexter) mechanism for energy transfer. This scheme is adapted from the book *Principles of Fluorescence Spectroscopy* by Joseph R. Lakowicz.[50]

While the FRET mechanism occurs at larger distances through dipole-dipole interactions between energy donor and acceptor, the exchange mechanism dealing through an electron transfer depends on the overlap integral, as in case of the Förster mechanism requiring a strong coupling, and is only valid at distances of a few angstrom.[51] Therefore, Dexter and Förster mechanism are competitive processes (see also **Figure 3.5**). In case of the exchange mechanism the energy transfer rate constant k_{EnT} is defined as:

$$k_{EnT}^{Dexter} = \frac{2\pi}{n} KJ \exp\left(-\frac{2R}{L}\right) \tag{3.6}$$

with L = Bohr radius, R = distance, and an experimental constant K.

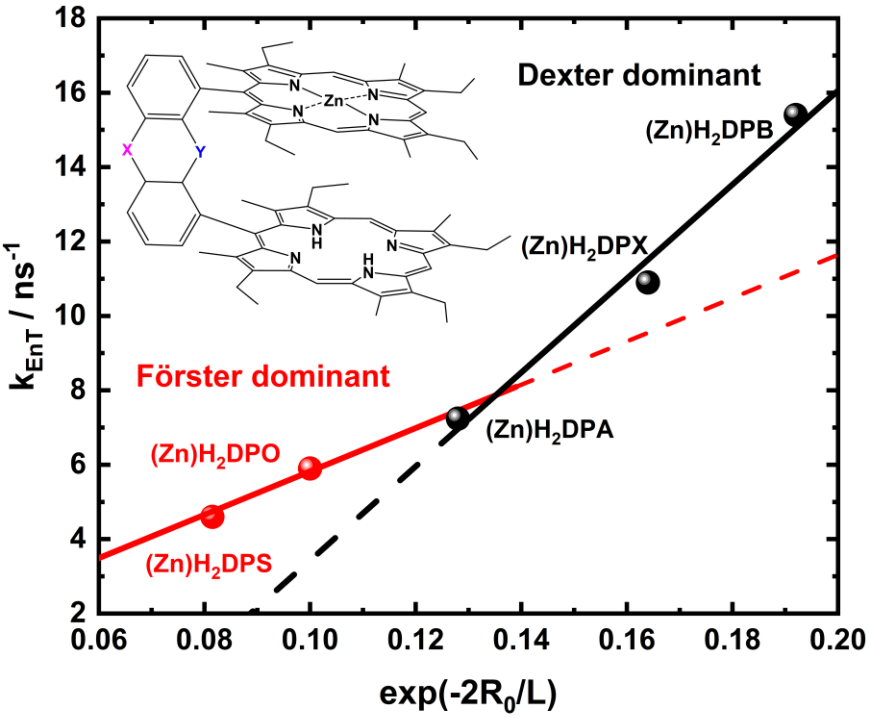

Fig. 3.5.: Plot of k_{ET} vs. exp(-2R/L) with R = 6.3 and L = 4.8 at T = 77 K. The straight lines are associated with the molecules operating with the Förster (red) and the Dexter (black line) mechanism, respectively. Here, **(Zn)H₂DPS** (with **X** = -; **Y** = S) and **(Zn)H₂DPO** (with **X** =; **Y** = O) are more Förster dominant, while **(Zn)H₂DPA** (with **X** = C; **Y** = C), **(Zn)H₂ DPX** (with **X** = CMe_2; **Y** = O), and **(Zn)H₂DPB** (with **X** = -; **Y** = -) are dominated by Dexter energy transfer. This graph is adapted from Faure *et. al.*[51]

Comparing equation (3.3) and (3.6), illustrates the distance dependence and the competitiveness between both mechanisms. However, in spin forbidden singlet-triplet transitions, in which J is very small, the FRET mechanism dominants as vice versa the Dexter mechanism in triplet-triplet energy transfer reactions. The latter one would be in case of a Förster mechanism energetically unfavored as it is based on a change in multiplicity.
Among small organic dyes, Triphenylamine shows interesting photophysical properties, not only as potential energy transfer chromophore,[52][53] but also as electron donor in electron transfer processes in solution[54] or solar cells[53][55] and, therefore, will be discussed in the next section.

3.4 Triphenylamine

One of the foremost properties for a suitable and long-living charge separated state is derived by thermodynamic values (see section **3.2**). Therefore, driving forces like a small reorganization energy value favors stable radical cation and anion formation and high PCE values leading to a sustainable and efficient solar energy conversion in solar cells. One of the most widely used electron donor materials[56] and most known class of dyes is the group of triphenylamines. First described in 1873 by Merz and Weith,[57] triphenylamines began their triumph especially due to their formation of long-lived aminium radical cations[58] and their easy fine-tuning properties. In fact, the formation of this radical cation is thermodynamically favored due to its small reorganization energy.[59] Consequently, the existence of long-lived charge recombination lifetimes, f.ex. in the microsecond regime at 77 K, are no absolute rarity.[60] In particular, a possible and versatile introduction of substituents at the para-positions of TPA leads to adjustable oxidation potential and finds its way in organic chemistry as oxidative catalyst[61][62] and gives the opportunity to form not only double decker units,[63] but also dendrimeric systems.[64]
Besides their synthetic versatility, triphenylamines are subject of interest in almost every field of modern research and in industry. Today, they find usage in conductive polymers, high spin poly-radicals,[65] molecule-based magnetic materials[63][66] or biological applications.[67] Todays most interest in triphenylamines lies in the field of LED based materials and solar cells. TPA units prevent aggregation due their non-planarity and have been intensively researched in dye-synthesized solar cells (DSSCs) showing high conversion efficiency values due to its excellent hole-transporting properties.[68] Recent research strives in the field of OLED devices focusing on

solution-processable molecules and low-cost and efficient polymers.[69] Triphenylamine and its derivatives have received considerable attention as excellent hole transport material due to their high hole mobility and low ionization potentials.[64][70][71][72]
As an interesting candidate, triphenylamines show, additional to that, fascinating charge transfer emission properties that are still moderately described in literature,[60][73][74] but may have enormous potential for sustainable and metal-free LED materials, additional to its hole-transporting properties.
Despite its tremendous potential in especially opto-electronical devices like OLEDs[75][76][77] and solar cells,[53][68] there are still some issues that has to be tackled nowadays. Probably the most important is the lack of absorption in the NIR region: In fact, triphenylamine shows, due a small π-conjugated system, absorption bands up to 350 nm and corresponding dendrimers cross only scarcely the 400 nm limit, at which the visible light range begins. As long as this 400 nm barrier is not consequently passed and exceeded, it will remain as the bottleneck for a sustainable and efficient solar energy conversion. In case of solar cell research, triphenylamine shows also issues with respect to the charge recombination on n-type semiconducting materials (see subsection **3.7.2**), dye aggregation, and an energy level imbalance with titania and the electrolyte.[68]
Notwithstanding some challenging issues, the family of triphenylamines captivates with an enormous potential in a multiverse of possibilities and already existing applications ranging from pure synthetic approaches over biological aspects to opto-electronical devices. FRET is, as described in section **3.3**, an energy transfer between two chromophores, in which the energy obtained by photoexcitation is transferred to the energy acceptor. One requirement for an efficient energy transfer process to be met are high fluorescence quantum yields, as well as a substantial overlap between the corresponding absorption and the emission and the distance between both chromophores. A property that could also be investigated in triphenylamine based systems. Organic dyes exploiting this effect are of great worth and have been widely used in bioimaging, biosensing, medical diagnosis and environmental detection.[78] Hence, the development of various small organic chromophores, such as BODIPYs,[79] rhodamines, coumarins,[80] and cyanines[81] have found their legitimacy, inter alia, in electron donor-acceptor systems.

3.5 Porphyrins as Pyrrolic Macrocycles and Chromophores

In addition to the use of, exemplarily, triarylmethane or azo dyes, as well as diketopyrrolopyrroles as chromophores, another dye with remarkable photophysical properties, which is not only used in artificial photosynthetic systems, but also directly in nature, exists: porphyrins. For example, chlorin, a subspecies of the porphyrin family, is found in the leaves as the so-called chlorophyll. Within plants it serves as a light harvester and transfers its energy to special proteins where the actual solar energy conversion via electron transfer processes takes place (see also section **3.1**).[82][83][84] Through the light reaction within the chloroplasts of plants, the formation of ATP and NADPH leads to the reduction of CO_2 (carboxylation) within the Calvin cycle and to the formation of the fixation product 3-phosphoglycerate and to the regeneration of the CO_2 acceptor (ribulose-1,5-bisphosphate).[85] In addition to this, porphyrins are found in our body as heme-group in the form of red blood cells and play, literally and figuratively, a vital role for us, since hemoglobin serves as an oxygen transporter. Hence, it conveys the oxygen, we breath in every day, from the alveoli through our blood to the body cells. The following **Figure 3.6** shows the chlorin containing magnesium metallated chlorophyll a and unmetallated pheophytin a, which are found both within the Photosystem II (PS II) (see also section **3.1**), as well as the heme pigment and the two alpha and beta subunits of hemoglobin.

Hence, and because of its natural proximity to natural processes like the natural photosynthesis, an immense interest in porphyrins and their diverse subunits, such as chlorin or metallo-porphyrins,[86] N-fused porphyrins,[87] π-extended ones like benzo- or naphthoporphyrins[88][89] or expanded porphyrin systems like sapphyrin or rubyrin[90][91] and porphyrin arrays[92] evoked. To date, there is a wide range of research fields that explain the triumph of porphyrins, such as biomimicking and -inspired photosynthetic artificial photosynthesis.[93] A further advantage to a variety of chromophores is their ability to cover the complete absorption spectrum of sunlight – from UV-vis to the NIR range (see **Figure 3.7**) – with extremely high extinction coefficients, and their high photostability, which makes them perfect candidates for opto-electronic devices like solar cells.

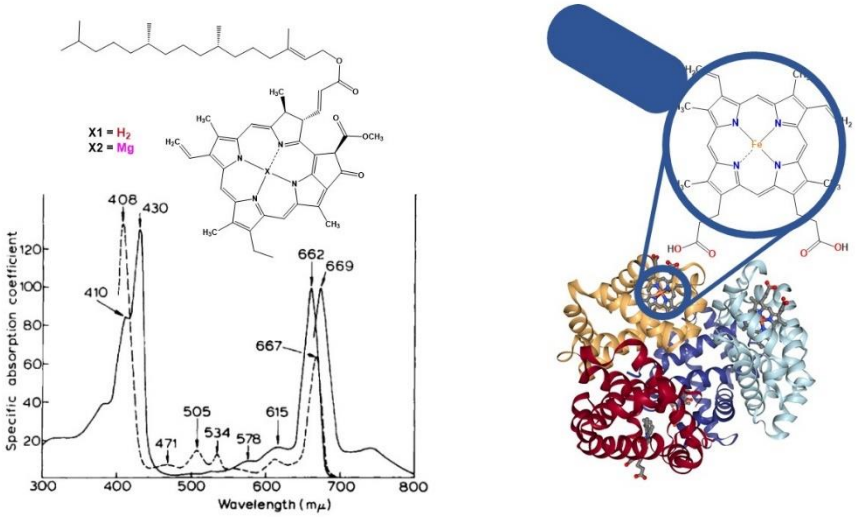

Fig. 3.6.: Absorption and fluorescence spectrum of chlorophyll a (—) and the absorption spectrum of pheophytin a (- - - -) in ether[94] (left) and the structure of human haemoglobin A α_1, α_2, β_1, and β_2 subunits containing the iron heme as prosthetic group adapted from the RCSB PDB database[95] (1GZX)[96] using the NGL viewer.[97]

In addition to their fundamental closeness to nature, porphyrins are also characterized by their simple synthesis, their high modifiability, and their versatility with relatively high yields. Thus, over the last decades, the development of new and better modifications and synthetic routes were carried out, ranging from one-pot over multi-steps to even microwave assisted synthetic approaches.[98]

One of the most utilized porphyrin synthesis procedures is certainly the Lindsey approach.[99][100] In this procedure, the required aldehydes are reacted with pyrroles under acidic conditions in a condensation reaction and under the usage of an oxidant like DDQ (2,3-dichloro5,6-dicyano-1,4-benzoquinone) to *meso*-tetraphenyl porphyrin (H_2P), based on several nucleophilic reactions. Nowadays, a large number of synthesis routes are known in the literature, which include linked porphyrin arrays, oligomeric chains up to dendrimeric systems completely made out of porphyrins or also in combination with other chromophores such as PDIs or phthalocyanines.[101] Porphyrins are also subject to the Hückel rule (4n+2 π-electrons) for the determination of aromaticity and can be described as diaza[18]annulene according to Sondheimer *et. al.*[102]

As described, porphyrins and their relatives show a high absorptivity over the entire spectral window of sunlight and can generally be divided into two distinct regions within their absorption spectrum. The first, and in the case of non-π-extended porphyrins most dominant band, is the so-called

Soret or B-band, in the range around 400 - 500 nm. The other ones are the Q-bands with usually much lower extinction coefficients, which, however, increase in intensity, if the π-system is enlarged (see also **Figure 3.7**). The absorption bands are described using the Gouterman model.[103][104] In general, it can be stated that, due to a higher symmetry by metallation of the porphyrins, two Q-bands, and, as in the case of H_2P, even two additional vibrionic peaks are formed.[105]

Exemplarily, *meso*-tetraphenyl-tetrabenzoporphyrin (see **Figure 3.7**) exhibits in toluene ground state absorption with two maxima as part of the Soret or B-band, as well as several Q-bands with maxima between 550 and 700 nm. Unlikely, *meso*-tetraphenyl-tetranaphthoporphyrin in toluene show three distinct absorption bands between 400 and 520 nm, accompanied by five absorption bands in the NIR with maxima between 620 and 750 nm. The latter ones are assigned to Q-band transitions, while the bands in the blue-green part of the optical spectrum are B-bands using the common nomenclature for porphyrinoids. However, describing the ground state absorptions by the simple, but for porphyrin commonly and successfully used four-orbital model by Gouterman *et. al.*[103][104] is rather problematical. The reason lies in the lifting of the quasi degeneration of the HOMO and HOMO-1 orbitals, as well as the insufficiently separated HOMO-1 and LUMO orbitals from the other occupied and virtual molecular orbitals.[89] Consequently, this results in additional (permitted and forbidden) transitions of the B-band region governing their electronic properties in the ground and excited states, likewise.[89][106] Interestingly, comparing their absorption spectra reveal that the expansion of the macrocycle leads to a red-shift of the maxima – for both, the B- and Q-bands. Hence, both π-extended porphyrin derivatives are sound candidates in opto-electronical devices and, consequently, renders them as promising alternatives to commonly used chromophores in photon up-conversion based systems.[107]

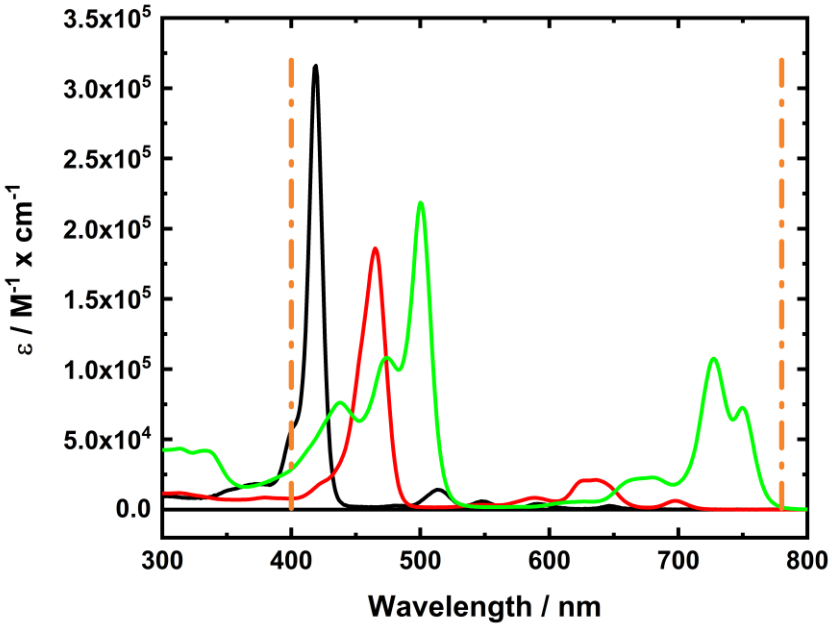

Fig. 3.7.: Absorption spectra of *meso*-tetraphenyl porphyrin (**H_2P**), tetrabenzo- (**TBP**), and tetranaphthoporphyrin (**TNP**) in toluene containing the limits of the solar spectrum depicted in orange.

Since the first synthesis of porphyrin derivatives by Fischer[108] in 1926, a lively branch of research has developed, which is not only characterized by the development, characterization, and analysis of porphyrin-based systems, but also by the attempt to use the knowledge gained in various biological,[109] sensing[110] and opto-electronical applications.[111][112] Especially the usage in supramolecular, as well as covalent, electron donor-acceptor systems in solution and in the solid state promises interesting and distinct properties and results.[113][114] Over recent years, porphyrins turned out to be very auspicious building blocks in the development of nanostructured architectures in photonmanaging systems tackling the ultimate goal of an efficient and sustainable solar energy conversion. In this regard, the design of the first porphyrin-fullerene based molecular electron donor-acceptor systems by Gust *et. al.*[115] evoked a vivid interest in the investigation of such systems, that lasts until now.

3.6 Fullerenes as Carbon Nanostructures

In nature, carbon occurs in two forms – diamond and graphite, which both have fascinating properties, starting with the highest natural hardness of diamond and the exceptionally high conductivity of graphite.[116] In general, carbon can form hybridized bonds (sp, sp^2, and sp^3), not only with other elements, but also with themselves, which is one reason for their endless synthetic possibilities.[117][118] Besides the natural carbon allotropes, this family has been artificially extended, since the development of fullerenes by Kroto, Smalley, and Curl.[119] As milestones in science, the first synthesis of carbon nanotubes by Iijiima[120] in 1991 and of graphene in 2004 are noteworthy here.[121] To this day, scientists continue to develop ever more novel "members" and classes, which in the broadest sense have their origin in the carbon allotropes family. The reason for the special capabilities of Buckminster fullerene as a carbon nanostructure and excellent electron acceptor lies in its molecular orbital (MO) structure. It corresponds to a closed-shell configuration, i.e. a complete MO configuration in all occupied MOs, consisting sixty π-electrons in thirty bonding molecular orbitals.[122] The occupied HOMOs (highest occupied MOs) have an energy level which is about 2 eV higher than the LUMO (lowest unoccupied MOs) and are, additionally, triply degenerated, as shown in **Figure 3.8**.[122][123]

The special properties of fullerenes such as Buckminster fullerenes are derived from their high symmetry (point group I_h).[124] In addition, more than forty-six vibrational mode frequencies exist. In fact, thirty-two are optically silent, ten Raman-active, and four IR-active, while the last ones are originating from the t_{1u} symmetry.[124] But the electronic structure, which is also valid for higher fullerenes like C_{70}, C_{78}, C_{82}, and C_{84}, has the ability to hold up to six electrons.[125] Thus, making them highly promising electron acceptors with a rich electrochemistry. Although C_{60} has double bonds, fullerenes are not classical aromatic compounds, as their C-C double bonds are only located between two six-membered rings, the so called 6,6-bonds, and not alternating with the single bonds at the five-membered rings and, thus, can be categorized as fused 1,3,5-cyclohexatrienes.[126]

Furthermore, the sp^2-hybridization of each carbon on the fullerene surface is low. The pyramidalization angle, which would be 90° in the case of σ-π bonds, is 11.6° in case of the Buckminster fullerene (compared to 0° for graphite).[127] This pyramidalization angle leads to an increased strain. Consequently, exohedral addition reaction to fullerenes are thermodynamically favored as strain can be released, while endohedral reactions will lead to an enhanced and induced strain. This always will result into synthetical issues

based on an inverse thermodynamic driving force.[126] In general, similar reaction patterns for C_{60}, C_{70}, and higher fullerene isomers can be observed. As cycloadditions, free radicals, and nucleophilic addition reactions can be seen as electron accepting alkenes, cycloadditions are an effective attaching choice to the 6,6-bonds of fullerenes.[126] Hence, the release of strain energy is the most important thermodynamic driving force, the production of monoadducts is a synthetic issue, since further reactions to form bis- or multiple-adducts are difficult to prevent.[126] Among the most well known addition reactions are the Bingel-Hirsch reactions[128][129] with diethylbromomalonates in the presence of DBU (1,8-Diazabicyclo[5.4.0]undec-7-ene) and the Prato-reaction, an example of a 1,3-cycloaddition reaction with azomethine ylides.[130] Especially, the latter offers an easy and simple functionalization method for fullerenes using reactive azomethine ylides. Up to now, they are a widely used approach leading to monofunctionalized fullerene adducts.[130][131] Moreover, regioselectivity plays a central role in synthesis. Nevertheless, even in the case of the Prato reaction, bis- and multiple adducts of fullerenes are isolated under an excess of ylide precursors.[132][133]

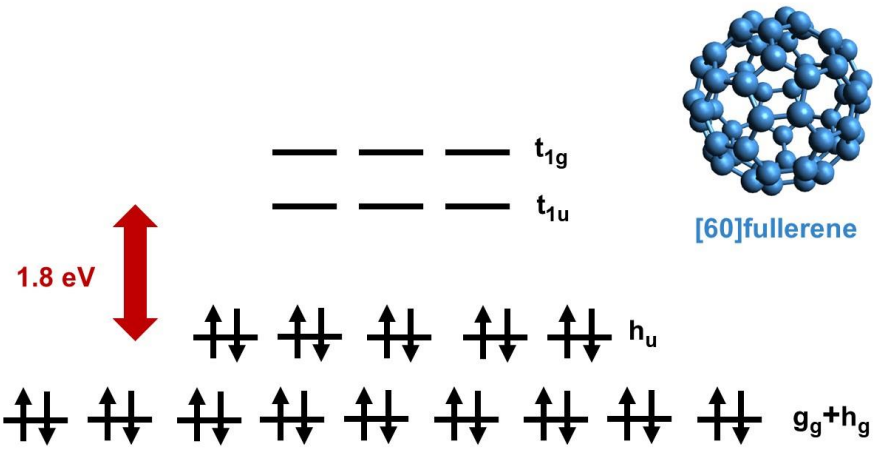

Fig. 3.8.: Schematic illustration of the π-orbital energy levels in C_{60}.[134]

In addition to the lively interest in synthetic variations and modifications, fullerenes are an equally interesting field of research for physicists, biologists, and material scientists alike. Thus, carbon nanostructures or fullerenes are used in a wide variety of applications ranging from pharmaceutical[135][136] or biological products[137][138] to the development of opto-electronic

devices.[139][140] Moreover, the low reorganization energy values (λ_R > 0.2 eV)[141] make fullerenes suitable for electron transfer processes. It originates from its high potential with respect to charge and energy delocalization.[142] Furthermore, the forward electron transfer from an electron donor like phthalocyanine or porphyrin (see section **3.5**) is highly energetically favored and results in fast charge separation. Conversely, the back reaction rate is lowered, shifting the BET into the inverse region of the Marcus parabola (see section **3.2**), an effect that makes fullerenes very promising for opto-electronic devices like solar cells. The interactions of fullerene-donor based molecular systems have been extensively studied over the years and revealed a high interaction potential, especially between porphyrins and fullerenes. For instance, their supramolecular recognition is significantly improved by the formation of C-H···π and π-π interactions between fullerenes and porphyrins or metallo-porphyrins, respectively.[113][143] Furthermore, this supramolecular interaction can be further improved by the simple synthetic modifiability described before, as well as the incorporation of one or more pyridyl ligands, e.g. on a Prato-functionalized fullerene. This, in turn, leads to a significant enhancement of the charge transfer processes between electron donor and fullerene and, thus, facilitates their use in photosynthetic artificial systems. The development of complex multi-component systems can also be enabled in this way.[144]

The implementation of carbon based materials in molecular electron donor-acceptor systems has already a long history,[113][145] but its development is far from over. Thus, newly developed forms of carbon allotropes,[146][147] together with other complementary forms like porphyrins,[148] corroles,[149] subphthalocyanines,[150] etc. have evolved. Especially the development of supramolecular multi-molecular frameworks offers a great playground for organic, physical, and material chemists, alike. Since its inception more than 50 years ago, supramolecular chemistry has played an invariably important role. Supported by people like Nobel Prize winner of 1987 Jean-Marie Lehn,[151] a multitude of synthetic strategies and designs, especially on a molecular level, have been developed through decades of research. Key objectives such as multi-molecular patterns mimicking artificially photosynthetic charge transfer events (see also section **4.2**) in the sense of a sustainable solar energy conversion, to name but one, play an eminently important role. But what is the basic principle behind it? In fact, the goal of supramolecular chemistry is the construction of highly complex host-guest architectures based on intermolecular interactions.[151] Moreover, the controlled formation and tunability of molecular self-assemblies is of major interest for mimicking natural systems.[152][153][154] Gaining control over their self-organization and -recognition is, therefore, of fundamental value and may

allow the development, integration, and optimization of molecular components as devices in catalysis, photonics, electronics or molecular information storage.[151][155] Especially, the introduction of fullerenes is an elegant way, due to their unique electronic- and photophysical properties,[156][157][158] as well as their ball-shaped morphology.
Besides self-assembly systems, fullerenes like $PC_{61}BM$ ([6,6]-phenyl-C_{61}-butyric acid methyl ester),[159] and $PC_{71}BM$ ([6,6]-phenyl-C_{71}-butyric acid methyl ester)[160] have been widely incorporated and investigated in polymer based films.[161][162][163] Interactions between fullerenes and polymer containing functional groups can lead f.ex. to an enhanced photoconductivity[164] and can play, therefore, a distinct part for the usage in solar energy conversion based systems like solar cells.

3.7 Semiconducting Materials

3.7.1 NiO as p-type Semiconductor Material in DSSCs

Dye-sensitized solar cells (DSSC) are a low cost and easy to manufacture technology for future energy supply, which are characterized by low production costs and power conversion efficiencies (PCE) similar to conventional silicon solar cells.[165] Due to the ever-increasing demand for energy, the production and combustion of fossil fuels such as natural gas or oil are increasing worldwide. However, due to the ongoing and worsening consequences of climate change (see chapter **1**) such as the increased number of bush fires in Australia in 2019/20, the perspective of many nations, including the European Union, which aims to be completely climate-neutral by 2050, and, therefore, relying on renewable energy sources and carriers such as wind and solar energy, is changing. The development and optimization of excellent performing and economically friendly solar cells is of highly interest. Especially with regard to n-type DSSCs, a high interest in TiO_2 as the first choice is evident, when it comes to be cost-effective, flexible, but highly efficient.[165] In general, the theoretical predicted power conversion efficiency (η) of one absorber DSSCs can reach up to about 31%, the so called Shockley-Queisser limit, an efficiency limit dependent on the bandgap material of a solar cell.[166] The most prominent representative is the Grätzel cell.[167]

In general, the efficiency of a solar cell is defined by the fraction of the product of the open-circuit voltage (V_{OC}), the short-circuit current density (J_{SC}), the fill factor (FF), and the power of incident light.[168]

$$\eta = \frac{P_{max}}{P_{in}} = \frac{V_{OC}\, J_{SC}\, FF}{P_{in}} \cdot 100\ \% \tag{3.7}$$

Consequently, V_{OC} is defined as the potential difference between the Fermi-level of electrons in the semiconducting film and the redox potential of the electrolyte, while the photocurrent J_{SC} is determined based on charge injection, collection, and the incident light harvesting efficiency.[168] J_{SC} is the flux of charge injection minus the charge recombination/interception reactions.[168] FF acts as ratio of the maximum power obtained to the product of both forms.
The basic operation principle of a dye-sensitized solar cell, which is already known since Antoine Henri Bequerel,[17] (see also chapter **1**), is simple. Sunlight hits the surface of the solar cell, which is covered with the dye. Thus, in turn, is excited and the so-called electron-hole pair (exciton) is formed. In the case of a n-type DSSC like the Grätzel cell, the electron is injected into the conduction band (CB) of TiO_2 and diffuses all the way through the film to the photoanode and is utilized to fulfill work at the external load. Meanwhile, the hole is reduced by the redox-couple (I^-/I_3^- or Co^{II}/Co^{III}) in the electrolyte. At the counter electrode, which is usually a platinum coated conductive glass electrode, the electron in the cycle reduces the hole. This closes the cycle and the DSSC is ready for the next incident light photon. This process can also be done inversely by passing the hole through the valence band (VB) of a p-type semiconductor, which leads to a reduction, and not to an oxidation as in the previous case. Which, in turn, reduces the redox-couple and is reoxidized at the counter electrode. Their combination, the so-called tandem cell, is shown in **Figure 3.9**.

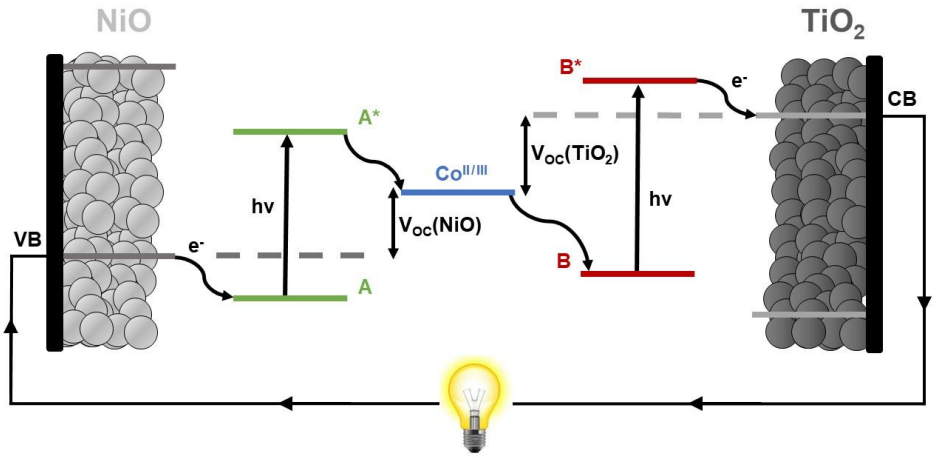

Fig. 3.9.: Schematic representation of a tandem dye-sensitized solar cell. TiO_2 CB and NiO VB represent the Fermi levels of TiO_2 and of NiO, respectively; A and A*, B, and B* represent the energetics of the sensitizers; $Co^{II/III}$ represents the redox potential of the electrolyte.[169]

In case of p-type DSSCs a lot of attention is paid to NiO as p-type semiconductor material,[168] f.ex also in combination with triphenylamines[170][171] (see section **3.4**). Especially with respect to highly efficient and sustainable tandem cells, the key lies in the improvement and further development of p-type solar cells, in contrast to n-type cells which have already been greatly improved and optimized.[169] Despite their still relatively weak values in terms of efficiency, (J_{SC} or V_{OC}) compared to TiO_2 based DSSCs,[168][169] much has happened since the first development of NiO based DSSCs by He *et. al*.[172] Nevertheless, some issues have emerged that need to be addressed, despite the progress that has been made: (i) the fast charge recombination between the hole in the VB of the NiO and the reduced species of the dye, (ii) the high dark current, (iii) and the small V_{OC} values.[168] In case of fast charge recombination, the low permittivity ($\varepsilon = 11.9$),[173] the low mobility of the holes in the NiO, and the lack of hole traps within the semiconductor, as well as the poor anchoring groups[174] leading to a fast recombination process between the reduced dye and the hole in the valence band of the NiO. Also the high dark current, which lowers the net current J(V) or J_{SC}, leads to low photocurrent and reduces, therefore, FF in addition to V_{OC}.[168] Charge collection efficiencies depend on the competing effects between the hole diffusion to the charge collector (hole transport time) and the rate of the reduction of the holes at the surface of the NiO (interception) or charge collectors by the reduced species in the electrolyte.[168] As with the recombination reaction between the dye and the hole in the NiO valence band,

the interfacial reaction with the electrolyte is particularly critical in p-DSSC and limits both, the V_{OC} (by affecting the position of the Fermi level) and the J_{SC}, leading to a high dark current and short hole lifetimes.[168] This increases the series resistance in the device, contributing to the low observed FF in p-DSSCs (≈ 0.3 - 0.4).[168]
The last and probably biggest problem causing the low efficiencies in p-type cells are their low V_{OC} values. The quasi-Fermi level is defined as the level in which the occupation probability of the electron at its specific energy level is one half, presented by the Fermi-Dirac distribution.[175][176] Any changes in this thermal equilibrium will change the population of the electron in the CB and the VB. If these changes are small or slow enough, the corresponding bands of the quasi thermal equilibrium, the so-called quasi-Fermi-level, relax.[168] These changes depend on the flat-band potential of the material of the hole concentration and the redox potential of the redox couple.[168] Since the in-built potential is small in the case of p-type materials, but the recombination and interception reactions are common, the combination of all factors results in reduced V_{OC} values.[168] If the use of the material, e.g. NiO or the redox-couple, is unchangeable, an improvement of the V_{OC} is only possible by extending the charge separated state lifetimes and, thus, reducing the charge recombination between the hole in the VB and the reduced dye species. The V_{OC} is a parameter of paramount importance to reach higher efficiencies and it can be enhanced with the use of new redox shuttles and new p-SCs, particularly those which will overcome the high dark current.[168] In p-DSSCs, the charge recombination and interception reactions are particularly important. As the photocurrent is mainly confined through the hole diffusion within the semiconductor film and the interception reaction between the redox mediator and the hole at its surface or on the exposed transparent conducting oxide (TCO) film.[168][174] Therefore, reducing losses by limiting the charge interception at the electrode/electrolyte interface will be an important improvement for both, J_{SC} and V_{OC}.

3.7.2 Brief Introduction to Black TiO_2 Nanoparticles in Photocatalytic Water Splitting

In addition to the production of electrical energy by light, which is exploited in the case of solar cells, the processing and production of solar fuels such as hydrogen, for example, plays an incredibly important role in the usage of fuel cell powered vehicles, operating CO_2-free. Because of this,

photocatalysis has been expanding quickly. However, one of the most commonly used materials for various photocatalytic applications, such as the production of H_2 from pure water or the disposal of industrial waste by organic decomposition,[177] are TiO_2 nanoparticles. As already mentioned in subsection **3.7.1**, TiO_2, as a n-type semiconductor, is a global player when it comes to the conversion of solar energy into electricity. But, titania is also considered as a perfect matching material in photocatalysis, if one talks about high stability, cost-effectiveness or non-toxicity, a major general drawback of nanoparticles, especially used as drugs or in biological applications.[178]

The starting signal for titania as photocatalyst was given in 1972 by Fujishima and Honda *et.al.*[25] with the first electrolysis of water using titania. Photoirradiation of rutile TiO_2 in aqueous solution led to the evolution of H_2 at the platinum counter electrode and of O_2 at the TiO_2 electrode after applying a negative bias voltage at the working electrode. Now, titania has widely researched for numerous photocatalytic, -electrochemical, and -electrical energy applications.[179] However, as the activity and performance in such systems requires a small band gap and a sufficient amount of incident light photons, pristine titania shows some issues that still need to be solved. Since titanium dioxide with its very large band gap ($\approx$ 3 eV) can only use about five percent of the solar spectrum (see also **Figure 3.10**), immense efforts are required to create a system that is not only functional but also economically efficient.[179][180]

An important milestone in the development of improved titania nanoparticles was the discovery of black TiO_2 nanoparticles, as it is not limited harnessing the light only in the UV range, as in the case of pristine TiO_2, but extending its usage up to the NIR range. This extension of absorption of the photocatalyst results in performance to be increased to a maximum.[181] Since its discovery ten years ago by Chen *et. al.*,[181] the focus has shifted to the development of defect-engineered black TiO_2 nanoparticles.[182] Besides the usual doping with metals or non-metals,[183] hydrogenation leads to a thin layer of disordered defects at the surface of the titania crystal causing a change in its electronic structure and, thus, leading to tunable optical properties.[180] The latter one is now one of the most widely used methods and of particular importance. In general, this process describes a chemical reduction by molecular hydrogen, which under mild reaction conditions results in a reduction of TiO_2 by hydrogen, while slowly increasing the temperature.[181][184] This can lead to the formation of O-H bonds during the hydrogenation process without developing metallic titanium. Under ideal reaction conditions oxygen vacancies, Ti-H bonds, and even Ti^{3+} interstitial sites are formed.[184] Despite this clear approach, the preparation, as well as

the structure and properties of black TiO_2, show a high dependency with respect to temperature. Moreover, the physiochemical properties of pristine TiO_2, with respect to size, morphology, etc., the hydrogenation time, as well as the hydrogen pressure and its purity, have an enormous impact and play pivotal role on the final result.[182] The black color of black TiO_2 nanoparticles seems to be possible due to incorporating hydrogen as dopant forming Ti-H and Ti-O-H bonds as mid-gap states.[181] A brief overview of the key parameters for black TiO_2 by high-pressure hydrogenation is given in the following table:

Table 3.1.: Key parameters of black TiO_2 nanomaterials by high-pressure hydrogenation adapted from reference.[184]

Starting TiO_2	Reaction temperature	Reaction time	H_2 pressure	Color	Surface disorder	Ref.
Anatase NP	200 °C	120 h	20 bar	Black	✓	[181]
Anatase NP	250 °C	24 h	20 bar	Pale yellow	×	[185]
Anatase NP	350 °C	24 h	20 bar	Grey	×	[185]
Anatase NP	450 °C	24 h	20 bar	Black	×	[185]
Anatase NP	450 °C	24 h	7 bar	Black	×	[186]
P25	15 °C	480 h	35 bar	Black	✓	[187]
Rutile Nanowire	350 °C	0.5 h	*N/S*	Yellow-green	×	[188]
Rutile Nanowire	≥ 450 °C	0.5 h	*N/S*	Black	×	[188]
Anatase Nanotube	450 °C	2 h	*N/S*	Black	×	[189]
Anatase Nanotube	200 °C	120 h	20 bar	Grey	×	[190]
Anatase Nanotube	500 °C	1 h	20 bar	Black	×	[190]

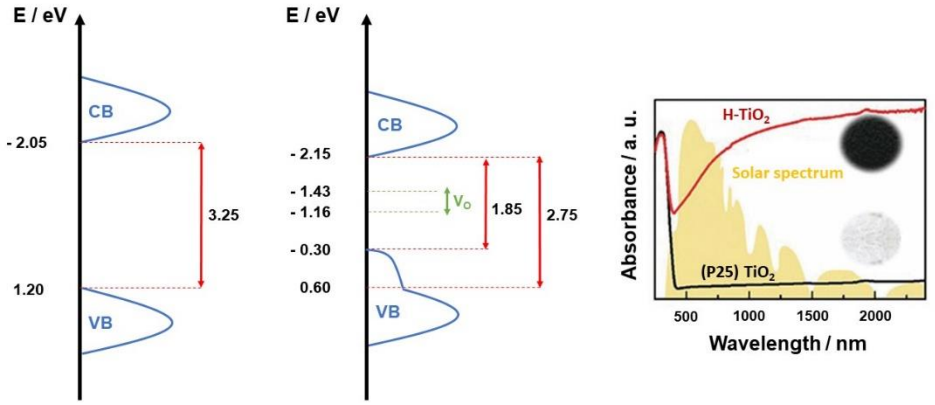

Fig. 3.10.: Adapted schematic energy diagram for TiO_2 P25 Degussa and black TiO_2 nanoparticles. The representations were developed using experimental data from SXRPD, XPS analysis, cathodoluminescence (CL), and UV-vis spectroscopy. The energy positions of the oxygen vacancies (green) localized states were calculated by subtracting components at 2.36 and 2.63 eV of black TiO_2 CL band from the valence band maximum in reference TiO_2.[191] (right) Adapted optical absorption spectra of pristine TiO_2 (white) and H-doped TiO_2 (black powder) obtained by hydrogen plasma treatment.[192]

In summary, it can be concluded that the formation of favorable surface disorders are preferred by persisting hydrogenation, high pressure, and low temperature reaction conditions.[184] But, why do oxygen vacancies, etc. contribute positively to the photocatalytic properties of black TiO_2? In general, oxygen vacancies are frequently found in different transition metals and, therefore, play a decisive role in metal oxides.[193] The oxygen vacancies, resulting from hydrogenation reduction, serve as active sites.[194]
One of the characteristics in the development of black TiO_2 is the shift of the VB to the Fermi level due to electronic modification, which is mainly caused by the synthetic conditions, doping or morphological properties.[179][191] The exact origin of controlling, evaluating, and tuning this deficiencies building is still not completely revealed and still under debate. Nevertheless, defects play an important role here. So tend modified TiO_2 to produce shallow and deep state traps nearing the CB minimum using typically Ti^{3+} states. Moreover, the development of disorder induced mid-gap states leading to an upshift of the VB edge in the TiO_2 and, therefore, to a so called band tailoring.[181] Besides the classical reduction methods like hydrogenation or ball milling treatment, which means the TiO_2 modification by strain introduction using a planetary mill with grinding balls made of

f.ex. ZrO_2 under pressure,[195] the optimization of the very slow H_2 evolution kinetics in non-bias applied photocatalysis is of major interest. This problem is usually solved by using noble metal co-catalysts like Pt, Pd, Au, etc. used as electron transfer mediator.[179][196] This enables an improved hydrogen generation rate, though involves high costs due to the exploitation of less abundant metals and, therefore, a less attractive overall package.[195] For this reason, the focus shifts to the development of noble metal and sacrificial-agent free black TiO_2 nanoparticles and will be a highly attention paid research field in the future, with its particularly cost-effectiveness and great performance potential. Subsuming, the synergy between the usage of solar energy in form of electrically and chemically bound energy carriers or sources has an enormous potential, as well as a rewarding research and civilian goal, making a prosper and sustainable future possible.

3.8 Experimental Methods and Analysis Techniques

3.8.1 Pulse Radiolysis

Thinking about experimental methods and analysis tools, a huge variety of measurement methods can be conducted using light, in general. But investigation of radiation or radiative processes contain not only electromagnetic wavelength in the range of the visible light, the UV or NIR region, but also in the magnitude of several centimeters up to γ-radiation or cosmic ray with several femtometers.
Another possibility of radiation can be achieved due to very fast particles, as f.ex. accelerated electrons (100 keV to several MeV). Those accelerated particles can be used as origin to detect radiation chemical processes or interactions due to secondary processes as a counterpart to the "pure" absorption based spectroscopy. This interaction with especially solvent molecules causes ionization or excitation through energy transfer due to Rutherford scattering or elastic scattering. Its exact mechanism is well described using the Spur model for radiation chemical primary processes by Magee and Samuel *et. al*.[197][198][199] Thus, in the path of the fast electrons, areas with groups of ionized or excited molecules (almost exclusively solvent molecules), radicals, and electrons are formed. Those are called spurs. These spurs can now undergo, on one hand, a recombination, and on the other hand, they may do expand by diffusion and are distributed homogeneously within the sample. These primarily formed reactive species can interact now via successive subsequent reactions with dissolved samples.

This technique is called electron pulse radiolysis and offers, therefore, the time-resolved investigation of reactive or excited species like triplets, oxidized or reduced radical species and their behavior over time.

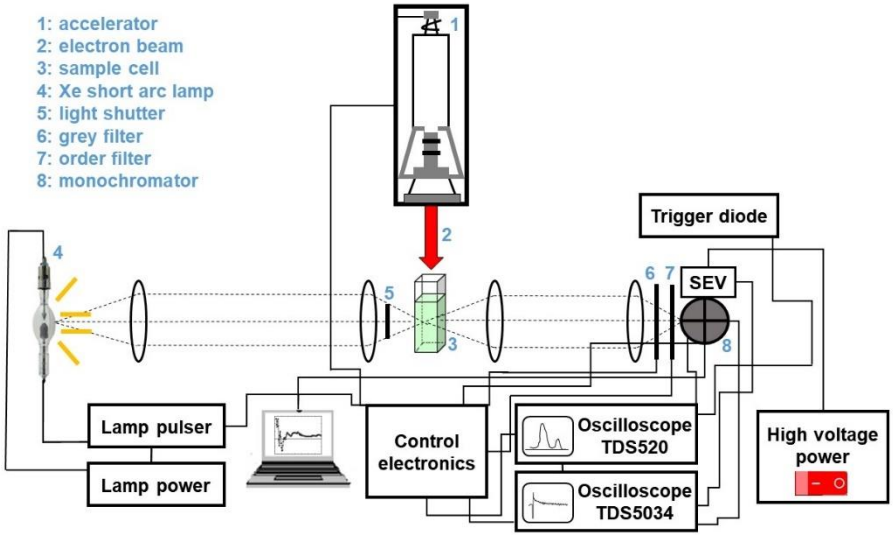

Fig. 3.11.: Scheme of the pulse radiolytic LINAC type electron accelerator ELEKTRONIKA-U003 setup at the IOM in Leipzig.

Using the experimental setup of the Leibniz Institute of Surface Engineering (IOM) in Leipzig, the electron accelerator used as electron gun speeds up the electrons using high-frequency alternating fields. In the vacuum chamber, the arranged metal plates are charged, similar to a capacitor in which a charge gradient is built up. Along this charge gradient the electrons are accelerated and experience an energy absorption of up to 10 MeV. Afterwards, they hit, after passing a tantalum plate, a very thin cuvette. In this cuvette the absorbed dose per pulse can be conducted up to 100 Gy with a pulse width of 15 ns. The detection of the formed transients is performed by means of time-resolved absorption spectroscopy (see also subsection **3.8.2**) using several detection instruments like, f.ex. secondary electron multipliers and photodiodes, and records the change in optical density as a function of time ($\Delta OD_\lambda = OD_\lambda - OD_{Ref}$). The basic principle arrangement of the measurement setup, which can be found at the Leibniz Institute of Surface Engineering (IOM), is shown in **Figure 3.11**. Here, pulse radiolysis measurements are conducted by irradiating the investigated samples with high energy electron pulses (10 MeV, 15 ns duration) by a LINAC type electron accelerator ELEKTRONIKA-U003 (Toriy, Moscow). The dose

delivered per pulse is measured by electron dosimetry. The optical detection system consists of a pulsed 1000 W xenon lamp (Osram, XBO1000), a Suprasil cell (light path 1 cm), a high intensity grating monochromator (Acton research, SP275), a R928 photomultiplier (Hamamatsu Photonics) or a fast InGaAs photodiode and a fast transient recorder (Tektronix, TDS5034). Thus, depending on the selected point at a specific time, the spectral characteristics of the formed primary transients, intermediate states or products therefrom are identified. Beyond this, additional kinetic information about the decaying transients or the formation of new ones, such as reaction rate constants, can be gathered.

3.8.2 Time Resolved Femtosecond and Nanosecond Transient Absorption Spectroscopy

Transient absorption spectroscopy offers a possibility to measure the absorptions of short lived species, namely transients, such as molecules in excited states or radical ion pairs, etc. This technique allows to investigate the reaction channels of such transients, revealing their reaction kinetics, mechanisms, and intermediates. Depending on the required time resolution, there are two different concepts of transient resolved spectroscopy – one based on femtosecond and the other one on nanosecond laser photolysis. The nanosecond transient spectroscopy is used to investigate photoinduced processes occurring in the range of several nanoseconds up to several ms. The femtosecond transient absorption spectroscopy allows for probing photoinduced processes in the time range between several hundred femtoseconds up to several nanoseconds and, therefore, gives information about elementary processes such as conformational changes, chemical reactions, or electron and energy transfer processes in solution or in the solid state.[200] The basic problem of femtosecond photolysis transient absorption spectroscopy is that no detectors with a sufficient time resolution are available. As a consequence, the information is transformed to another dimension, in this case the distance of light. **Figure 3.12** displays a schematic setup. A pump/probe laser system is used, whose laser pulse of a certain wavelength is slivered at the beam splitter. Both laser beams pass through the probe together and are transferred afterwards to a Charge Coupled Device (CCD) camera.

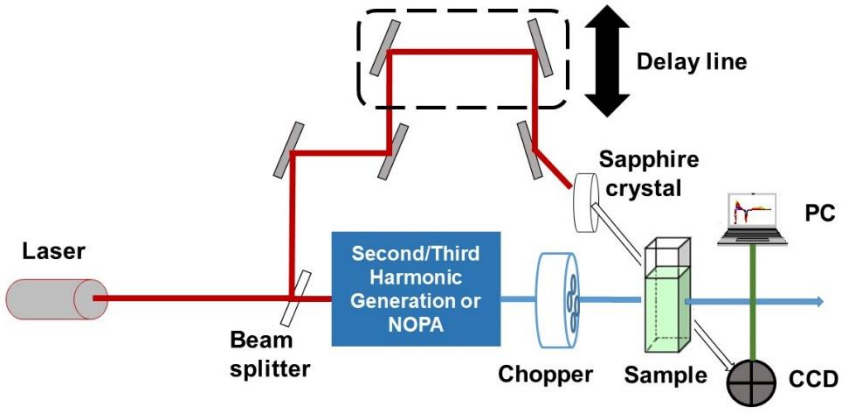

Fig. 3.12.: Schematic setup of a femtosecond resolved transient absorption spectroscopy setup.

One of the two pulses – the pump pulse – excites the molecule from the ground state into a higher excited singular state. The wavelength adjustment of the pump pulse is achieved by either second harmonic or third harmonic generation of a pulsed titanium:sapphire laser with a 775 nm output, leading to excitation wavelengths of 387 (second harmonic) and 258 nm (third harmonic generation) or with the help of a two-stage non-collinear optical paramagnetic amplifier (NOPA) with wavelengths between 450 and 1200 nm. The other pulse, the probe pulse, which is formally white light generated by the sapphire crystal, follows another adjustable path (delay line) and passes the probe some time afterwards. After the transfer to the CCD camera, the absorption spectrum of the transient is calculated. To enable the uptake of differential absorption spectra, a chopper is interposed between NOPA and probe. The chopper blocks every second pulse, thereby only every second excitation, but every request pulse is measured. This procedure leads to differential spectra. These differential spectra are equal to time-depending alteration of the optical density (ΔOD). In this case, measurements are performed on a titanium:sapphire laser system and three CCD cameras for the Vis (420 - 765 nm) and the NIR (780 - 1630 nm) are used. In general, three different forms of physical processes are known. The first, the ground state bleaching, which originates from the decreased number of molecules in the ground state compared to those in the excited state caused by the pump pulse producing a negative differential absorption – a

mirror image of the ground state absorption maxima. The second one is due to stimulated emission, at which the excited molecules decay via f.ex. fluorescence back to the ground state. The third and most interesting one originates from transient absorptions of the excited states leading to a positive signal, which may evolve over time due to solvent, geometry relaxations or changes in the nature of the molecule.
Additional to ultra-short-lived transients, also transients with longer lifetimes like triplet excited states can be investigated. Therefore, transient absorption spectroscopy in the nanosecond range can be carried out. Here, the pump and the probe beam are evolved separately. Both are hitting the probe perpendicular. In case of the laser system, a Q-switched Nd:YAG laser with a pulse width of 5 ns is used. With the assistance of a high-pressure XBO lamp, the white light for the request pulse is generated. The prefixed pulser allows a higher intensity of the beam, which is transferred, after hitting the probe, to the monochromator. The monochromator filters a certain wavelength, which is also transferred to a photomultiplier (measurements in the UV-Vis) or an indium-gallium-arsenide (InGaAs) photodiode (measurements in the NIR). The signal is led to the oscilloscope, which transfers the information to the computer. A second option is using the Ti:sapphire laser system with a detached laser source as white light generator. Hence, a chopper is not required as the pulse generation is managed electronically.

3.8.3 Multiwavelength Analysis Technique – the Glotaran program

After the processing of datasets by different time-resolved techniques like time-resolved emission or transient absorption spectroscopy (see also subsection **3.8.2**), an intensive analysis is necessary to evaluate and interpret the collected information in the best possible way. This is where the Glotaran[201] program helps. Glotaran stands for global and target analysis and is a graphical user interface for the TIMP[202] program. TIMP is a well described[203] package of the statistical programming language *R*[204] for computational modelling, which allows to analyze several datasets simultaneously. Therefore, Glotaran or TIMP follows the scientific model, discovery of specification, parameter estimation, and validation, which is an iterative simulation process.

But, how exactly does TIMP work? In general, a spectroscopic dataset can be considered as a matrix, which is described as the following:

$$\Psi_{\mathrm{q}} = \begin{pmatrix} \psi(\mathrm{t}_1, \lambda_1) & \psi(\mathrm{t}_1, \lambda_2) & \cdots & \psi(\mathrm{t}_1, \lambda_{\mathrm{n}}) \\ \psi(\mathrm{t}_2, \lambda_1) & \psi(\mathrm{t}_2, \lambda_2) & \cdots & \psi(\mathrm{t}_2, \lambda_n) \\ \vdots & \vdots & \ddots & \vdots \\ \psi(\mathrm{t}_m, \lambda_1) & \psi(\mathrm{t}_m, \lambda_2) & \cdots & \psi(\mathrm{t}_m, \lambda_{\mathrm{n}}) \end{pmatrix} \tag{3.8}$$

Each row of the matrix Ψ_{q} is a spectrum containing the spectral variable λ (often the wavelength or wavenumber). Spectra are represented at m instances of independent experimental variables such as the time t.[202] This matrix can be divided into a matrix *P*, which has the concentration or population properties, and a second matrix *S*, which has the spectral components.[202] Each individual matrix contains *n* components, spectrally distinct units representing the concentration or population in time and the associated spectra with respect to the wavelength,[205] and can be noted in the superposition model as the following:

$$\Psi_{\mathrm{q}} = \begin{pmatrix} \mathrm{c}(\mathrm{t}_1, 1) & \cdots & \mathrm{c}(\mathrm{t}_1, n) \\ \mathrm{c}(\mathrm{t}_2, 1) & \cdots & \mathrm{c}(\mathrm{t}_2, n) \\ \vdots & \ddots & \vdots \\ \mathrm{c}(\mathrm{t}_m, 1) & \cdots & \mathrm{c}(\mathrm{t}_m, n) \end{pmatrix} \begin{pmatrix} \epsilon(\lambda_1, 1) & \cdots & \epsilon(\lambda_1, n) \\ \epsilon(\lambda_2, 1) & \cdots & \epsilon(\lambda_2, n) \\ \vdots & \ddots & \vdots \\ \epsilon(\lambda_m, n) & \cdots & \epsilon(\lambda_m, n) \end{pmatrix}^{\mathrm{T}} = PS^{\mathrm{T}} \tag{3.9}$$

By modelling multiwavelength dataset Ψ_{q}, the inverse problem of recovery of the entries of *P* or *S*, in terms of physically significant parameters, (e.g. the lifetime of a component, or the associated spectra like a certain maximum of a transient in the spectrum), using (3.9), is of particular interest.[202] As *P* or *S* are nonlinear, and are usually comprised of many submodels, an appropriate parametrization of them is necessary to gather various model aspects.[202][206] Consequently, scientists use spectroscopic and microscopic measurement techniques to study the mechanisms and the behavior of complex systems. Thus, the resulting physical processes underlying these data, advanced modeling and data analysis techniques are essential.[201] The first step in modeling is the deconvolution with the aid of the singular value decomposition of the dataset.

The singular value decomposition (SVD) is in fact a matrix factorization technique to investigate the number of spectrally and temporally independent components within the data matrix.[201][207] This in fact, plays a

crucial role to obtain and define an initial model. The SVD[201] of the data matrix is defined as:

$$\Psi_q(\lambda, t) = \sum_{n=1}^{n_{max}} u_n(t) w_n(\lambda) SV_n \tag{3.10}$$

The involved number of individual components within the system is defined by singular values, while n_{max} is described as the number of rows and columns of it.[201] With n independent components you get exactly n significant singular values, which are different from zero and can be defined as: $SV_1 \geq SV_2 > SV_n > SV_{n+1} = \ldots = 0$.[201]
After this pre-processing of the data, a first attempt can be made to model and fit the dataset, whereby often the simplest and most reasonable model is the best approach. Existing interactions between the individual states, or even between several systems, can be applied by the compartment model, which is used in particular in pharmacology.[208][209] The crossover between the compartments, such as the interacting subsystems as rate constants, represent the off-diagonal elements of the transfer matrix K.[202][210] In fact, the diagonal elements of K are containing the decay rates or lifetimes of each subsystem of the model.[202] Thus, a linear compartmental model with n compartments is described by a differential equation[202] for these concentrations:

$$\frac{d}{dt} c(t) = Kc(t) + j(t) \tag{3.11}$$

where the input, that means the corresponding pathways, to the system are described by vector j. In general, two modes for analyzing the compartment model can be distinguished: The global analysis and the target analysis, where the former describes a unified separable non-linear model containing multiple independent variables.[202] Again, two model modes exist – the parallel and the sequential model. The latter describes a system in which the components, and in consequence the species, obtained by the SVD, decay in parallel to the ground state.

Fig. 3.13.: Diagram of a compartmental model of three components, all of which decay in sequential (left) and parallel (right) to the ground state.[202]

The sequential model, on the other hand, describes a system, in which these k-components decay sequentially, i.e. one after the other and without losses, into the ground state. As an example, **Figure 3.14** shows the procedure using a femtosecond transient absorption spectroscopy dataset from the acquisition of the raw data of a calix[4]arene-perylene bisimide dye, through SVD analysis, modeling, and optimization of the result.[211]

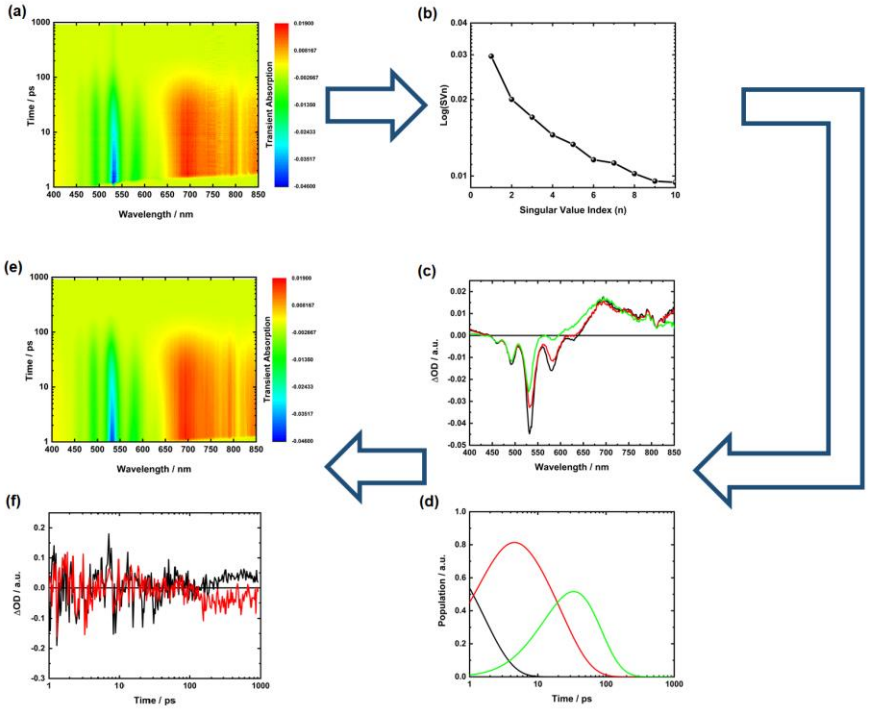

Fig. 3.14.: Schematic representation of data from capturing over analyzation to representation of components after selective modeling and component deconvolution. Starting from the collected raw data transient spectra as a 3D map **(a)**, followed by a singular value decomposition **(b)**, deconvolution, and visualization of both matrices **(c)**-**(d)**, and its optimized and modelled results **(e)** containing the left singular vector as a fit to raw data relation **(f)**.[211]

But this is exactly where the disadvantage of global analysis becomes apparent – the simplicity of the described model. Most of the time, the samples to be investigated show a much more complex photophysical behavior, which cannot be described either loss-free or by a mere parallel or sequential model, but rather by a combination of both. The solution to the problem is provided by target analysis, which requires, however, the implementation of a reasonable target model. In general, it can be summarized that the more complicated the system under investigation and the fewer variables or paths within the model are known, the more the use of global analysis is recommended. Whereas a precise description of the photophysical states and their dynamics can only be achieved by implementing a target model.

4 Results and Discussion

4.1 Fundamental Characterization of New Carbon Rich Materials – Development of New Electron Donor-Acceptor Systems

4.1.1 Controlling and Fine-Tuning Charge Transfer Emission in 2,6-Dicyanoaniline Multichromophores Prepared through Domino Reactions: Entry to a Potentially New Class of OLEDs

- Fabian Plass,* Sebastian Bönisch,* Felix Held,* Tobias Ullrich, Florian E. J. Fischer, Anton Guryev, Andreas Görling, A. Kahnt, Svetlana B. Tsogoeva, Controlling and Fine-Tuning Charge Transfer Emission in 2,6-Dicyanoaniline Multichromophores Prepared through Domino Reactions: Entry to a Potentially New Class of OLEDs, *J. Org. Chem.*, **2021**, *86*, 6111-6125

The development and characterization of new materials – especially on carbon basis – is of fundamental importance. Not only focused on the synthesis of new carbon allotropes like fullerenes, nanotubes, etc., but also as major component in novel molecular electron donor-acceptor systems. On the basis of them, almost endless possibilities are conceivable. One interesting, but not commonly described option is their implementation as OLED based materials.[212] In fact, in the nearby future, organic light emitting diodes (OLEDs) are assumed to usurp other electroluminescent devices or liquid crystal display (LCD) technology.[213] Nowadays, OLEDs are already commercially available and integrated as thin layers in a variety of electronical devices like cellphones. Therefore, a tremendous increase in the demand and production of OLEDs is expected.[214] OLEDs are currently still grounded on coordination complexes consisting of rare metals such as Iridium.[215][216][217] But, their usage comes with several drawbacks, especially due to their rare abundance, which makes them unsustainable and highly expensive.[218] There are existing, but still challenging alternatives like triplet harvesting in phosphorescent OLEDs (PHOLEDs), thermally activated delayed fluorescence (TADF),[219] rotationally accessed spin-state inversion (RASI),[220] doublet exciton emission,[221][222] and triplet-triplet annihilation (TTA).[223] A different concept on the basis of charge recombination processes from charge transfer states is mechanistically sparsely described in

electron donor-acceptor systems.[74] In general, molecules with electron donor-acceptor moieties are of great interest, since these molecular architectures facilitate electron and hole injection.[224][225] Until now, several different electron donor and electron acceptor systems have been successfully implemented,[226][227] yielding electroluminescence ranging from blue to red.[228][229]

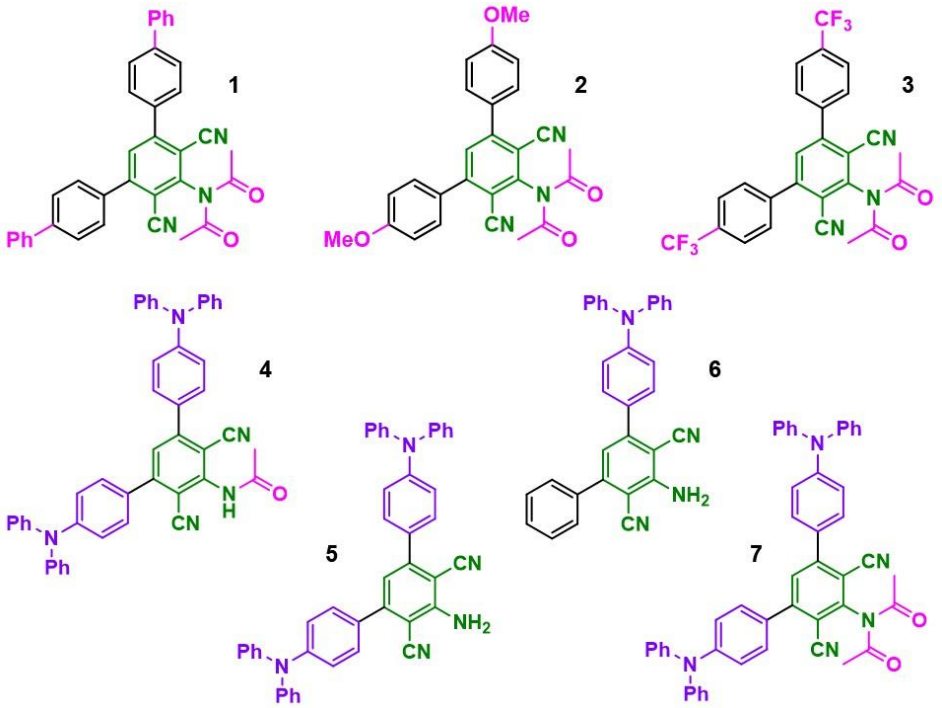

Fig. 4.1.: Schematic structure of all investigated references (from top left to right), namely **1**, **2**, and **3** and the molecular electron donor-acceptor systems (from left to right), namely **4**, **5**, **6**, and **7**. The 2,6-dicyanoaniline and TPA units are depicted in olive and violet, while the different units attached are shown in pink.

A promising and rather new class is 2,6-dicyanoaniline, as it can be used as building block, for example, in electron donor-acceptor triades, in plastics, and synthetic fiber textile printing.[230] The most studied derivatives of 2,6-dicyanoanilines are 3,5-disubstituted-2,6-dicyanoanilines. Recently, several methods for their synthesis have been reported.[231] However, they show a couple of disadvantages like high costs or long reaction times,[232][233] excess of volatile and toxic organic solvents,[234] and relatively low yields, though.[235][236]

Therefore, the group of Prof. Svetlana B. Tsogoeva developed a new synthetic strategy using an one-pot method using two multi-step domino reactions to develop a set of 2,6-dicyanoaniline based systems, also in combination with triphenylamines (see **Figure 4.1**). The resulting symmetric systems, namely **4**, **5**, and **7**, as well as an asymmetric analog of **5**, namely **6**, exhibit outstanding photophysical properties and are described in the following.
In the beginning, work was performed on the references without TPAs (**1**, **2**, and **3**). Exemplarily, steady state absorption measurements of **3** reveal absorption maxima at 300 and 370 nm and very high fluorescence quantum yields, as well fluorescence in the UV and blue region of the optical spectrum (see **Figure 4.2**), as well as a small red-shift following higher solvent polarity.

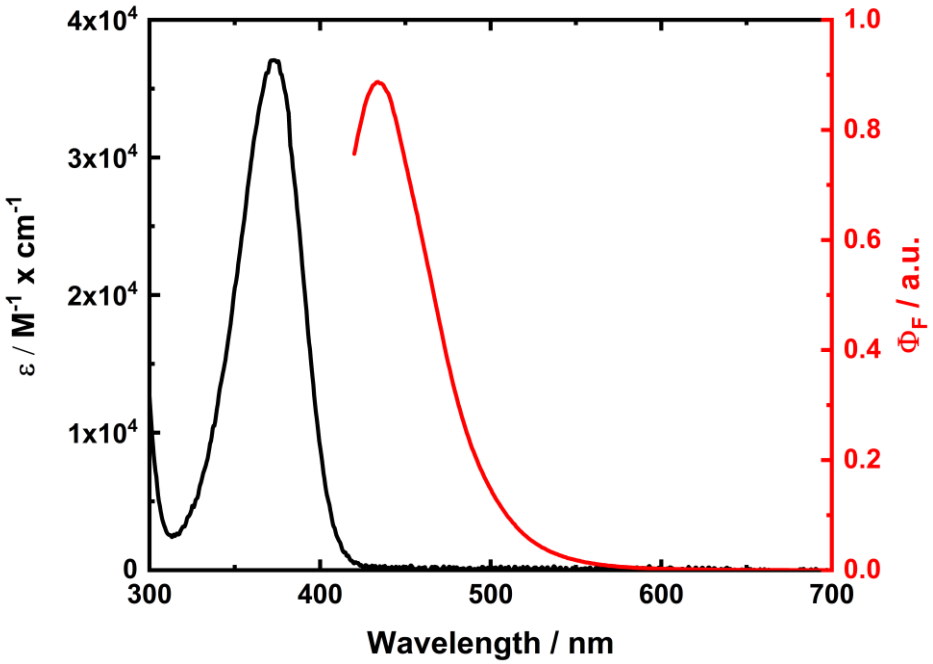

Fig. 4.2.: Absorption and fluorescence spectrum of **3** in anisole upon photoexcitation at 390 nm.

Accordingly, transient absorption laser photolysis experiments were conducted to provide insights into the photophysical nature of the dicyanoaniline backbone. Exemplarily again, for **3** in THF upon photoexcitation at 387 nm, a SVD and global analysis of the transient raw data matrix using the multiwavelength analysis tool Glotaran[201] (see also subsection **3.8.3**),

revealed the existence of three distinguishable species (see **Figure 4.3**). Interestingly, it could be demonstrated that the first two species show both singlet character with lifetimes of 71 ps and 3.23 ns, while the latter is comparable to the one obtained by fluorescence lifetime measurements.
The existence of two singlet states can be easily reasoned, as two different spatial conformations of the reference exist. This fact was also corroborated by theoretical calculations by the group of Prof. Andreas Görling. Here, both outer aryl rings stand perpendicular or almost planar to each other, while the latter is less energetically favored and, therefore, higher in energy and less stable, which is corroborated by the sequential model of the global analysis and due to its shorter lifetime. Moreover, the existence of two singlet states can be further corroborated by the observable fluorescence in the evolution associated spectra (EAS, see also **Figure 4.3b**) at around 460 and 480 nm, perfectly matching the fluorescence maxima obtained by steady-state fluorescence spectroscopy. The third species obtained by global analysis could be related to the corresponding triplet manifold, as their transients are in sound agreement with the pulse radiolysis measurements in pure toluene. Under these conditions[237] and after triplet formation of the toluene, a Dexter energy transfer process to the reference **2** occurs forming ^{3*}**2** (see **Figure 4.4**).

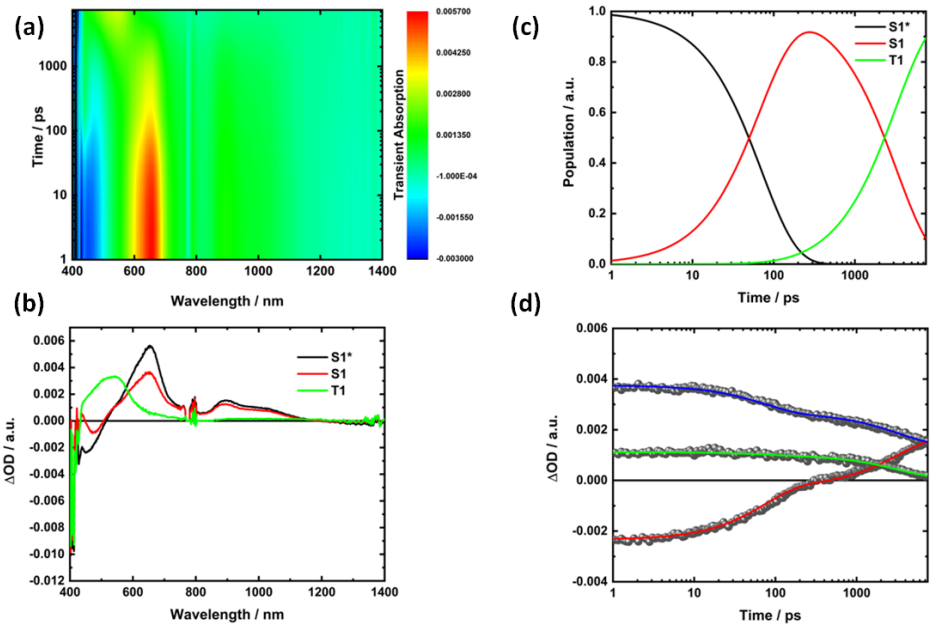

Fig. 4.3.: Transient absorption spectra obtained upon femtosecond laser flash photolysis (387 nm) of **3** in THF. **(a)** The data matrix analyzed by SVD analysis presents three different species, while the first two are related both to first singlet excited states occurring due to the existence of two spatial conformers of **3**. The third species is their corresponding triplet state. **(b)** and **(c)** represent the fitted spectral and time species, respectively, while **(d)** shows exemplarily the corresponding kinetics containing the raw data points (grey circles) and the corresponding fits at 452 (red), 604 (blue), and 860 nm (green line) using a sequential global analysis model.

After establishing the photophysical fundamentals of the references, the view turned to the investigation of the corresponding molecular electron donor-acceptor systems, namely **4**, **5**, **7**, and the asymmetric **6**. Accordingly, the class of dicyanoaniline was assumed to act as electron acceptor forming with triphenylamine an electron donor-acceptor system. To shed light on the reductive nature of them, pulse radiolysis studies under reducing conditions were conducted. Hence, solutions of **2** in mixtures of 80 Vol.-% toluene, 10 Vol.-% acetone, and 10 Vol.-% isopropanol were prepared. In this environment, it results in the formation of $(CH_3)_2\dot{C}OH$,[238][239] which is known to be a strong reductant[240] forming, as a consequence, $\mathbf{2}^{\bullet-}$. For **2**, the radiolytic reduction results in transient absorption bands in the UV and visible part of the optical spectrum with maxima at 340 and 500 nm, accompanied by a transient minimum around 410 nm (see **Figure 4.4**).

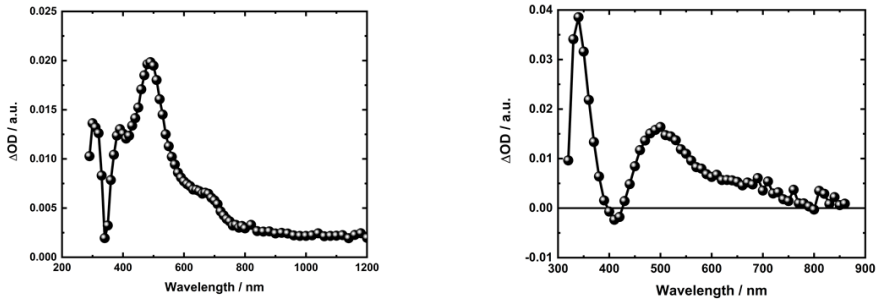

Fig. 4.4.: Pulse radiolysis measurements of **2** (100 Gy) in toluene 2 µs after the electron pulse (left) and of a mixture of toluene/acetone/2-propanol (80/10/10 v/v/v) after 70 ns.

Steady-state absorption and fluorescence spectroscopy measurements of the electron donor-acceptor systems **4**, **5**, **6**, and **7** demonstrated strong ground state interactions between triphenylamine (see section **3.4**) and dicyanoaniline. In fact, an additional absorption band with a maximum at 400 (**4**), 403 (**5**), 380 (**6**) or 391 nm (**7**) in acetonitrile, which is not related to pure TPA, nor dicyanoaniline ground state absorption, has been detected and was later on related to a charge transfer (CT) band. Such ground state interactions in TPA based electron donor-acceptor systems are not completely new and have been observed previously.[241] Moreover, conducted photoluminescence measurements showed a strong solvent polarity dependency of all investigated electron donor-acceptor systems. Furthermore, photoluminescence quantum yields showed exemplarily for **5**, high quantum yields between 70% and 95% and lifetimes of up to about six nanoseconds in benzonitrile. This radiation process is neither related to the fluorescence of TPA,[242] nor originates from the fluorescence of dicyanoaniline. Hence, this makes such systems a promising new class candidate in opto-electronic devices such as OLEDs. Nevertheless, the exact origin behind this radiative process needed clarification, since CT emission in molecular electron donor-acceptor systems are rather limited described and often do not deeply cover the photophysical mechanism in these systems.
In principle, two feasible rationales for such a wide, solvent dependent shift of the emission were possible for this charge transfer emission. Either from excited-state symmetry breaking[243][244] or resulting from a radical ion pair recombination.[74][245] The former – excited-state symmetry breaking (SB) – was excluded due to several facts like the long photoluminescence lifetimes, the resulting quantum yields in comparison to known SB-systems,[243][244] as well as the exhibition of emission in the asymmetric electron

donor-acceptor system **6**. Moreover, the experimental results and conclusions are well in line with the obtained theoretical calculations indicating a charge transfer characterization of the calculated corresponding transition.

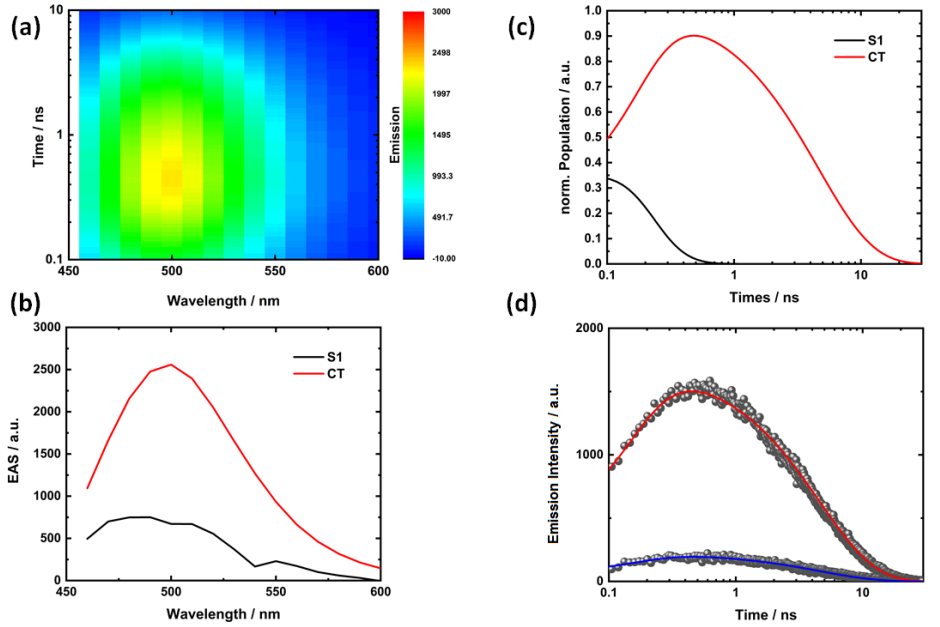

Fig. 4.5.: Time-resolved emission spectra obtained upon photoexcitation (430 nm) and photoemission detection between 460 and 600 nm of **5** in Me-THF at RT. **(a)** The data matrix analyzed by SVD analysis presents two different species, while the first is related to a first singlet excited state and the second one to a radiative CT (CT2) state. **(b)** and **(c)** represent the fitted spectral and time species, respectively, using a sequential global analysis model, while **(d)** shows the raw data points (grey circles) and the corresponding fits at 530 (red) and 590 nm (blue line.)

As the origin of this radiative process could be unraveled, the mechanism behind this newly developed molecular electron donor-acceptor class needed explanation. Hence, temperature-dependent time-resolved photoluminescence spectroscopy (TRES) measurements of **5** in Me-THF helped to gain information about the charge transfer processes as a function of time. Interestingly, at room temperature (see **Figure 4.5**) two different species have been determined by using the multiwavelength analysis tool Glotaran with lifetimes of 115 ps and 4.62 ns.
Noteworthy, the implementation of TRES data matrices in Glotaran has been conducted for the first time. While the first was attributed to a fluorophoric process and, in consequence, to the first excited singlet state, the

second (radiative) species originates from a energetically lower lying radical ion pair state.

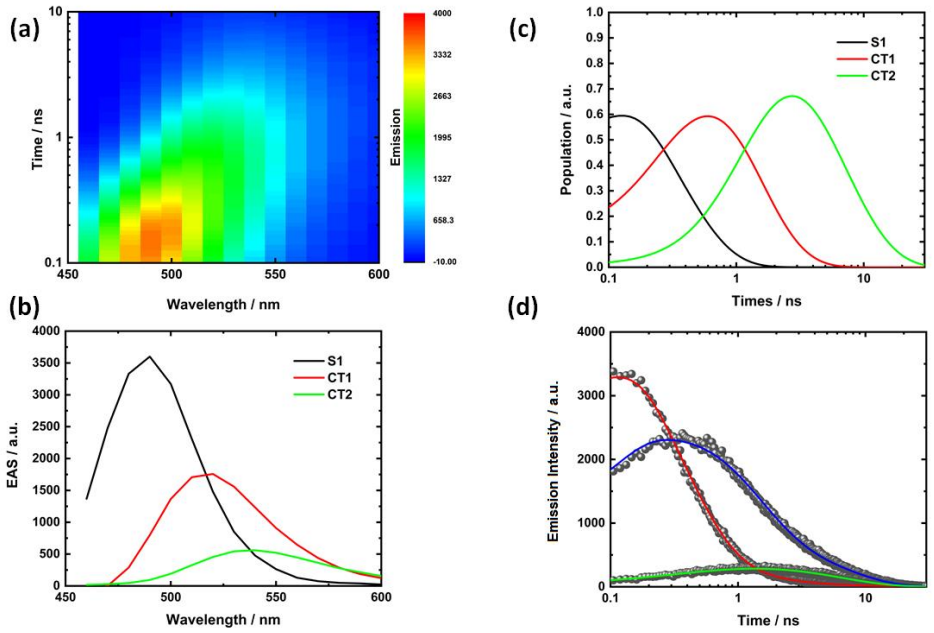

Fig. 4.6.: Time-resolved emission spectra obtained upon photoexcitation (430 nm) and photoemission detection between 460 and 600 nm of **5** in Me-THF at 140 K. **(a)** The data matrix analyzed by SVD analysis presents three different species, while the first is again related to a first singlet excited state, the two other species could be revealed as both radiative CT states, namely CT1 and CT2. **(b)** and **(c)** represent the fitted spectral and time species, respectively, while **(d)** shows exemplarily the corresponding kinetics containing the raw data points (grey circles) and the corresponding fits at 480 (red), 520 (blue), and 590 nm (green) obtained by global analysis.

Remarkably, if one cools down to 140 K (see **Figure 4.6**), three spectral species can be identified, exhibiting emission lifetimes and maxima at 490 (0.3 ns), 510 (1.1 ns), and 530 nm (6.0 ns). Again, the first species is related to the S_1 state of **5**, while the other ones originate from (radiative recombining) radical ion pair states (CT states). The core of two different CT states lies again in the structural nature of the molecular electron D-A system, as again two possible spatial conformers, like in the reference system, are existing.

Finally, transient absorption spectroscopy based on femtosecond laser photolysis at RT helped to corroborate the notion of a charge transfer process from TPA to the dicyanoaniline. Upon photoexcitation at 420 nm of **5** in

argon saturated THF at RT, three different states have been revealed after a target analysis using the program Glotaran.[201] The accuracy of the target analysis model is further proven by the fact that the obtained values by temperature dependent TRES and transient absorption spectroscopy are independently matching perfectly to each other.

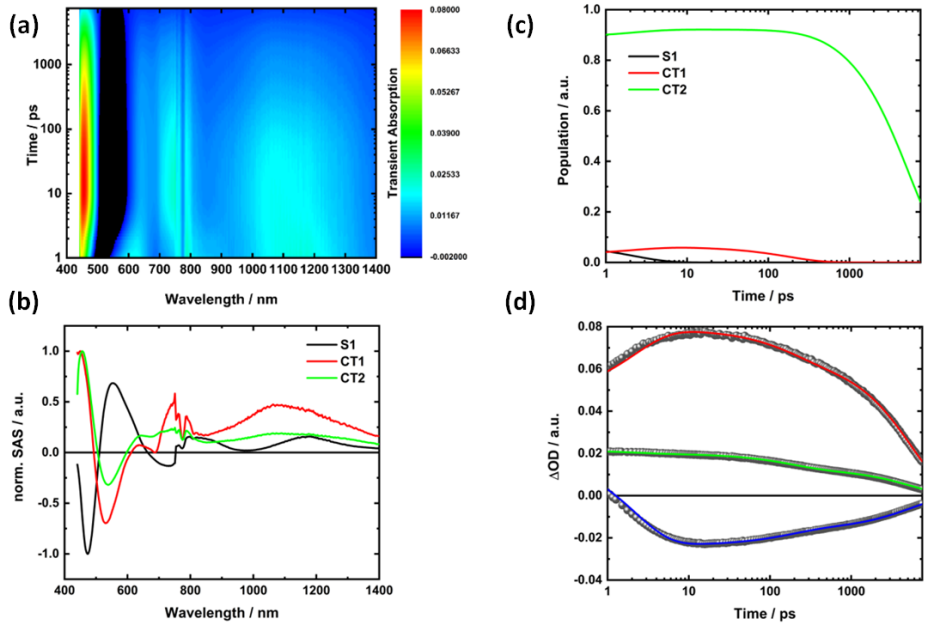

Fig. 4.7.: Transient absorption spectra obtained upon femtosecond laser flash photolysis (420 nm) of **5** in THF. **(a)** The data matrix analyzed by SVD analysis presents three different species, which are related to the first singlet excited state (S_1), the first CT state originating from the LUMO+1 state and the second charge transfer state (LUMO state). **(b)** and **(c)** show the corresponding normalized species associated spectra and the population, while **(d)** shows exemplarily the raw data (grey dots) and the obtained fit at 450 (red), 550 (blue), and 1100 nm (green line).

Three distinct maxima, one at 455 nm, one around 760 nm, and one at 1100 nm, could be obtained, matching perfectly literature reported transients for the TPA radical cation,[241][242][246][247] and the transient absorption obtained from the reduction of the reference **2** by pulse radiolysis (see **Figure 4.4**). As a result, and due to the close distance between triphenylamine and dicyanoaniline, it is reasonable to claim the formation of a $TPA^{\bullet+}$-$dicyanoaniline^{\bullet-}$ radical ion pair state. The validity of the implemented target analysis model, especially for the existence of three distinguishable states, as well as the excitation scaling factors are further corroborated taking temperature-dependent time resolved emission spectroscopy (TRES) measurements and theory into account. Noteworthy, at room temperature for **5**, only one

photoluminescent CT state is observed, while transient absorption data suggest the existence of two CT states. But, as the shorter-lived CT state at room temperature is below the temporal detection limit of our TCSPC setup, it is, in contrast to the fs-transient absorption spectroscopy technique, not resolvable.

As a result of the target analysis, **4** and **7** show both short-lived S_1 state lifetimes in the picosecond range, while their CT state lifetimes differ substantially. In fact, they are mainly shorter in case of **4**. A similar observation was also made for the other electron donor-acceptor systems **5** and **6**. The corresponding target model for the asymmetric one showed smaller scaling factors, though, and, in result, smaller contribution for the formation of both CT states. But this is again a reasonable finding, as only one TPA unit contributes to the CT formations. By virtue of the results, photoexcitation values of 0.07 (S1), 0.04 (CT1), and 0.89 (CT2) for **5** and 0.11 (S1), 0.19 (CT1), and 0.70 (CT2) for **6** could be obtained. Noteworthy, since these molecular electron donor-acceptor systems exhibit a strong $TPA^{\delta+}$-$dicyanoaniline^{\delta-}$ ground state absorption, a direct excitation into the radical ion pair states CT1 and CT2 is reasonable.[245] Interestingly, temperature-dependent TRES measurements of **5** demonstrated an increase of the population of the S_1 state by a simultaneously decrease of the population value of CT2 state, while decreasing the temperature from 300 to 140 K.

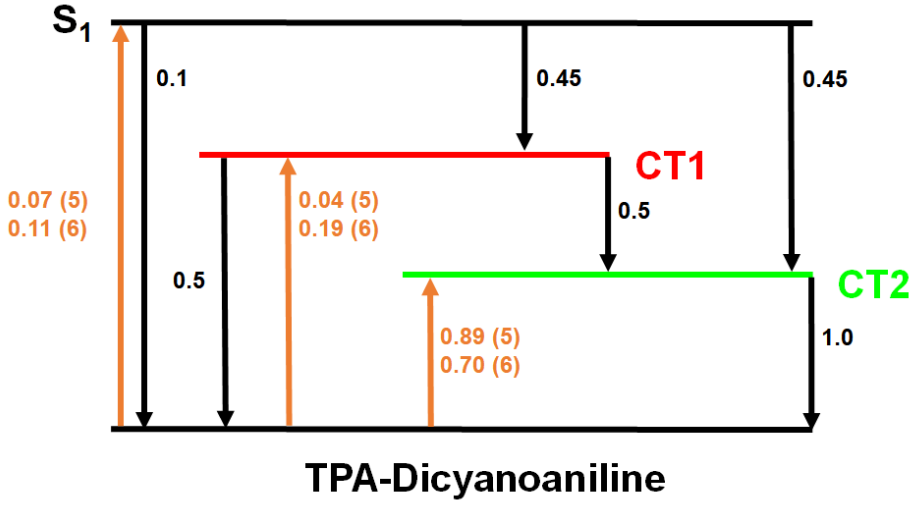

Fig. 4.8.: Target analysis model showing the photochemical events of **5** and **6** upon photoexcitation.

Additional to the photophysical values, thermodynamic results using Marcus theory (see also section **3.2**) could be determined. As a result, a reorganization energy of 1.96 eV and an electronic coupling of 1.9 cm^{-1} were determined.
To conclude, triphenylamine based dicyanoaniline systems demonstrated intriguing photophysical charge transfer properties making them interesting candidates for future opto-electronic applications like OLEDs and a potential alternative to rare metal based complexes in this field. As the investigated systems are, moreover, cost-effective due to their one-pot synthesis, high controllability, and easy fine-tuning and, in consequence, attractive carbon rich electron donor-acceptor based materials.

4.2 Supramolecular and Covalent Architectures for Solar Energy Conversion – From Principle to Application

4.2.1 Interfacing Tetrapyridyl-C_{60} with Porphyrin Dimers via π-Conjugated Bridges: Artifical Photosynthetic Systems with Ultrafast Charge Separation

- Christina Stangel,* Fabian Plass,* Asterios Charisiadis, Emmanouil Giannoudis, Georgios Charalambidis, Kostas Karikis, Georgios Rotas, Galateia E. Zervaki, Nektarios N. Lathiotakis, Nikos Tagmatarchis, Axel Kahnt, and Athanassios G. Coutsolelos, Interfacing Tetrapyridyl-C_{60} with Porphyrin Dimers via π-Conjugated Bridges: Artificial Photosynthetic Systems with Ultrafast Charge Separation, *Phys. Chem. Chem. Phys.* **2018**, *20*, 21269-21279

Besides the field of covalently linked systems, researchers turn their views nowadays to the development of molecular electron donor-acceptor systems based on supramolecular binding, mimicking bio-inspired artificial photosynthetic systems as described in section **3.1**. Therefore, the preparation of novel or optimized light harvesting antenna molecules, as well as the research on the nature and the impact of the bridge between electron donor and acceptor play a crucial role. Hence, the implementation of photosensitive groups leads to photoactive receptors as light-conversion and charge-separation centers. Moreover, redox-active polyolefinic chains act as electron transporting wires in membranes, while molecular self-

assemblies can result to complex double-helical structures using appropriate ligands.[248] This transfer of information and signal processing on a molecular level is inter alia defined by stacking and molecular recognition through binding.[248]

One problem, that has to be addressed, is the evolution of long-lived radical ion pairs with fast charge separation, which can be used in solar cells[249][250] or even as reaction centers in photocatalytic water splitting processes releasing H_2.[251][252] Artificial photosynthetic systems based on porphyrins as electron donors feature themselves with vast absorption coefficients, high synthetic flexibility, and photochemical stability (see also section **3.5**). In combination with fullerenes as electron acceptors, they are potent candidates. Moreover, fullerenes are very convenient electron acceptors due to their small reorganization energy in electron transfer reactions (see also section **3.6**). The additional implementation of especially π-conjugated spacers, such as oligo(p-phenylenevinylene) (oPPV), are, however, very beneficial, as they result in smaller electron transfer recombination rate constants, a strong electronic coupling, and also low attenuation factors.[253][254][255][256] Additionally, supramolecular electron donor-acceptor systems have the advantage of being "self-repairable" – no matter if in polymers or in solution.[257][258]

Despite a sheer endless manifesting number of publications dealing with the preparation and photophysical examination of self-assembled architectures mimicking the biological processes, there have been only a few donor–bridge–acceptor (D–B–A) systems, in which the electron donor–acceptor entities are connected through long π-conjugated phenyl bridges via supramolecular interactions.[259][260] Moreover, up to this date, a noticeable absence of multiple bound porphyrinoids on one fullerene exists in the literature and is only limited to two-fold systems.[261][262][263] However, their introduction would have exceptional advantages, though: On the one hand, as described in section **3.5** and section **3.6**, the possibility to push a higher electron charge density into the fullerene by the increased number of electron donors, as well as an enhanced association by using an appropriate key-lock binding motive improving the overall structural stability.

This promising approach has already been demonstrated using a two-fold system in combination with mono and dimeric zinc porphyrin units.[261] Consequently, the research group of Prof. Athanassios G. Coutsolelos expanded this approach and developed a novel four-fold fullerene based system containing one pyridyl ligand on each branch (see **Figure 4.9**).

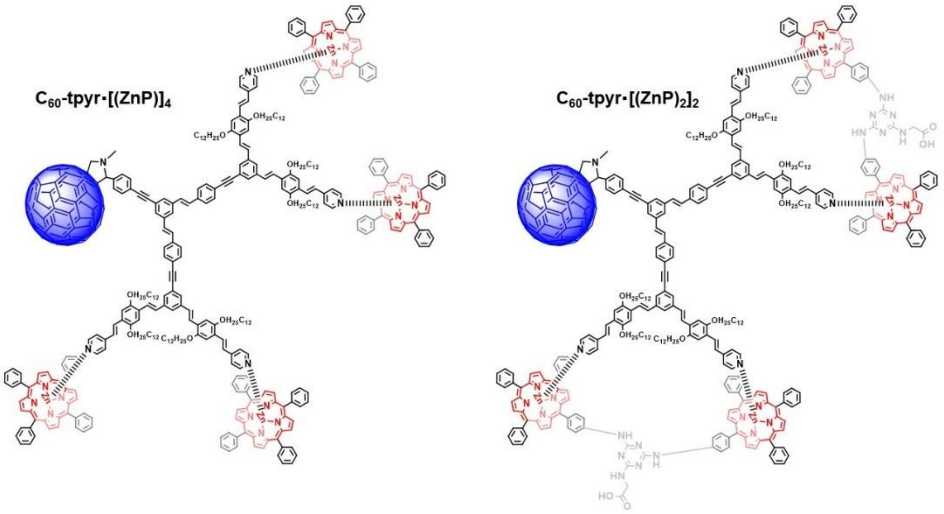

Fig. 4.9.: Illustrative structures of **C_{60}-tpyr·[(ZnP)]$_4$** and **C_{60}-tpyr·[(ZnP)$_2$]$_2$**. The fullerene and the porphyrin macrocycle are depicted in blue and red, respectively.

In this study, it could be demonstrated that using a supramolecular hybrid system consisting of an oPPE/oPPV functionalized C_{60} derivative with four pyridyl groups enables the formation of four metal-to-ligand coordinations. For **(ZnP)$_2$**, a 2:1 formation was confirmed by means of Job plot titration experiments and the binding constant with the electron-donating zinc porphyrin dimer was calculated to be 5 x 10^5 dm^3mol^{-1} in anisole matching perfectly the value that was previously reported in the literature.[261][262][263]
Femtosecond based transient absorption spectroscopy measurements and target analysis of the corresponding raw data using Glotaran[201] revealed, that after photoexcitation, the charge separated state is rapidly generated via electron transfer from the first singlet excited state of **(ZnP)$_2$** to C_{60}. Of particular importance is the formation of the charge separated state of **C_{60}-tpyr·[(ZnP)$_2$]$_2$** – within a few picoseconds and a lifetime of up to 2.4 ns in toluene, which is almost 40% longer compared to the previously reported dipyridyl model binding to one **(ZnP)$_2$**. This, in fact, shows again the promising concept of adding multiple binding motives harnessing electron donating units within a molecular electron donor-acceptor system. This promotes not only the charge separation process, but also supports longer-lived radical species and high association constants. Hence, this leads to an enhanced chemical stability of the overall supramolecular system.
Furthermore, by studying **C_{60}-tpyr** with four monomeric **ZnP**s, a smaller binding constant (9 x 10^3 dm^3mol^{-1}) was obtained, which resembles the values known in the literature.[264] Moreover, longer charge separation and

shorter charge recombination lifetimes of 105 ps and 1300 ps in anisole, respectively, compared to the corresponding supramolecular **C_{60}-tpyr·[(ZnP)$_2$]$_2$** system were determined.

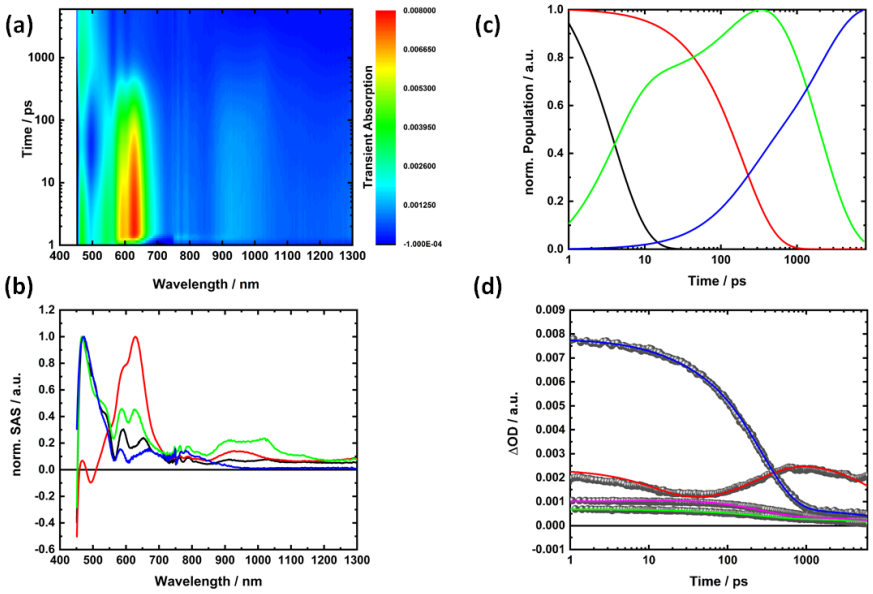

Fig. 4.10.: Transient absorption spectra obtained upon femtosecond laser flash photolysis (430 nm) of **C_{60}-tpyr** and **(ZnP)$_2$** in a 1:2 (5 x 10^{-6} and 1 x 10^{-5} M, respectively) mixture in anisole. **(a)** The data matrix analyzed by SVD analysis presents three different species, which relate to the first singlet excited state, the charge separated state, and the corresponding triplet excited state. **(b)** and **(c)** represent the normalized and fitted spectral and time species, respectively, while **(d)** shows exemplarily the corresponding kinetics containing the raw data points (grey circles) and the corresponding fits at 460 (red), 627 (blue), 850 (green), and 1003 nm (magenta) obtained by target analysis. Adapted for thesis publication.

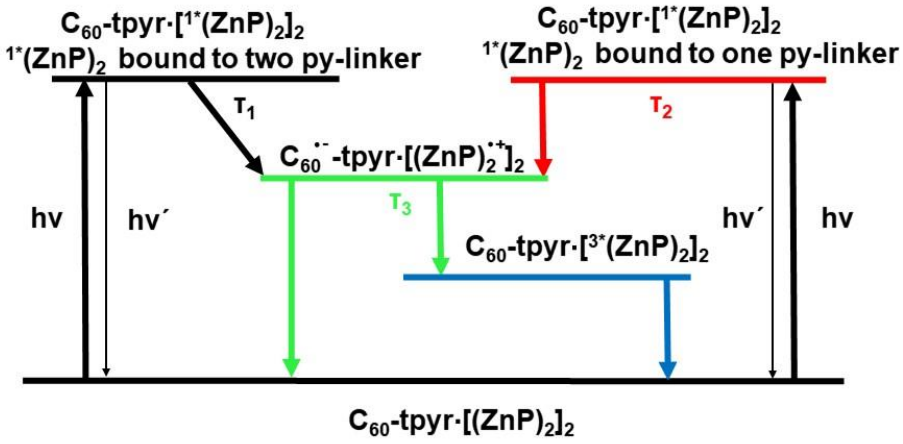

Fig. 4.11.: Simplified energy-level diagram showing the photochemical events of **C_{60}-tpyr** and **(ZnP)$_2$**. The lifetime (τ) values are given in **Table 4.1**.

Table 4.1.: Transient absorption spectroscopy values upon photoexcitation at 430 nm using the target analysis model shown in **Figure 4.11**. As a result, two different first singlet excited state (S_1) lifetimes (τ_1 and τ_2) depending on the binding motif of **ZnP_2**, as well as the corresponding charge separated state lifetimes (τ_3), were identified. The triplet excited state of **C_{60}-tpyr·[(ZnP)$_2$]$_2$** resembles the triplet manifold of **ZnP_2** in shape and lifetime, which is in the microsecond regime.

Compound		toluene	anisole	chlorobenzene
C_{60}-tpyr·[(ZnP)$_2$]$_2$	τ_1 [ps]	5.0	3.6	2.8
	τ_2 [ps]	234	195	76
	τ_3 [ps]	2390	2050	1180

As a result, the favorable role of incorporating multiple binding sites containing dimeric porphyrins is emphasized by, firstly, the formation of ensembles with higher association constants and, secondly, by a fast forward and a slow backward electron transfer. In conclusion, such concept based on multiple bearing electron donor-bridge-acceptor systems can be a guidance or template for the design of even more promising next generation hybrid systems for solar-energy conversion.

4.2.2 Controlling the Charge Transfer Mechanism and Efficiency by Means of Different C_{70} Regioisomeric Adducts

- Fabian Plass, Daniil A. Lukyanov, Alexander S. Konev, Axel Kahnt, Konstantin Y. Amsharov, Alexander F. Khlebnikov, and Dirk M. Guldi, Controlling the Charge Transfer Mechanism and Efficiency by Means of Different C_{70} Regioisomeric Adducts, *Small Struct.* **2020**, *1*, 2000012

Exciton diffusion lengths are a bottleneck in organic solar cells. However, as described in section **3.6**, the use of fullerenes, especially in solar energy based architectures such as in molecular electron donor-acceptor systems, as well as in polymer-based solar cells, stands out. Within polymer systems, bulk heterojunction (BHJ) solar cells are not only the most commonly used, but also represent nowadays a kind of standard in organic photovoltaics.[265] The principle of BHJs is: Using blended electron donor and acceptor materials forming a bicontinuous interpenetrating pattern with large interfacial areas, in which the photogenerated excitons easily dissociate and are collected.[265]

The purpose of suitable electron donors and acceptors plays an important role in the development of sustainable solar energy conversion based systems. One of the most important parameter (see also section **3.7.1**) is undisputedly V_{OC}. Among them, it is classified as the energy difference between the HOMO of the donor and the LUMO level of the electron acceptor material.[266][267] However, simply enlarging the HOMO-LUMO gap, for example by lowering the HOMO level, is only partially promising, since this increases the optical bandgap and, thus, also the J_{SC} value, which in turn reduces the power energy conversion performance.[268] Yet, fullerene based materials provide besides deep level HOMOs, well matching LUMOs, and high hole-blocking properties.[265] Moreover, implementing fullerene bisadducts foster due to up-shifting the LUMO levels and, therefore, increase the V_{OC} and PCE value of the corresponding solar cell.[269][270][271]

Aside from that, the current existing synthetic procedures generate a mixture of regioisomers, especially in the case of bisadducts.[268][272] Nevertheless, the usage of regioisomeric fullerene adducts demonstrate a decent impact on the PCE values in organic photovoltaics. Hitherto, the main explanation is focusing on the existing structural and morphological differences of the corresponding regioisomers. As a matter of fact, morphology and, in

consequence, packing effects influencing the performance of solar cells are undeniable.[268][273][274]
However, there are more reasons to discover. Namely, the idea that is that fullerene based regioisomeric adducts may also affect the electron transfer processes within such systems is barely discussed. Consequently, the group of Prof. Alexander F. Khlebnikov synthesized a hitherto unpublished electron donor-acceptor system consisting of a covalently linked *meso*-tetraphenyl porphyrin and regioisomeric α- and β-C_{70} fullerenes. The use of C_{70} as an electron acceptor is particularly suitable for two reasons. On the one hand, C_{70} has been described and studied scarcer than C_{60}, and, on the other hand, a highly selective synthetic functionalization process using diethyl N-arylaziridine-2,3-dicarboxylates easily yield α- and β-C_{70}-fulleropyrrolidine adducts.[275] The system of an α- and β-regioisomeric fullerene-porphyrin molecular electron donor-acceptor system is demonstrated in the following figure.

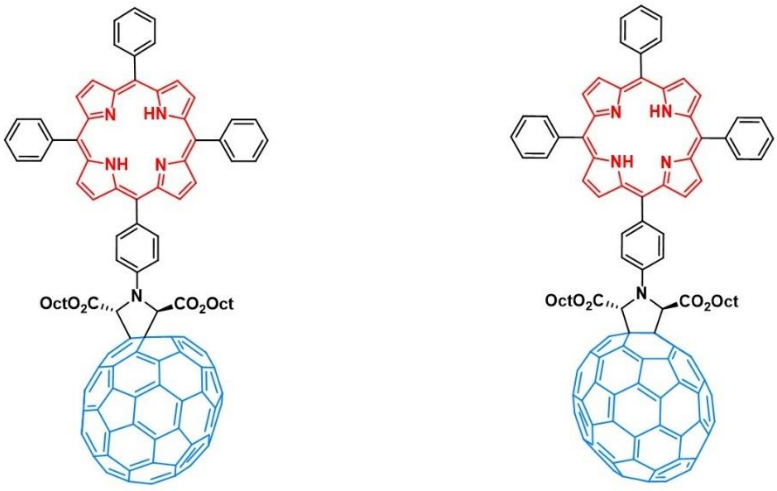

Fig. 4.12.: Schematic illustration of both C_{70}-fulleropyrrolidine regiosisomers, namely **8** (β-isomer) and **9** (α-isomeric adduct) containing a single *meso*-tetraphenyl porphyrin. The fullerene and the porphyrin are depicted in blue and red, respectively.

As a first step, steady-state absorption and emission spectroscopy measurements were conducted with the corresponding **H_2P** reference, a *meso*-tetraphenyl porphyrin, and three C_{70} fulleropyrrolidine systems, namely C_{70}-H, C_{70}-Br, and C_{70}-CH_3. Afterwards, the fullerene derivatives have been investigated with means of radiation chemical measurements, namely pulse radiolysis. As a result, information of the one-electron reduced state of C_{70},

as well as the reaction rate constants with $(CH_3)_2C^{\cdot}(OH)$ were gained. This radical is formed after radiation of a mixture of toluene/acetone/isopropanol (80/10/10 v/v/v) and is a strong reducing agent. The fingerprint spectrum of the C_{70} radical anion species is seen in **Figure 4.13**. The obtained spectra, fluorescence quantum yields and lifetimes, using time-resolved fluorescence lifetime measurements, namely TCSPC (time-correlated single photon counting), and transient absorption spectroscopy measurements of all references are in sound agreement with the literature, and are exemplarily shown in case of the **H_2P** reference in **Table 4.2**. The corresponding first singlet excited state lifetimes of the molecular electron donor-acceptor targets **8** and **9** show shorter lifetimes. Due to the limitation of the TCSPC setup, as its pulse width is ≤ 150 ps, the exact lifetimes could not fully revealed.

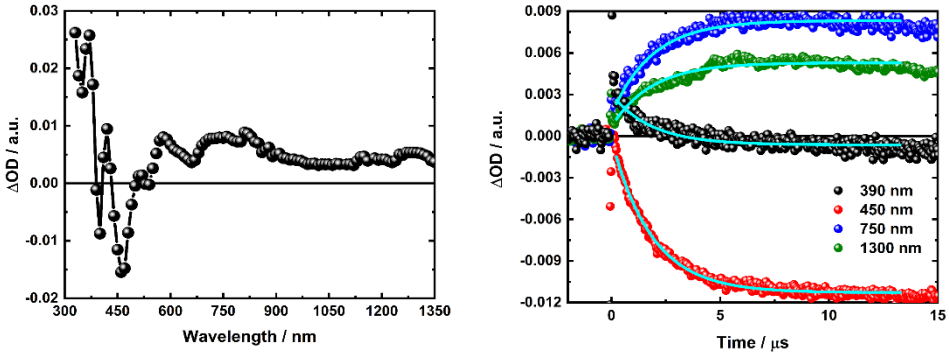

Fig. 4.13.: (Left) Pulse radiolysis spectrum of C_{70}-H in n a nitrogen saturated mixture of toluene, acetone, and isopropanol (8:1:1 v/v/v), 1.3 µs after the electron pulse and (right) the corresponding time absorption profiles at 390 (black), 450 (red), 750 (blue), and 1300 nm (olive circles) with the corresponding monoexponential global fit depicted in cyan. Adapted for thesis publication.

Table 4.2.: Fluorescence lifetimes and quantum yields in different solvents at 25°C. [a]Corresponding singlet excited state lifetimes using time-correlated single photon counting. [b]Fluorescence quantum yields determined by using a *meso*-tetraphenyl porphyrin reference.

Cmpd	Toluene		Anisole		THF		benzonitrile	
	τ_{Fl} [ns]	Φ_{Fl}	τ_{Fl} [ns]	Φ_{Fl}	τ_{Fl} [ns]	Φ_{Fl}	τ_{Fl} [ns]	Φ_{Fl}
H_2P[a]	9.77 ± 0.15	0.1028	10.74 ± 0.15	0.1160	10.49 ± 0.15	0.1033	10.67 ± 0.15	0.1165
8[ab]	< 0.150	0.0008	< 0.150	0.0015	< 0.150	0.0011	< 0.150	0.0013
9[ab]	< 0.150	0.0015	< 0.150	0.0016	< 0.150	0.0007	< 0.150	0.0009

However, both electron donor-acceptor systems display a strong fluorescence quenching up to 99% with respect to the porphyrin reference. This indicates an additional deactivation channel, either energy transfer or electron transfer. In fact, after performing the radiation chemical reduction of the fullerene references (see also subsection **3.8.1**) and conducting transient absorption spectroscopy measurements also on both electron donor-acceptor systems **8** and **9**, a charge transfer process yielding a charge separated state, was corroborated, as shown in **Figure 4.14** of **8** in toluene. Moreover, by means of radiation chemical measurements based on pulse radiolysis and, after an extensive photophysical investigation with both electron donor-acceptor systems in toluene, anisole, and THF, and a SVD analysis using a target analysis model, revealed the existence of three different species of which one displays the charge separated state. In fact, in benzonitrile, the triplet energy level of the *meso*-tetraphenyl porphyrin lies below the charge separated state and cannot be formed in contrast to the other solvents. Interestingly, an exceptional impact on the relative distribution and, in turn, charge transfer processes of regioisomeric systems was demonstrated.

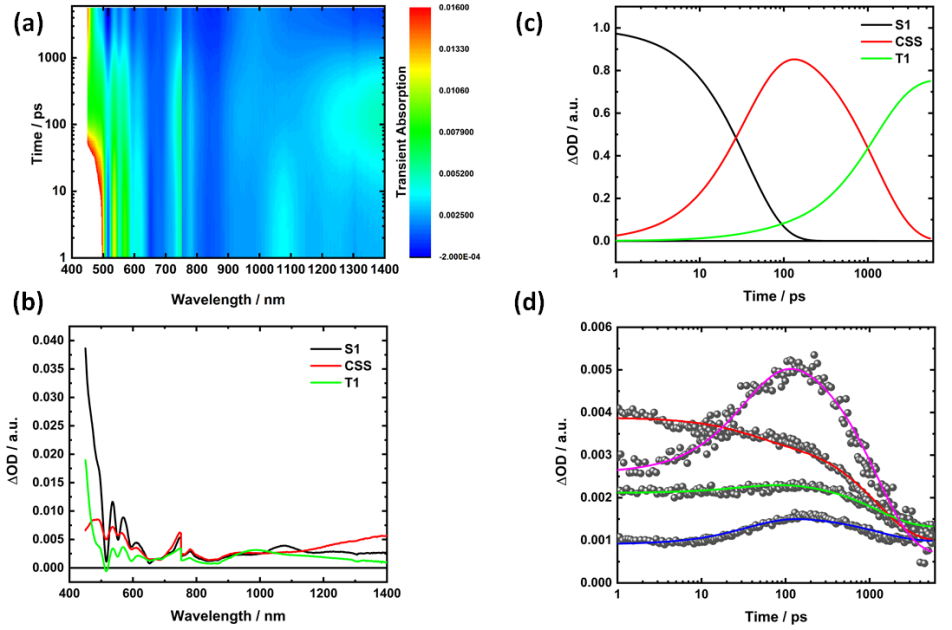

Fig. 4.14.: Transient absorption spectra obtained upon femtosecond laser flash photolysis (430 nm) of **8** in toluene. **(a)** The data matrix analyzed by SVD analysis presents three different species, which relate to the first singlet excited state, the charge separated state, and the corresponding triplet excited state. **(b)** and **(c)** represent the fitted spectral and time species, respectively, while **(d)** shows exemplarily the corresponding kinetics containing the raw data points (grey circles) and the corresponding fits at 592 (red), 650 (blue), 903 (green), and 1383 nm (magenta line) obtained by target analysis. Adapted for thesis publication.

Furthermore, **8** compared to **9** show significantly shorter charge separation lifetimes (49 ± 1 vs. 65 ± 2 ps, see for further detail **Table 4.3**), but similar charge recombination lifetimes (559 ± 11 vs. 571 ± 8 ps) in a solvent like anisole. As a consequence, β-regioisomeric fullerene adducts are prone to develop less triplet excited state as compared to α-adduct **9**, which makes sense by comparing the corresponding lifetimes and reaction rate constants, respectively.

This electronic effect of inducing different distributions of electron transfer processes in regioisomeric systems in fullerene based systems was up to this date hardly known and shows the importance of fullerene based studies, notwithstanding their numerous amount in literature. This interesting effect, which emphasizes the different charge transfer behavior of regioisomers independently from pack- or stacking effects. Notwithstanding **8**'s faster charge separation in anisole, the overall charge recombination lifetimes of α-adduct **9** are up to 1.5 fold enhanced. This effect can be explained, as the alpha adducts are more superior due to their unique electron

delocalization within the carbon cage of C_{70} made out of "corannulenoid" fragments relative to the equator region of fullerenes featuring extended "phenanthrenoid" rings.

Table 4.3.: First singlet excited state (S_1), charge separated state (CS), and first triplet excited state (T_1) lifetimes in different solvents at 25 °C. All transient absorption spectra were performed upon photoexcitation at 430 nm.

Compound		**H_2P**	**8**	**9**
toluene	S_1 [ps]	10487 ± 76	39 ± 2	48 ± 2
	CS [ps]	×	1203 ± 16	1160 ± 19
	T_1 [µs]	40.80 ± 0.72	23.22 ± 0.51	1.23 ± 0.06
anisole	S_1 [ps]	11229 ± 113	49 ± 1	65 ± 2
	CS [ps]	×	559 ± 11	571 ± 8
	T_1 [µs]	18.90 ± 0.29	4.09 ± 0.11	9.68 ± 0.27
THF	S_1 [ps]	11230 ± 103	11 ± 1	12 ± 1
	CS [ps]	×	138 ± 2	195 ± 3
	T_1 [µs]	13.80 ± 0.32	12.80 ± 0.39	20.80 ± 0.43
benzonitrile	S_1 [ps]	10800 ± 93	10 ± 1	14 ± 1
	CS [ps]	×	125 ± 3	136 ± 4
	T_1 [µs]	48.90 ± 0.85	×	×

Hence, we demonstrated that the use of regioisomeric fullerene adducts has a significant impact on the charge transfer processes. Moreover, the implementation of C_{70} α-adducts is more promising in future solar energy conversion systems with respect to the superior electron delocalization compared to β-adducts. From this point of view, the possible control- and tunability using not only solvents with different polarity, but also viscosity, represents an intriguing option for future bio-mimicking and sustainable molecular electron donor-acceptor based solar cell systems. Moreover, the implementation of different fullerene regioisomeric adducts is an interesting direction towards the control of the distribution of states in advanced electron donor-acceptor systems.

4.2.3 Effect of the Triazole Ring in Zinc Porphyrin-Fullerene Dyads on the Charge Transfer Processes in NiO-Based Devices

- Vasilis Nikolaou,* Fabian Plass,* Aurélien Planchat, Asterios Charisiadis, Georgios Charalambidis, Panagiotis A. Angaridis, Axel Kahnt, Fabrice Odobel, and Athanassios G. Coutsolelos, Effect of the Triazole Ring in Zinc Porphyrin-Fullerene Dyads on the Charge Transfer Processes in NiO-Based Devices, *Phys. Chem. Chem. Phys.* **2018**, *20*, 24477-24489

The implementation of novel types of molecular electron donor-acceptor systems in the field of opto-electronical devices, just like organic light emitting diodes (OLEDs) and photovoltaic cells, is of tremendous importance. Probably it is THE key factor to tackle climate change, as the biggest obstacle of the 21st century for humankind. Nevertheless, to hold our gained prosperity and not to risk any employments, we have to develop and optimize environmentally friendly technologies such as photovoltaic systems, which are capable of sufficiently converting solar energy into electricity and solar fuels.[276][277][278] Hence, the preparation of new photo- and electroactive conjugates (see also section **4.1** and **4.2**) remains of particular relevance, especially in the case of molecular organic solar cells, which evince already high carrier collection efficiencies or power conversion efficiencies[279] of non-fullerene based systems of around thirteen percent.[280]
Moreover, a big advantage of covalently linked systems is the possible introduction of π-bridges or spacers, as efficient electron funnels, between donor and acceptor. The influence of its nature is of great significance for maintaining long-lived charge separated states and, therefore, an efficient conversion of photons into usable electrical or storable energy like solar fuels (see also section **4.3**). Besides the research of photoelectrochemical devices based on n-type semiconductor materials like TiO_2 or ZnO, there is also the opportunity to use p-type solar cells.
In this context (see also subsection **4.2.3**), nickel oxide (NiO) is one of the most commonly used p-semiconductors for both – dye-sensitized photoelectrochemical cells[281][282][283][284] and dye-sensitized solar cells (p-DSSCs).[285][286][287] The best performing NiO based p-DSSC was recently published by Perera *et al.*, which exhibited an overall power conversion efficiency of 2.51%.[288] DSSCs based on porphyrinic compounds have already been extensively studied and achieved exceptional performances in n-type solar cells up to almost 13%. Yet, p-type solar cells using these

systems as sensitizer are disappointingly inefficient. One main reason is the ultrafast charge recombination in p-DSSCs limiting the photocurrent density and the voltage delivered by the solar cell.[288][289][290][291]
In this study, three different modified new zinc porphyrin-fullerenes, namely **C_{60}ZnP**, **C_{60}*tr*ZnP**, and **C_{60}*tr*ZnP*tr*** were reported. The idea was, that in the presence of a secondary electron acceptor, the fast charge recombination process could be diminished and, therefore, increasing the efficiency of the poor performing sensitizer.[286][292][293][294] These conjugates are composed of zinc porphyrin (ZnP) containing a benzoic acid anchoring group immobilizing it on the NiO film and additionally linked to C_{60}. Thus, to determine the effect of distance and optimal combination a triazole bridge was inserted as a spacer between ZnP, the fullerene, and the anchor, which should enhance and improve any charge transfer.[295][296][297]

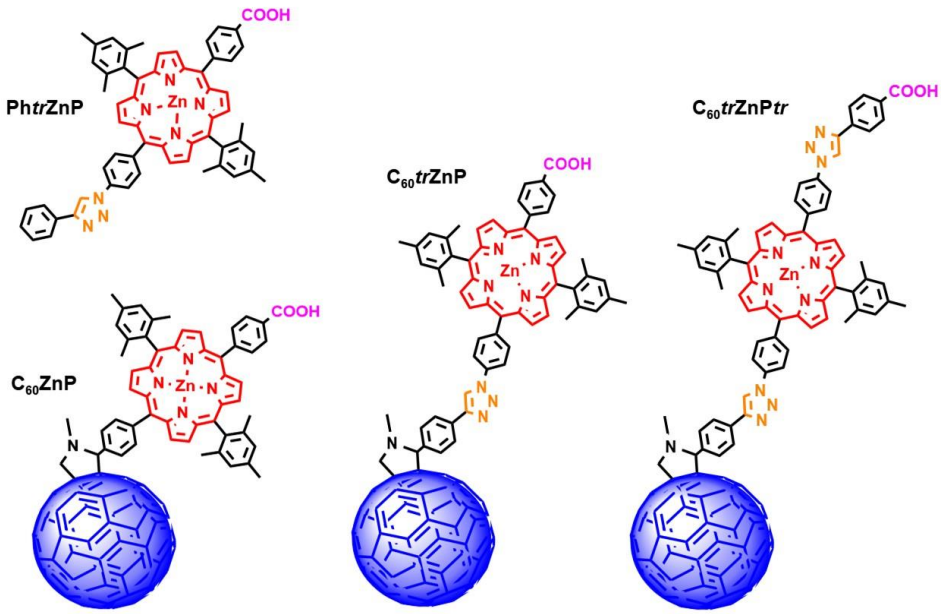

Fig. 4.15.: Schematic structure of the investigated carboxylic acid zinc porphyrin and zinc porphyrin-C_{60} systems. Zinc porphyrin and fullerene are depicted in red and blue, respectively, the triazole ring and the carboxylic acid end group in orange and pink, respectively.

Hence, it shows not only an up to 5.5 fold higher V_{OC}, but also a threefold higher J_{SC}. However, the photoelectrochemical measurements (see **Table 4.4**) induce, that the implementation of two triazoles shows no distinct improvement. This might be surprising, as one can believe that the introduction of a longer spacer between the electron donor and the acceptor leads to a better charge delocalization and, in consequence, an enhanced performance of the solar cell. But it has, in fact, a reason, why this is not the case for **C_{60}*tr*ZnP*tr***: the distance/morphology.
In fact, theoretical calculations showed that the morphology of the electron donor-acceptor systems **C_{60}*tr*ZnP*tr*** and **C_{60}*tr*ZnP** is quiet different, as **C_{60}*tr*ZnP*tr*** tend to bent towards the NiO surface, which actually minimizes the real distance, between NiO and the electron donor-acceptor system. This is also the reason for larger J_{SC}, especially compared to different electron donor-acceptor systems (see **Table 4.4**), due to the introduced charge transfer resistance with the electrolyte.[298] Which in fact demonstrates that a larger distance is favorable, but not in case of the triazole rings, as it reduces the desired space due its interaction with NiO.
Nevertheless, photovoltaic measurements revealed that the power conversion efficiencies were more than three times higher compared to the **Ph*tr*ZnP**@NiO reference system. This confirms the impact of electron donor-acceptor systems in the opto-electronical devices like solar cells or photoelectrochemical cells.

Table 4.4.: Photoelectrochemical metrics (within 3 different cells) of p-DSSCs sensitized with porphyrins and employing either the iodide/ triiodide or the cobalt electrolyte recorded under AM 1.5G simulated sunlight (1000 W m^{-2}). V_{OC} = open circuit voltage, J_{SC} = short circuit current density, FF = fill factor, and PCE = $V_{OC} \cdot J_{SC} \cdot FF$ / power(light), [a,b]Data adapted from reference[299] and reference,[300] respectively.

Dye	Electrolyte	J_{SC} [mA cm^{-2}]	V_{OC} [mV]	FF [%]	PCE [%]
C_{60}*tr*ZnP	I_3^-/I^-	1.86 ± 0.10	109 ± 3	37 ± 0.5	0.076 ± 0.0040
	$Co^{III/II}$	0.63 ± 0.03	244 ± 6	35 ± 0.1	0.054 ± 0.0040
C_{60}*tr*ZnP*tr*	I_3^-/I^-	1.82 ± 0.04	84 ± 5	33 ± 1	0.050 ± 0.0020
	$Co^{III/II}$	0.76 ± 0.05	269 ± 14	36 ± 1	0.074 ± 0.0010
C_{60}ZnP	I_3^-/I^-	1.68 ± 0.10	103 ± 10	37 ± 1	0.063 ± 0.0010
	$Co^{III/II}$	0.71 ± 0.02	175 ± 10	28 ± 0.1	0.035 ± 0.0030
Ph*tr*ZnP	I_3^-/I^-	0.69 ± 0.03	68 ± 5	33 ± 0.2	0.015 ± 0.0010
	$Co^{III/II}$	0.22 ± 0.01	48 ± 10	24 ± 1	0.002 ± 0.0006
ZnP-NDI[a]	I_3^-/I^-	1.38	127	32	0.056
	$Co^{III/II}$	0.50	195	31	0.090
ZnP-PyC_{60}[b]	I_3^-/I^-	1.50	158	38	0.090
	$Co^{III/II}$	1.50	260	35	0.130

Additional to the investigation of the carboxylic acid containing systems, photophysical measurements – steady-state and time-resolved – on the carboxylic acid ester systems have been conducted and showed in solution the formation of a charge separated state with lifetimes up to 2.6 ns. However, the mechanism of the carboxylic acid systems immobilized on NiO is rather complex, see **Figure 4.16**.

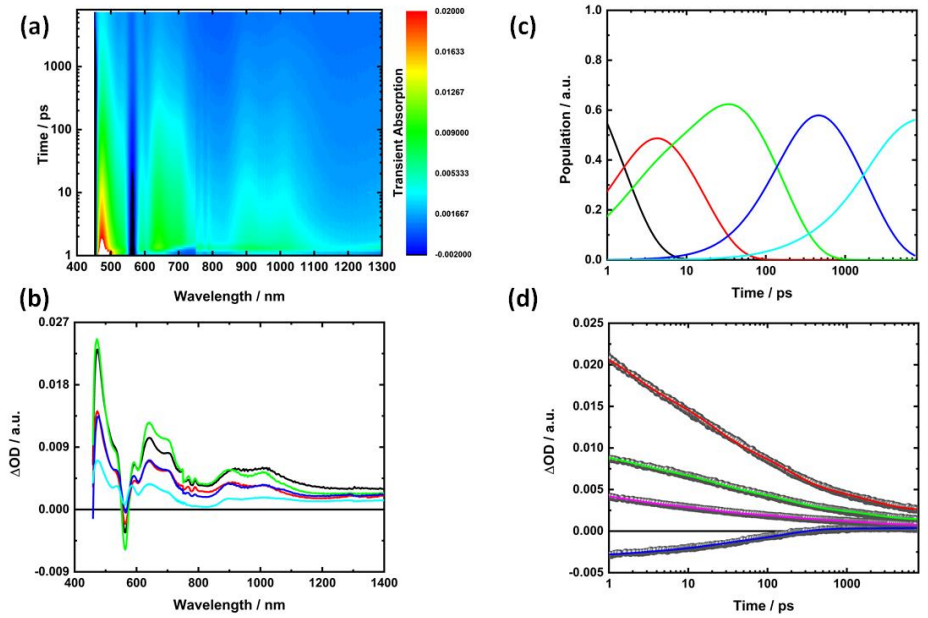

Fig. 4.16.: Transient absorption spectra obtained upon femtosecond laser flash photolysis (430 nm) of **C_{60}*tr*ZnP** on NiO. **(a)** The data matrix analyzed by SVD analysis presents five species, which were assigned to NiO-^{1*}ZnP–C_{60} (black), NiO^{+}-ZnP$^{\bullet-}$-C_{60} (red), NiO-ZnP$^{\bullet+}$-$C_{60}^{\bullet-}$ (green), (NiO–ZnP)$_{(h+,VB)}^{+}$-$C_{60}^{\bullet-}$ (blue), and a fifth species (cyan line), which could be revealed as a combined feature of (NiO-ZnP)$_{(h+,TR)}^{+}$-$C_{60}^{\bullet-}$ and NiO-^{3*}ZnP-C_{60}, respectively. **(b)** and **(c)** represent the corresponding fitted spectral and time species, while **(d)** shows the corresponding kinetics containing the raw data points (grey circles) and the corresponding fits at 460 (red), 560 (blue), 640 (green), and 1010 nm (magenta line) using target analysis. Adapted for thesis publication.

Upon photoexcitation at 430 nm the singular value decomposition (SVD) analysis of the transient absorption raw data using Glotaran[201] disclosed the presence of five individual species, which were assigned to be NiO-^{1*}ZnP–C_{60}, NiO^{+}-ZnP$^{\bullet-}$-C_{60}, NiO-ZnP$^{\bullet+}$-$C_{60}^{\bullet-}$, (NiO–ZnP)$_{(h+,VB)}^{+}$-$C_{60}^{\bullet-}$, (NiO-ZnP)$_{(h+,TR)}^{+}$-$C_{60}^{\bullet-}$, and NiO-^{3*}ZnP-C_{60}.[291][294][301][302][303]
Furthermore, nanosecond based transient absorption spectroscopy measurements revealed three species. Here, the first one can be described as the sum of the previous four species and the last two ones are assigned to (NiO-ZnP)$_{(h+,TR)}^{+}$-$C_{60}^{\bullet-}$, and NiO-^{3*}ZnP-C_{60}, while the first one is the charge separated state between a NiO hole residing in a trapped state and an electron in the fullerene. According to the literature,[302] this trapped hole is related to a Ni^{4+} signal with unique features at 380, 400, and 430 nm and lifetimes, which are in sound agreement with those reported by Hammarström and co-workers.[302][303]

As a consequence, a highly complex kinetic model for the process was obtained matching the lifetimes and characteristics, which were reported earlier.[291][294][301][302][303] The remarkable finding is that, the rate constants found in all three dyads are similar to each other, except for the rate constants for the recombination of NiO^{+}-$ZnP^{\bullet-}$-C_{60} back to the ground state (k_8). Remarkably, the values of k_8 show that the linkage between ZnP and NiO lead to an enhanced lifetime of the corresponding charge separated state due to the larger separation between $ZnP^{\bullet-}$ and NiO^{+}.

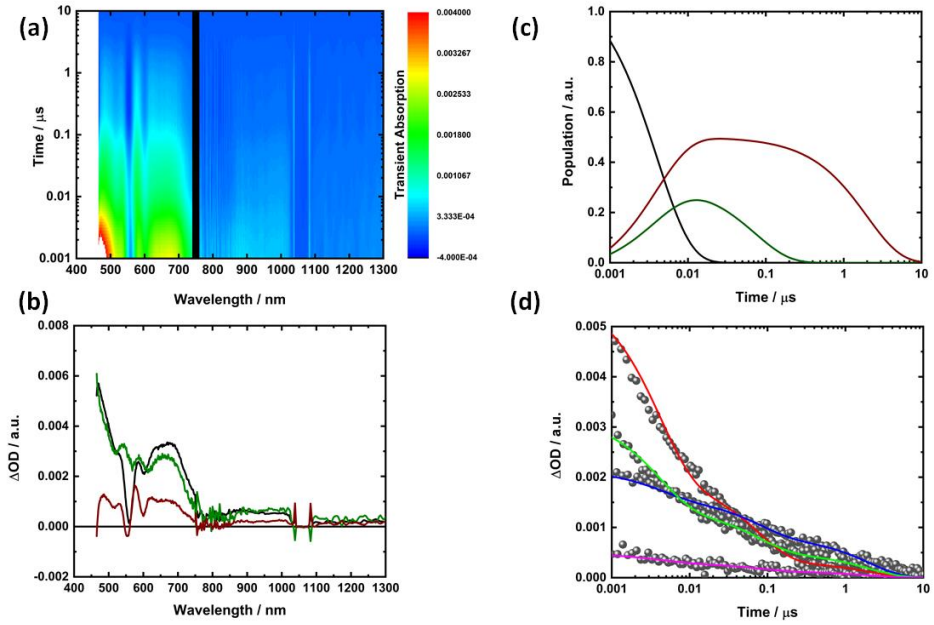

Fig. 4.17.: Transient absorption spectra obtained upon femtosecond laser flash photolysis (430 nm) of **C_{60}*tr*ZnP** on NiO. **(a)** The data matrix analyzed by SVD analysis presents three species, which were assigned to four combined states (black) obtained from femtosecond transient absorption spectroscopy measurements (see **Figure 4.16**), the $(NiO\text{-}ZnP)_{(h+,\ TR)}{}^{+}$-$C_{60}{}^{\bullet-}$ (olive) and $NiO\text{-}{}^{3*}ZnP\text{-}C_{60}$ state (brown line), respectively, while **(b)** and **(c)** represent the corresponding fitted spectral and time species, while **(d)** shows the corresponding kinetics containing the raw data points (grey circles) and the corresponding fits at 470 (red), 577 (blue), 640 (green), and 1010 nm (magenta line). Adapted for thesis publication.

These findings are in perfect agreement with the performed photovoltaic studies. Interestingly, compared to the results obtained by transient absorption spectroscopy, the triazole linker exhibits only a marginal effect on the charge separation and recombination. A feasible explanation is that the fullerene attaches towards the NiO and the electron from the corresponding radical anion is formed via a through-space electron transfer mechanism, as well as the surface coverage by the dyes. In summary, the influence of the triazole ring in this particular system is rather limited and demonstrates that the implementation of especially nitrogen containing bridges on NiO surfaces might be less promising, as the charge separated state formation (with about 42 %) and the lifetimes in all systems show only slightly differences (see also **Table 4.5**).

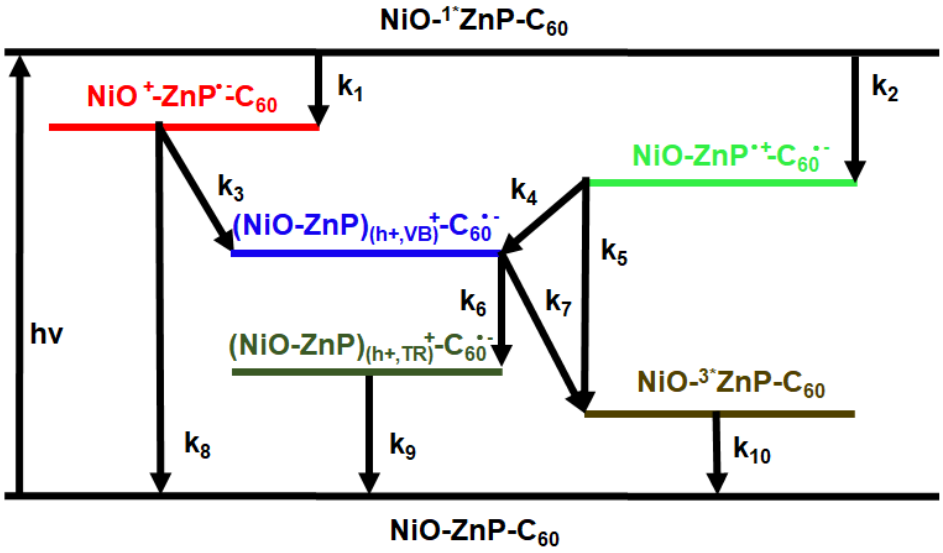

Fig. 4.18.: Energy Diagram for the excitation of **C_{60}*tr*ZnP**, **C_{60}*tr*ZnP*tr***, and **C_{60}ZnP** on NiO.

Table 4.5.: List of individual rate constants obtained from target analysis of the time evolution of transient absorption spectra for **C_{60}*tr*ZnP**@NiO, **C_{60}*tr*ZnP*tr*@NiO, and **C_{60}ZnP**@NiO according to the kinetic model depicted in **Figure 4.18**.

Rate Constant	**C_{60}*tr*ZnP**@NiO	**C_{60}*tr*ZnP*tr*@NiO**	**C_{60}ZnP**@NiO
k_1 [s^{-1}]	2.76 x 10^{11}	2.15 x 10^{11}	2.76 x 10^{11}
k_2 [s^{-1}]	1.65 x 10^{11}	1.65 x 10^{11}	1.22 x 10^{11}
k_3 [s^{-1}]	3.86 x 10^{10}	3.86 x 10^{10}	2.29 x 10^{10}
k_4 [s^{-1}]	4.35 x 10^{9}	4.74 x 10^{9}	5.49 x 10^{9}
k_5 [s^{-1}]	3.97 x 10^{8}	4.93 x 10^{8}	4.69 x 10^{8}
k_6 [s^{-1}]	7.34 x 10^{7}	9.01 x 10^{7}	8.47 x 10^{7}
k_7 [s^{-1}]	1.24 x 10^{8}	1.72 x 10^{8}	1.23 x 10^{8}
k_8 [s^{-1}]	2.01 x 10^{10}	6.44 x 10^{9}	2.01 x 10^{10}
k_9 [s^{-1}]	1.36 x 10^{7}	1.46 x 10^{7}	1.69 x 10^{7}
k_{10} [s^{-1}]	5.00 x 10^{5}	5.00 x 10^{5}	5.00 x 10^{5}

In summary, the issue stays, as the ultrafast charge recombination between the NiO surface and porphyrins plays a major problem for the corresponding overall efficiencies. In this study, photophysical measurements revealed that about 2/3 of the excitation energy leads to the formation of NiO^{+}-$ZnP^{\bullet-}$-C_{60} and only 1/3 to NiO-$ZnP^{\bullet+}$-$C_{60}^{\bullet-}$ as the initial charge transfer process. For the development of more efficient systems, the suppression of the formation of the NiO^{+}-$ZnP^{\bullet-}$-C_{60} is the bottleneck, while simultaneously the formation of NiO^{+}-ZnP-$C_{60}^{\bullet-}$ should be enhanced. In other words, decreasing the rate constants k_1 and k_8, while favoring the reaction pathways of k_2 and k_3. Furthermore, the presence of a highly efficient charge shift (k_4) has to be ensured. This detailed knowledge about the inner mechanistic pathways for NiO-ZnP-C_{60} systems will lead the way towards better performing p-DSSCs with the ultimate goal of establishing more sustainable materials for solar energy conversion.

4.3 Progress in Photocatalytic Water Splitting Using TiO_2 – The Rise of the Sustainable Hydrogen Economy

4.3.1 Long-Living Holes in Grey Anatase TiO_2 Enable Noble-Metal-Free and Sacrificial-Agent-Free Water Splitting

- Ning Liu,* Shiva Mohajernia,* Nhat T. Nguyen, Seyedsina Hejazi, Fabian Plass, Axel Kahnt, Tadahiro Yokosawa, Andres Osvet, Erdmann Spiecker, Dirk. M. Guldi, and Patrik Schmuki, Long-Living Holes in Grey Anatase TiO_2 Enable Noble-Metal-Free and Sacrificial-Agent-Free Water Splitting, *ChemSusChem* **2020**, *13*, 4937-4944

Despite all the advantages that are existing by using solar cells, especially their CO_2-free energy production, an one-sided focus on them is not very helpful. Instead, it is important to develop a "healthy" energy mix of different renewable energy sources such as wind, biomass, but also solar energy. In addition, the production of hydrogen and its use as an energy source is playing an increasingly important role. Thus, there is little hope for only pure electric cars in the future, which is partly due to the weight, manufacturing costs of the batteries, as well as their, at the moment, achievable ranges that are not yet competitive compared to conventional drive technology. For long-distance vehicles, such as trucks, ships and freight trains, a short stop at the power socket is, therefore, impossible. This is why a great interest in hydrogen-powered vehicles, so-called Hydrails, exists. Those have already made it to market. To mention here are Alstom's *Coradia iLint* (train), Toyota's *Mirai* (car), the *Viking Lady* (ocean-going cargo vessel) or the *HY4* (four-seater passenger aircraft). The development and optimization of existing systems for hydrogen production is of immense importance. In addition to electrolytic water splitting, the industrial core, which is, exemplarily, being promoted by the company group of Siemens, namely *Hydrogen Solutions*, photocatalytic water splitting is of great importance. Up to now, (see also subsection **3.7.2**) Titanium dioxide (TiO_2) is the standard semiconductor used in photocatalysis.[25][304] Besides TiO_2, a variety of semiconductor based photocatalysts with suitable band edges exist, showing only limited photocatalytic activity in the absence of sacrificial-agents.[305][306] Leading examples are binary oxides which split water in aqueous alkaline solutions and neutral water, like $K_4Nb_6O_{17}$[307] and

$Sr_2Ta_2O_7$.[308] However, the advantages of titania are obvious, as it is cheap and shows outstanding photocorrosion resistance.[25][179]
Nevertheless, decomposing water into stoichiometric amounts of H_2 and O_2, containing also a sufficient activity, is still challenging and their yields are, if any, moderate,[179][309] even, when using noble metal based co-catalysts in combination with TiO_2. The bottleneck lies in their slow charge transfer kinetics across the TiO_2/water interface. Consequently, optimization is required, as separating photogenerated charge carriers, as well as preventing recombination processes, are the keys. As described earlier, (see also subsection **3.7.2**) the hydrogenation process forming black titania nanoparticles extend their absorption capability from the visible region up to the NIR and is a milestone in photocatalysis, in particular. An exact and proper mechanism allowing the development of appropriate photocatalysts is needed, though, as well as an increase of efficiency. Moreover, as the use of noble metals as co-catalysts or other sacrificial-agents is rather expensive, the production and research of photocatalysts preventing their usage is consequently favorable.
An alternative candidate as co-catalyst with low overpotentials in the hydrogen generation process reducing protons is the more abundant metal nickel.[25][196] The hole-transfer process can be warranted by using sacrificial-agents like alcohols. Without using them, a complete water oxidation demands for photogenerated holes. This is problematical as, as described in section **3.1**, four electrons and protons are required to photogenerate oxygen, resulting in high overpotentials for titania.[310] As a competing process, H_2O_2 can be formed by just handling two electrons. In fact, the adsorbed hydroxyl units trap the photogenerated holes and form $^{\bullet}OH$ radicals, which then react to H_2O_2.[311] This hole trapping leads a priori to the reaction of the conduction band with its environment, an effect firstly described by Grätzel *et. al.*[309] using P25 titania and platinum as co-catalyst. This is nevertheless an unsustainable process.
As a consequence, the group of Prof. Patrik Schmuki, developed an utmost active "grey" anatase TiO_2 photocatalyst, after hydrogenation in the presence of nickel. The designation of grey instead of black anatase titania relates to its defect engineered process. Grey titania exhibits a specific defect center that, if present, can act in non-hydroxylated anatase as an intrinsic catalytical center for the hydrogen evolution. However, black titania demonstrates higher degree of hydroxylation and more paramagnetic Ti^{3+} states, which may act as recombination centers for charge carriers (see **Figure 4.19**).[312]
As a first step, the group of Prof. Patrik Schmuki optimized the hydrogenation conditions resulting in an one hour H_2 treatment at 500 °C. The use of

higher hydrogenation temperatures like 600 or 700 °C produces, on the one hand, darker forms and, on the other hand, less photocatalytically active ones.[191] In fact, this investigated new photocatalyst has a stunning performance concerning neutral water splitting. Here, the production of H_2 and H_2O_2 is possible without any noble metals or sacrificial-agents. Most importantly, a hydrogen evolution rate of ~700 $molh^{-1}g^{-1}$, resulting in a quantum conversion of about 2.3% upon photoexcitation at 325 nm, could be achieved. This is one of the highest values in this field. Moreover, the resulting Ni@grey anatase TiO_2 nanoparticles do not need noble metals or any sacrificial-agents to enable photoexcited holes to surface-oxidize water to peroxide, on one hand, and to transfer efficiently electrons to Ni on the other hand (see **Figure 4.19**).

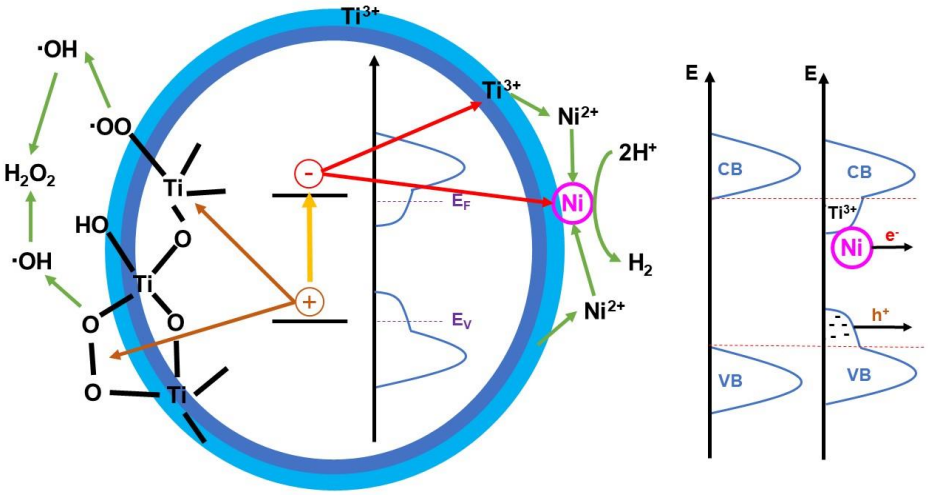

Fig. 4.19.: Photocatalytic generation of H_2 and H_2O_2 on Ni@grey anatase TiO_2 under illumination. Light absorption by Ni@grey anatase TiO_2 generates electrons and holes; electrons travel to the Ni-decorated surface and lead to proton reduction; holes are trapped on deep states (become long-lived) and, thus, enable water oxidation to H_2O_2. Adapted for thesis publication.

By virtue of its potential to render a substantial photocatalytic production of hydrogen, the photocatalyst showed, moreover, long-term stability over a time period of more than 100 h and several repetitions of 24 h intervals. Hence, the efficiency under AM 1.5 (100 mW/cm^2) illumination is remarkably higher than that ever reported for titania based catalysis in pure water.[309][313] Consequently, these findings by our cooperation partners stand out, and the question of its origin, and potentially its optimization potential, arose.

As a matter of fact, the hole transfer to water on the surface of anatase is largely suppressed. Reports regarding Ni on plain anatase for the use in water splitting are rather scarce.[310] The newly developed Ni@grey anatase TiO_2 catalyst is though different. In-situ femtosecond and nanosecond transient absorption measurements revealed the existence of free electron lifetimes in the range of picoseconds for anatase TiO_2, black anatase TiO_2, and Ni@grey anatase TiO_2. These results are in good agreement with the literature.[314]

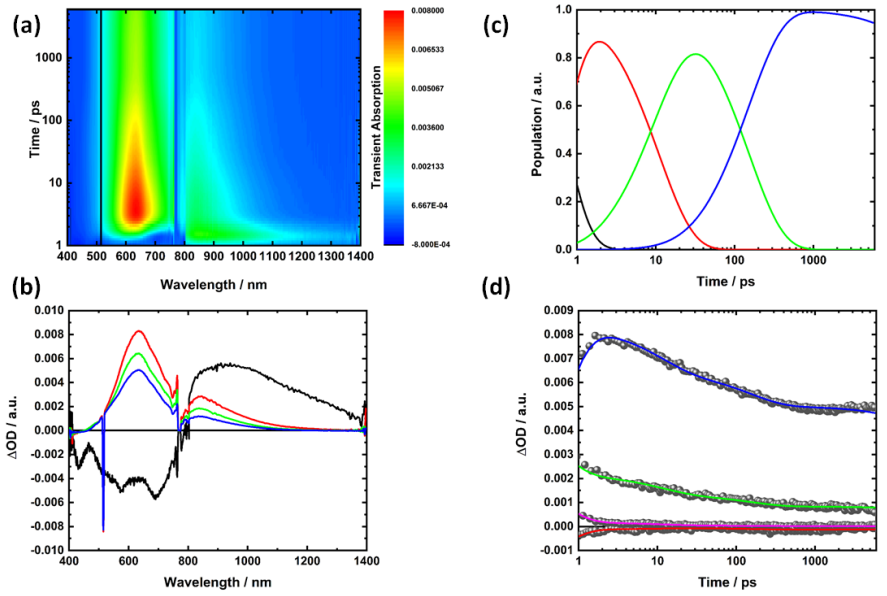

Fig. 4.20.: Transient absorption spectra obtained upon femtosecond laser flash photolysis (258 nm) of Ni@grey anatase TiO_2 in pure neutral water. **(a)** The data matrix analyzed by SVD analysis presents four different species which can be related to free electron processes, as well as longer-lived species (blue), which can be attributed to deep trap states using nanosecond transient absorption spectroscopy upon photoexcitation at 258 nm, being in sound agreement with the literature. **(b)** and **(c)** represent the fitted spectral and time species, respectively, while **(d)** shows exemplarily the corresponding kinetics containing the raw data points (grey circles) and the corresponding fits at 440 (red), 640 (blue), 900 (green), and 1200 nm (magenta line) obtained by global analysis. Adapted for thesis publication.

Moreover, nanosecond transient absorption measurements evince the existence of (trapped) holes with lifetimes ranging from nano- to microseconds (see **Figure 4.21**). These holes can be categorized, in particular, into two types of trap states: shallow ones with absorptions between 400 to 450 nm and deep traps in the range from 500 to 700 nm.[315] Taking a look at the

hydrogenated samples of TiO_2, remarkable differences with respect to the obtained lifetimes for the deep trap states could be revealed. By virtue of global fitting, relative to anatase titania, the deep trapped hole lifetimes increased from 64 ns (anatase TiO_2) to 820 ns (black anatase titania) up to remarkable fifteen microseconds for Ni@grey anatase TiO_2 (see **Table 4.6**). As a result, the existence of long-lived deep level traps may be of particular importance and, moreover, its optimization may have enormous impact, not only on the conduction, but also on the valence band. However, it promotes a better electron transfer.[315][316] Moreover, it demonstrates very different state distributions of valence or deep trap states of the analyzed white (plain titania), black (hydrogenated titania), and grey titania tailoring the bandgap of titania, as described in subsection **3.7.2**.[179][312][316]

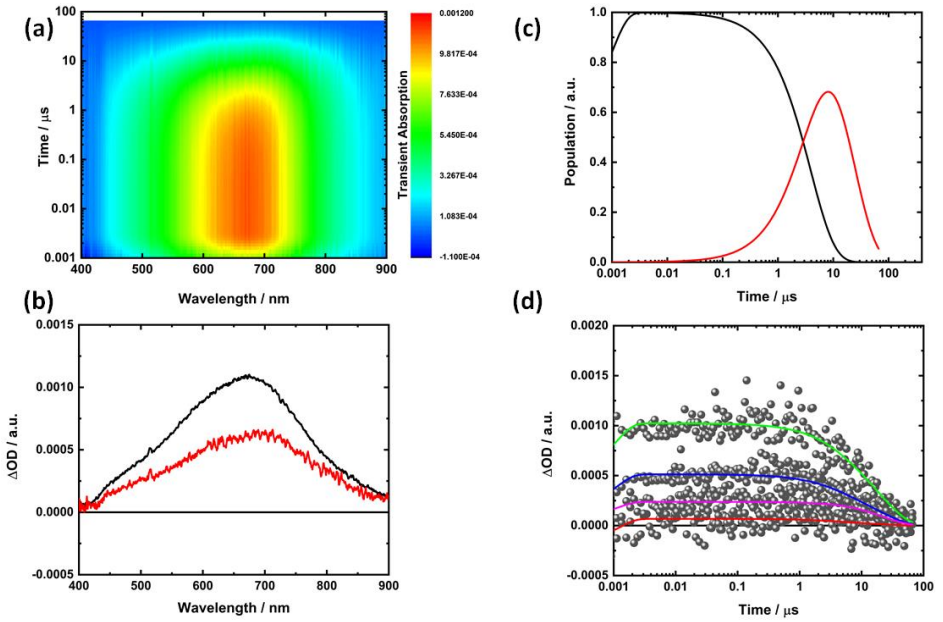

Fig. 4.21.: Transient absorption spectra obtained upon nanosecond laser flash photolysis (258 nm) of Ni@grey anatase TiO_2 in pure neutral water. **(a)** The data matrix analyzed by SVD analysis presents two different species which are related to deep trapped hole states. **(b)** and **(c)** represent the spectral and time species, respectively, while **(d)** shows exemplarily the corresponding kinetics containing the raw data points (grey circles) and the corresponding fits at 411 (red), 525 (blue), 700 (green), and 850 nm (magenta line) obtained by global analysis. Adapted for thesis publication.

Table 4.6.: Transient absorption spectroscopy data of anatase, black anatase, and Ni@grey anatase TiO_2 in pure neutral water upon photoexcitation at 258 nm using global analysis.

Suspension in H_2O					
Compounds	τ_1 [ps]	τ_2 [ps]	τ_3 [ps]	τ_4 [ns]	τ_5 [ns]
Anatase	0.92	15.4	283	5.8	64.3
Black anatase	0.87	6.4	170	14	820
Ni@grey anatase TiO_2	0.45	11	153	3210	14830

Exemplarily, the valence band maximum is shifted by about 0.5-0.7 eV towards the vacuum level compared to the VB of anatase titania.[179][312] The shift in fully black anatase is even three fold larger than that.[317] This dramatic shift in grey anatase nanoparticle is also in line with recent DFT calculations for hydrogenated materials.[179][317]

Only those samples, which feature Ni, give rise to the substantial differences in lifetimes. For partially oxidized samples of Ni@grey anatase TiO_2, not only the lifetimes, but also the hydrogen evolution efficiencies become comparable to those obtained for anatase TiO_2 or black anatase TiO_2. In the case of Ni@grey anatase TiO_2, the drastically enhanced hole lifetime goes hand-in-hand with a strong increase in H_2O_2 formation. No appreciable O_2 formation was, however, detected in any of the experiments. In other words, water splitting by this photocatalyst proceeds via a two-electron process to form H_2 and H_2O_2. However, past findings on the two-electron reactions using TiO_2 showed in addition to free H_2O_2 also a considerable amount of surface-bound oxygen species in terms of –Ti-O-O-Ti-.[309]

In summary, our findings confirm the notion of a valence band tailoring (or deep trapping states) in grey titania. Energetically, these holes are in optimal position to be transferred to cause water oxidation, forming H_2O_2 exhibiting remarkable long lifetimes. For Ni@grey anatase, photoluminescence measurements also showed a substantial photoluminescence quenching and, in return, eliminates radiative recombinations of valence band carriers with deep-trapped holes. A key feature of this Ni@grey TiO_2 catalyst is, that Ni in its metallic state (as a maximum efficient co-catalyst for H_2 production) is formed and stabilized by UV illumination. The reason is again the consequence of the excellent hole trapping features of grey titania.

As a summary, key to its high efficiency is, on one hand, a drastically enhanced lifetime of photogenerated holes in Ni@grey anatase TiO_2, which, in turn, enables efficient peroxide formation via a two-electron pathway and, on the other hand, the metallic state of Ni is photo-stabilized and acts as a stable electron transfer mediator for the hydrogen reduction reaction. In conclusion, these findings can be an intriguing option for a better understanding teamed up with better performance in the field of titania based photocatalysis.

5 Conclusion

The projects presented in this thesis provide a broad and new perspective on the development, analysis, and optimization of solar energy conversion based systems on a molecular, as well as nanostructured, basis in solution and in the solid state. Starting with the fundamental characterization of new carbon rich materials (see section **4.1**), over the influence of supramolecular and covalent architectures on a fundamental basis, the implementation, and optimization in devices (see section **4.2**), to the improvement of photocatalytic and photonmanaging processes for the sustainable production of solar fuels, such as hydrogen and hydrogen peroxide (see section **4.3**). In its entirety, the interplay of targeted molecular design, state-of-the-art spectroscopic, and radiation chemical measurement methods provided the basis for the elucidation of the complex interrelationships, especially in the development of modern and economical-friendly electron donor-acceptor systems.

This necessary development requires, however, the research and understanding of novel photoactive systems, which is described in the first part of this thesis. In the first project, in which the compound class of 2,6-dicyanoanilines together with triphenylamines as electron donors, exceptionally high photoluminescence quantum yields originating from charge transfer emission were found. Their strong emission makes them interesting and possible alternatives in future applications like OLEDs. Moreover, electron donor-acceptor systems with such strong emissive properties are quite unusual in literature up to this date. Not only the exact photophysical mechanism could be demonstrated, but also tunable optimization potential that especially is derived by the introduction of appropriate solvents. As a matter of fact, a huge variety of solvents was investigated resulting in emission colors ranging from blue to red of the optical spectrum. The obtained lifetimes have been corroborated with complementary time-resolved photoluminescence and transient absorption spectroscopy measurements. Moreover, it could be photophysically demonstrated, together with theory, that two possible spatial forms of the molecular electron donor-acceptor systems are existing. These lead to two distinguishable CT states. Using complementary temperature dependent time-resolved photoluminescence and transient absorption spectroscopy techniques, a full-fledged image at RT and low temperatures could be drawn. Exemplarily for **5**, photoexcitation values of 0.07 (S_1), 0.04 (CT_1), and 0.89 (CT_2) could be determined and completely attributed also on a theoretical basis.

Moreover, it could be shown that the introduction of multiple electron donor units can influence and, in consequence, tune the distribution of each involved state. Additionally, thermodynamic values using Marcus Theory could be derived, exemplarily **5** demonstrated a reorganization energy of 1.96 eV, a value which is up to eight-fold higher than in the case of fullerenes.

The next project dealt with the investigation of new supramolecular electron donor-acceptor based systems. Here, together with the group of Prof. Athanassios G. Coutsolelos, a self-assembled molecular electron donor-bridge-acceptor system containing π-conjugated spacers, such as oligo(pphenylenevinylene) (oPPV) together with four pyridyl endgroups, was investigated in combination with mono and dimeric zinc porphyrins. Together with titration based absorption and transient absorption spectroscopy measurements, strong binding constants in the range of several hundred thousand could be determined, which are in sound agreement with known literature values. Moreover and of particular importance, it could be demonstrated that the introduction of multiple binding motives can have an enormous positive impact on, not only the binding strength, but also on the charge transfer lifetimes enabling a faster charge separation process, too. Here, it could be demonstrated that the system containing four pyridyl-ligands elongates the lifetimes up to 40% to a similar fullerene bridged zinc porphyrin system with only two binding motives. Together with target analysis of the corresponding transient absorption spectroscopy raw data, a precise model was derived. As a result, the approach of multiple bearing electron donor-bridge-acceptor systems is highly intriguing. The further development of such next generation hybrid systems is, therefore, very promising. The discussed results are a guideline for the design of even more sustainable ones.

One of the most discussed and investigated systems in terms of electron donor-acceptor systems containing fullerenes, are dyads including C_{60}. The research of higher fullerenes is, in consequence, less present, but needs to be addressed. Another interesting aspect is the electronic and photophysical behavior of regioisomeric fullerene systems in combination with porphyrins as electron donors. As a result, together with the group of Prof. Alexander F. Khlebnikov, two C_{70} regioisomers have been synthesized, including an α- and a β-fullerene, in combination with *meso*-tetraphenyl porphyrin as electron donor. As a first step, all reference molecules, namely *meso*-tetraphenyl porphyrin and three different C_{70} derivatives have been measured. Here, steady-state absorption and emission spectroscopy

measurements, time-resolved fluorescence and transient absorption spectroscopy measurements came into play. In the case of the three fullerene samples, also radiation chemical measurements, namely pulse radiolysis, have been conducted to obtain insights into the one-electron reduced state of C_{70}. This information was highly important to corroborate the occurring electron transfer from the porphyrin to the fullerene in the corresponding electron donor-acceptor systems. Afterwards, these systems have been investigated intensively and, together with the multi-wavelength analysis tool Glotaran, very interesting insights were gathered. Both dyads exhibit a charge separated state in a variety of solvents also with different viscosity, but show different electronic behavior. As a matter of fact, the α-regioisomeric system is much more superior as the electron delocalization within the carbon caps of fullerenes are made out of "corannulenoid" fragments relative to the equator region of fullerenes featuring extended "phenanthrenoid" rings. This can be demonstrated taking a look on the lifetimes, which are up to 1.5 fold higher in case of the α-regioisomer in contrast to the β-regioisomer, but show faster charge separation processes in viscous solvents. But this is not the only interesting aspect, one can obtain from this template system. Hence, significant regioisomeric differences in the charge recombination kinetics are distinguishable. Here, the α-regioisomer shows an enhanced formation of triplet excited state of the porphyrin after recombining from its charge separated step in relation to its β-brother. These findings are actually highly interesting, as regiosiomeric fullerenes implemented in bulk heterojunction solar cells exhibit substantial performance differences. Those are mainly explained due to packing effects, but an additional explanation could be their dissimilar electronic behavior as well. The introduction of electron donating porphyrins or phthalocyanines into C_{70}-based solar cells may demonstrate not only differences in the power conversion efficiency due to morphological effects, but also derived from their electronic distribution originating from their charge separated state. As a consequence, the implementation of different fullerene regioisomeric adducts can be an attractive direction to control and tune the distribution of states in advanced electron donor-acceptor systems, not only in solution, but also in the solid state.

The corresponding chapter revisited the implementation of molecular electron donor-acceptor architecture in the solid state. However, the ultimate goal is to develop new systems, as well as to optimize existing forms for a sustainable solar energy conversion. The two former projects already demonstrated, how regioisomeric effects, as well as multiple bearing systems positively influence the charge separated state in solution. The

question is now, is it possible to implement the gained knowledge on, exemplarily spacer length, on a solid state material in a solar cell? Therefore, together with the group of Prof. Athanassios G. Coutsolelos and Prof. Fabrice Odobel, three different covalently linked fullerene-zinc porphyrin systems have been investigated in solution, as well as on p-type NiO, forming p-DSSCs. Moreover, an exact model including states, their distribution, and explanation, why the recombination process between zinc porphyrins and NiO is so fast, and to improve this condition, is demanded to obtain higher power conversion efficiencies. The introduction of triazole as linker between the zinc porphyrin and the C_{60} is reasoned, as a larger distance between the electron donor and the acceptor may enhance the lifetimes in the solid state. However, as a first step, photophysical measurements in solution have to be examined to obtain information of the molecular electron donor-acceptor system itself. As a consequence, a charge separated state in all three dyads could be determined together with lifetime differences. Afterwards, all systems, together with a zinc porphyrin system, containing a benzoic acid anchoring group to immobilize on NiO, have been investigated. Hence, a target analysis of the corresponding femtosecond and nanosecond transient absorption spectroscopy raw data revealed the existence of six distinguishable states in the case of the electron donor-acceptor systems. Moreover, not only the states, but also the distribution pathways, as well as the rate constants for each process could be determined.
Furthermore, photoelectrochemical measurements of our partner demonstrate that the power conversion efficiencies of all systems on NiO could be optimized by a factor of almost 40. This is a great improvement. However, the initial problem stays: The ultrafast charge recombination between the NiO surface and porphyrins is the major bottleneck for the corresponding overall efficiencies. In this project, it could be revealed that about 2/3 of the excitation energy leads to the formation of the NiO^{+}-$ZnP^{\bullet-}$-C_{60}. For the development of more sustainable systems, the inhibition of its formation, by strengthen the charge separation process between the zinc porphyrin and the fullerene, is the main key to solve this problem. All photophysical, electrochemical, and theoretical results explain the slight performance differences in all systems.
To recap the beginning assumption: The idea was to enhance the lifetimes of the charge separated state and, in consequence, to achieve a better performance by enhancing V_{OC} and by reducing the charge recombination process between the hole in the VB in the NiO and the reduced ZnP. However, the electron donor-acceptor DSSC shows not only an up to 5.5 fold higher V_{OC} and three times higher J_{SC}, but theoretical calculations could show that the morphology of the electron donor-acceptor systems **C_{60}*tr*ZnP*tr*** and

C_{60}*tr*ZnP is quite different. As a result, it bends more towards the NiO surface, which actually reduces the real distance. This enhanced surface coverage originates from the triazole ring itself interacting substantially with the NiO surface. This also affects J_{SC} by enhancing the charge transfer resistance of the electrolyte with the system. This is indeed a special case, though, as it still counts that an elongation of electron donor-acceptor distance is favorable. These results are very important for the design and development of future based solar cell systems.

The last chapter took the step beyond a limited view of using sunlight only in terms of opto-electronical devices like solar cells or OLEDs to the development of photonmanaging and photocatalytic applications for solar fuels. An interesting approach, which, instead of forming electrical energy from sunlight, has its idea to store this solar energy into chemical one. Together with renewable energy sources like wind and sun light, solar fuels like hydrogen are highly demanded energy sources. This is reflected, exemplarily, by the hydrogen strategy by the federal government of Germany. Up to now, titania is the standard, if one talks about cheap and effective photocatalysis, as it is abundant, easy to produce, and handle. Nevertheless, the efficiencies are very low due to their low charge transfer kinetics. As a result, together with the group of Prof. Patrik Schmuki, a very photoactive "grey" anatase titania photocatalyst, after hydrogenation with present nickel, stated remarkable hydrogen evolution rates in neutral water without using sacrificial-agents or noble-metals. This low-price and highly promising alternative to known noble-metal based photocatalysts or binary oxides, also produces hydrogen peroxide in a significant amount.
The exact mechanism in the field of black or grey titania is still under debate. As a consequence, photophysical measurements, namely transient absorption spectroscopy, could prove the existence of different shallow and deep trap states. As a matter of fact, for the special photocatalyst, deep trap state lifetimes up to almost 15 µs could be determined, almost 250 times longer than in pure (white) titania, which resembles very well the hydrogen evolution rate. Moreover, the existence of long-lived deep level traps is crucial, and its optimization has exceptional influence on both conduction and valence bands. Those samples including nickel exhibit substantial differences in lifetimes, partially oxidized samples show comparable hole lifetime as black and white titania. Those derived differences in the distributions of valence or deep trap states of the analyzed plain (white) titania, black (hydrogenated titania), and grey titania have their origin from the proceeding band tailoring of the band gap of titania, coming from Ti^{3+} states acting as intrinsic photocatalytic center. The corresponding

photocatalytic efficiency using a laser system photoexciting at 325 nm leads to the formation of a quantum conversion of about 2.3%. A remarkable high value in this field. Moreover, the increased deep level state lifetimes go hand-in-hand with a strong increase in hydrogen peroxide formation, demonstrating that the water splitting, by this also very stable photocatalyst, occurs via a two-electron process to form both hydrogen and hydrogen peroxide. These are very important results, which can be seen as guidance for future photocatalytic systems containing (black) titania and gives us a better understanding of the fundamental processes to improve its performance even more.

6 Prospective

Despite all the progress that has been made in the evolution of molecular electron donor-acceptor systems, as well as in the field of photocatalytic water splitting, there is still a long way to go. For the development of novel classes for use as OLED material such as 2,6-dicyanoaniline derivatives, the development is in its beginning. One possibility is to use 2,6-dicyanoaniline as a ligand, in addition to the attempt to implement it directly as an OLED material. On the one hand, basic properties of the resulting metal-ligand complexes can be determined and would possibly lead to a reduction in the use of expensive rare metals like iridium in opto-electronic applications such as OLEDs. The first attempts to coordinate derivatives of this class with cheaper metal centers are already very promising.
Another possibility in the case of an increased lifetime of charge transfer states would be an extension of the junction length between the electron donor triphenylamine and the electron acceptor 2,6-dicyanoaniline. The implementation of such bridges would have two advantages: On the one hand, it would lead to a probable increase of the recombination lifetimes of the two charge transfer states and, on the other hand, it would also lead to a possible energetic degradation of such states. This would be explained by the local difference of the two possible partial charges, as well as by thermodynamic influences such as a reduced reorganization energy, especially in less polar solvents. A reduction of the energetic state, in turn, leads to a further redshift of the emission. Conversely, this enables to tune the color, i.e. the energy, of the recombination emission. Hence, the development of far-red OLED materials is of highly interest.

For the application in solar cells, this work showed that supramolecular, as well as covalent systems are equally advantageous. In terms of an economical solar energy conversion, it is, therefore, advisable to consider the introduction of π-extended porphyrins, such as benzo- and naphthoporphyrins. On the one hand, they would contribute to an increased absorption capacity of the system in the red region of the optical spectrum and, in addition, they show increased extinction coefficients. These molecule classes can be used as pure dye solar cells, e.g. on n- or p-semiconductors, in covalently linked electron donor-acceptor systems, as well as supramolecular systems. A study of zinc benzo- or naphthoporphyrins with multi-membered interaction possibilities, such as a fullerene with four pyridyl units, would be an interesting idea and an extension of the approach of the project mentioned

in the second chapter. Another interesting approach would be the investigation of such non-planar porphyrins on NiO. Precisely because of its planarity and interaction of the pyrrol ring with the surface of the NiO, there is significant optimization potential for porphyrins. The saddle-distorted form of the π-extended systems increases their distance to the surface, which should lead to a reduction of the recombination between the radical anion of the dye and the hole in the valence band of the NiO. The project presented in this thesis shows very clearly that this is the bottleneck for increased power conversion efficiency. An increased lifetime of this electronic state would lead to an enhanced delocalization and, thus, further processing of the electron at the porphyrin. This would not only result in an increased application potential within the system, but finally also in an improved performance.

The development of black or grey titanium dioxide also offers further potential for optimization. Thus, as in the project presented, it is of decisive importance to further increase the lifetime and frequency of deep level trap states. This can be achieved, for example, by incorporating novel compounds, such as metals or new classes that act directly, as another deep level state, or indirectly, as a passivation option for the nanoparticle, in general. Another possibility is the use of materials, whose absorption is further in the visible range or red part, respectively, of sunlight. This would result, as in the case of solar cells, to an increased absorption of the entire solar spectrum, and, thus, further promotes the efficiencies of water splitting in terms of solar fuels such as hydrogen. The use of black or grey titanium dioxide is, therefore, particularly suitable, especially because of its inexpensive production, but also because it can be easily modified. As it has been shown, this is another area in which a great demand for research exists, as well as it is a promising field for the future, which must be further pursued.

Bibliography

[1] K. Burke, S. I. Rasool, and M. F. Uman, System Interactions: Atmosphere, Oceans, Lands and Humans, in *One Earth, One Future: Our Changing Global Environment*, Ed. C. S. Silver and R. S. DeFries, National Academy Press, **1990**.

[2] K. Burke, J. Kutzbach, S. I. Rasool, and M. F. Uman, Lessons from the Geologic Past, in *One Earth, One Future: Our Changing Global Environment*, Ed. C. S. Silver and R. S. DeFries, National Academy Press, **1990**.

[3] R. Dickinson, J. Mahlman, and S. H. Schneider, Global Warming, in *One Earth, One Future: Our Changing Global Environment*, Ed. C. S. Silver and R. S. DeFries, National Academy Press, **1990**.

[4] Y. G. Zhang, M. Pagani, Z. Liu, S. M. Bohaty, R. DeConto, *Phil. Trans. R. Soc. A.* **2013**, *371*, 20130146.

[5] E. Buchner, W. H. Schwarz, M. Schmieder, M. Trieloff, *Meteorit. Planet. Sci.* **2010**, *45*, 662–674.

[6] Regenwald Report 01/2010, opened on the 12.03.2020 at 3:49 pm, https://www.regenwald.org/regenwaldreport/2010/302/tropenholz-heizt-das-klima-an-holzeinschlag-im-regenwald-setzt-massiv-kohlendioxid-frei.

[7] J. Gradwohl, R. Peters, and J. Richey, Vanishing Forest and Vanishing Species, in *One Earth One Future: Our Changing Global Environment*, Ed. C. S. Silver and R. S. DeFries, National Academy Press, **1990**.

[8] K. L. O'Brien, *Prog. Phys. Geog.* **1996**, *20*, 311–335.

[9] Global Time Series, opened on the 11.03.2020 at 8:21 pm, National Centers for Environmental Information, https://www.ncdc.noaa.gov/cag/global/time-series.

[10] Paris Agreement, English, opened on the 03.02.2020 at 7:32 am, United Nations, **2015**, https://unfccc.int/process-and-meetings/the-paris-agreement/the-paris-agreement.

[11] Kassensturz für den Weltklimavertrag - Der Budgetansatz, opened on the 12.03.2020 at 3:10 pm, Wissenschaftlicher Beirat der Bundesregierung Globale Umweltveränderungen, **2009**, https://www.wbgu.de/de/publikationen/publikation/kassensturz-fuer-den-weltklimavertrag-der-budgetansatz.

[12] SolarCity 2015 Impact Report, opened on the 07.02.2020 at 5:51 pm, **2014**, http://www.socialvalueuk.org/report/solarcity-2015-impact-report/.
[13] U.S. Energy Information Administration, International Energy Outlook 2017, opened on the 08.01.2020 at 2:12 pm, **2017**, https://www.iea.org/reports/world-energy-outlook-2017.
[14] BP Energy Outlook 2019 edition, opened on the 19.02.2020 at 1:43 pm, **2019**, https://www.bp.com/content/dam/bp/ business-sites/en/global/corporate/pdfs/energy-economics/energy-outlook/bp-energy-outlook-2019.pdf.
[15] U. Nations, U. N. D. Programme, *World Energy Assessment: Energy and the Challenge of Sustainability*, United Nations, **2001**.
[16] G. Ciamician, *Science* **1912**, *36*, 385–394.
[17] A. E. Becquerel, *C. R. Acad. Sci. Paris* **1839**, *9*, 145–149.
[18] D. M. Chapin, C. S. Fuller, G. L. Pearson, *J. Appl. Phys.* **1954**, *25*, 676–677.
[19] M. A. Green, K. Emery, D. L. King, S. Igari, W. Warta, *Prog. Photovol: Res. Appl.* **2001**, *9*, 49–56.
[20] A. Goetzberger, J. Luther, G. Willeke, *Sol. Energy Mater. Sol. Cells* **2002**, *74*, 1–11.
[21] M. A. Green, K. Emery, Y. Hishikawa, W. Warta, E. D. Dunlop, *Prog. Photovol: Res. Appl.* **2016**, *24*, 905–913.
[22] J. Barber, P. D. Tran, *J. R. Soc. Interface* **2013**, *10*, 20120984.
[23] V. Balzani, A. Credi, M. Venturi, *Curr. Opin. Chem. Biol.* **1997**, *1*, 506–513.
[24] A. A. Ismail, D. W. Bahnemann, *Sol. Energy Mater. Sol. Cells* **2014**, *128*, 85–101.
[25] A. Fujishima, K. Honda, *Nature* **1972**, *238*, 37–38.
[26] Y. Sasaki, H. Kato, A. Kudo, *J. Am. Chem. Soc.* **2013**, *135*, 5441–5449.
[27] H. Kato, K. Asakura, A. Kudo, *J. Am. Chem. Soc.* **2003**, *125*, 3082–3089.
[28] H.-Y. Lin, H.-C. Huang, W.-L. Wang, *Microporous Mesoporous Mater.* **2008**, *115*, 568–575.
[29] J. R. Bolton, D. O. Hall, *Photochem. Photobiol.* **1991**, *53*, 545–548.
[30] X.-G. Zhu, S. P. Long, D. R. Ort, *Annu. Rev. Plant Biol.* **2010**, *61*, 235–261.
[31] R. E. Blankenship, D. M. Tiede, J. Barber, G. W. Brudvig, G. Fleming, M. Ghirardi, M. R. Gunner, W. Junge, D. M. Kramer, A. Melis, T. A. Moore, C. C. Moser, D. G. Nocera, A. J. Nozik, D. R. Ort, W. W. Parson, R. C. Prince, R. T. Sayre, *Science* **2011**, *332*, 805–809.
[32] D. Gust, T. A. Moore, A. L. Moore, *Acc. Chem. Res.* **2001**, *34*, 40–48.

[33] M. R. Wasielewski, *Chem. Rev.* **1992**, *92*, 435–461.
[34] G. J. Kavarnos, *Fundamentals of Photoinduced Electron Transfer*, Wiley-VCH, **1993**.
[35] B. Wardle, *Principles and Applications of Photochemistry*, Wiley-VCH, **2009**.
[36] N. J. Turro, J. C. Scaiano, V. Ramamurthy, *Principles of Molecular Photochemistry: An Introduction*, University Science Books, **2009**.
[37] W. F. Libby, *J. Phys. Chem.* **1952**, *56*, 863–868.
[38] R. A. Marcus, *J. Chem. Phys.* **1956**, *24*, 966–978.
[39] G. I. Likhtenshtein, *Solar Energy Conversion: Chemical Aspects*, Wiley-VCH, **2012**.
[40] M. Rudolf, *Endohedral metallofullerenes: novel biomimetic approaches for solar energy conversion*, Doctoral thesis, Friedrich-Alexander Universität Erlangen-Nürnberg, **2015**.
[41] R. A. Marcus, *Angew. Chem.* **1993**, *105*, 1161–1172.
[42] J. R. Miller, L. T. Calcaterra, G. L. Closs, *J. Am. Chem. Soc.* **1984**, *106*, 3047–3049.
[43] K. Ohkubo, S. Fukuzumi, *J. Porphyrins Phthalocyanines* **2008**, *12*, 993–1004.
[44] T. Förster, *Die Naturwissenschaften* **1946**, *33*, 166–175.
[45] J. W. Verhoeven, *Pure Appl. Chem.* **1996**, *68*, 2223–2286.
[46] R. Emerson, W. Arnold, *J. Gen. Physiol.* **1932**, *16*, 191–205.
[47] J. Perrin, *Gauthier-Villars Paris S* **1925**, *322*.
[48] F. Perrin, *Ann. Chim. Phys. (Paris)* **1932**, *17*, 283–314.
[49] B. W. van der Meer, Förster Theory, in *FRET - Förster Resonance Energy Transfer*, Ed. I. Medintz and N. Hildebrandt, Wiley-VCH, **2013**.
[50] J. R. Lakowicz, *Principles of Fluorescence Spectroscopy*, Springer-Verlag New York Inc., **2006**.
[51] S. Faure, C. Stern, R. Guilard, P. D. Harvey, *J. Am. Chem. Soc.* **2004**, *126*, 1253–1261.
[52] J. Qu, N. G. Pschirer, D. Liu, A. Stefan, F. C. D. Schryver, K. Müllen, *Chem. Eur. J.* **2004**, *10*, 528–537.
[53] H. Tian, X. Yang, J. Pan, R. Chen, M. Liu, Q. Zhang, A. Hagfeldt, L. Sun, *Adv. Funct. Mater.* **2008**, *18*, 3461–3468.
[54] P. Leriche, P. Frère, A. Cravino, O. Alévêque, J. Roncali, *J. Org. Chem.* **2007**, *72*, 8332–8336.
[55] S. Roquet, A. Cravino, P. Leriche, O. Alévêque, P. Frère, J. Roncali, *J. Am. Chem. Soc.* **2006**, *128*, 3459–3466.
[56] S. Qu, J. Hua, H. Tian, *Sci. China Chem.* **2012**, *55*, 677–697.
[57] V. Merz, W. Weith, *Ber. Dtsch. Chem. Ges.* **1873**, *6*, 1511–1520.

[58] J. Louie, J. F. Hartwig, A. J. Fry, *J. Am. Chem. Soc.* **1997**, *119*, 11695–11696.
[59] M. Malagoli, J. Brédas, *Chem. Phys. Lett.* **2000**, *327*, 13–17.
[60] M. Lor, J. Thielemans, L. Viaene, M. Cotlet, J. Hofkens, T. Weil, C. Hampel, K. Müllen, J. W. Verhoeven, M. V. der Auweraer, F. C. D. Schryver, *J. Am. Chem. Soc.* **2002**, *124*, 9918–9925.
[61] S. Dapperheld, E. Steckhan, K.-H. G. Brinkhaus, T. Esch, *Chem. Ber.* **1991**, *124*, 2557–2567.
[62] N. G. Connelly, W. E. Geiger, *Chem. Rev.* **1996**, *96*, 877–910.
[63] Y. Yokoyama, D. Sakamaki, A. Ito, K. Tanaka, M. Shiro, *Angew. Chem. Int. Ed.* **2012**, *51*, 9403–9406.
[64] Y. Shirota, *J. Mater. Chem.* **2005**, *15*, 75–93.
[65] K. R. Stickley, T. D. Selby, S. C. Blackstock, *J. Org. Chem.* **1997**, *62*, 448–449.
[66] T. Zhang, I. E. Brumboiu, C. Grazioli, A. Guarnaccio, M. Coreno, M. de Simone, A. Santagata, H. Rensmo, B. Brena, V. Lanzilotto, C. Puglia, *J. Phys. Chem. C.* **2018**, *122*, 17706–17717.
[67] X. He, M. Tian, X. Liu, Y. Tang, C. F. Shao, P. Gong, J. Liu, S. Zhang, L. Guo, Z. Liu, *Chem. Asian J.* **2018**, *13*, 1500–1509.
[68] A. Mahmood, *Sol. Energy* **2016**, *123*, 127–144.
[69] A. J. Sandee, C. K. Williams, N. R. Evans, J. E. Davies, C. E. Boothby, A. Köhler, R. H. Friend, A. B. Holmes, *J. Am. Chem. Soc.* **2004**, *126*, 7041–7048.
[70] C. Adachi, K. Nagai, N. Tamoto, *Appl. Phys. Lett.* **1995**, *66*, 2679–2681.
[71] Y. Shirota, *J. Mater. Chem.* **2000**, *10*, 1–25.
[72] Y. Shirota, H. Kageyama, *Chem. Rev.* **2007**, *107*, 953–1010.
[73] K. C. Moss, K. N. Bourdakos, V. Bhalla, K. T. Kamtekar, M. R. Bryce, M. A. Fox, H. L. Vaughan, F. B. Dias, A. P. Monkman, *J. Org. Chem.* **2010**, *75*, 6771–6781.
[74] A. G. Bonn, O. S. Wenger, *J. Org. Chem.* **2015**, *80*, 4097–4107.
[75] E. Ripaud, T. Rousseau, P. Leriche, J. Roncali, *Adv. Energy Mater.* **2011**, *1*, 540–545.
[76] G. Zhou, W.-Y. Wong, B. Yao, Z. Xie, L. Wang, *Angew. Chem. Int. Ed.* **2007**, *46*, 1149–1151.
[77] Y. Tao, Q. Wang, C. Yang, C. Zhong, J. Qin, D. Ma, *Adv. Funct. Mater.* **2010**, *20*, 2923–2929.
[78] L. D. Lavis, R. T. Raines, *ACS Chem. Biol.* **2008**, *3*, 142–155.
[79] M. J. Leonardi, M. R. Topka, P. H. Dinolfo, *Inorg. Chem.* **2012**, *51*, 13114–13122.

[80] W. Lin, L. Yuan, Z. Cao, Y. Feng, J. Song, *Angew. Chem. Int. Ed.* **2009**, *49*, 375–379.
[81] K. Fujii, N. Iyi, H. Hashizume, S. Shimomura, T. Ando, *Chem. Mater.* **2009**, *21*, 1179–1181.
[82] J. Deisenhofer, H. Michel, *Angew. Chem. Int. Ed.* **1989**, *28*, 829–847.
[83] A. Hoff, J. Deisenhofer, *Phys. Rep.* **1997**, *287*, 1–247.
[84] N. Nelson, C. F. Yocum, *Annu. Rev. Plant Biol.* **2006**, *57*, 521–565.
[85] C. A. Raines, *Photosynth. Res.* **2003**, *75*, 1–10.
[86] S. Fukuzumi, K. Ohkubo, H. Imahori, J. Shao, Z. Ou, G. Zheng, Y. Chen, R. K. Pandey, M. Fujitsuka, O. Ito, K. M. Kadish, *J. Am. Chem. Soc.* **2001**, *123*, 10676–10683.
[87] M. Toganoh, H. Furuta, *Chem. Lett.* **2019**, *48*, 615–622.
[88] S. Ito, T. Murashima, N. Ono, H. Uno, *Chem. Commun.* **1998**, 1661–1662.
[89] J. E. Rogers, K. A. Nguyen, D. C. Hufnagle, D. G. McLean, W. Su, K. M. Gossett, A. R. Burke, S. A. Vinogradov, R. Pachter, P. A. Fleitz, *J. Phys. Chem. A* **2003**, *107*, 11331–11339.
[90] S. Saito, A. Osuka, *Angew. Chem. Int. Ed.* **2011**, *50*, 4342–4373.
[91] V. V. Roznyatovskiy, C.-H. Lee, J. L. Sessler, *Chem. Soc. Rev.* **2013**, *42*, 1921–1933.
[92] T. Tanaka, A. Osuka, *Chem. Soc. Rev.* **2015**, *44*, 943–969.
[93] S. Fukuzumi, Artificial Photosynthetic Systems Composed of Porphyrins and Phthalocyanines, in *Handbook of Porphyrin Science, Volume 10, Catalysis and Bio-Inspired Systems*, Ed. K. M. Kadish, K. M. Smith and R. Guilard, World Scientific Publishing, **2010**.
[94] J. C. Goedheer, Visible Absorption and Fluorescence of Chlorophyll and Its Aggregates in Solution, in *The Chlorophylls*, Ed. L. P. Vernon and G. R. Seely, Academic Press, **1966**.
[95] H. M. Berman, *Nucleic Acids Research* **2000**, *28*, 235–242.
[96] M. Paoli, R. Liddington, J. Tame, A. Wilkinson, G. Dodson, *J. Mol. Biol.* **1996**, *256*, 775–792.
[97] A. S. Rose, A. R. Bradley, Y. Valasatava, J. M. Duarte, A. Prlić, P. W. Rose, *Bioinf.* **2018**, *34*, 3755–3758.
[98] N. Ono, H. Yamada, T. Okujima, Synthesis of Porphyrin Fused with Aromatic Rings, in *Handbook of Porphyrin Science, Volume 2, Synthesis and Coordination Chemistry*, Ed. K. M. Kadish, K. M. Smith and R. Guilard, World Scientific Publishing, **2010**.
[99] J. S. Lindsey, R. W. Wagner, *J. Org. Chem.* **1989**, *54*, 828–836.
[100] P. Rothemund, *J. Am. Chem. Soc.* **1935**, *57*, 2010–2011.
[101] N. Aratani, A. Osuka, Synthetic Strategies Toward Multiporphyrinic Architectures, in *Handbook of Porphyrin Science, Volume 1,*

Supramolecular Chemistry, Ed. K. M. Kadish, K. M. Smith and R. Guilard, World Scientific Publishing, **2010**.
[102] F. Sondheimer, R. Wolovsky, Y. Amiel, *J. Am. Chem. Soc.* **1962**, *84*, 274–284.
[103] M. Gouterman, *J. Mol. Spectrosc.* **1961**, *6*, 138–163.
[104] M. Gouterman, G. H. Wagnière, L. C. Snyder, *J. Mol. Spectrosc.* **1963**, *11*, 108–127.
[105] M. Gouterman, *J. Chem. Phys.* **1959**, *30*, 1139–1161.
[106] O. S. Finikova, S. E. Aleshchenkov, R. P. Briñas, A. V. Cheprakov, P. J. Carroll, S. A. Vinogradov, *J. Org. Chem.* **2005**, *70*, 4617–4628.
[107] J. R. Sommer, A. H. Shelton, A. Parthasarathy, I. Ghiviriga, J. R. Reynolds, K. S. Schanze, *Chem. Mater.* **2011**, *23*, 5296–5304.
[108] H. Fischer, B. Walach, *Liebigs Ann.* **1926**, *450*, 164–181.
[109] K. Berg, P. K. Selbo, A. Weyergang, A. Dietze, L. Prasmickaite, A. Bonsted, B. O. Engesaeter, E. Angell-Petersen, T. Warloe, N. Frandsen, A. Hogset, *J. Microsc.* **2005**, *218*, 133–147.
[110] R. Paolesse, D. Monti, S. Nardis, C. Di Natale, Porphyrin-based Chemical Sensors, in *Handbook of Porphyrin Science, Volume 12, Applications*, Ed. K. M. Kadish, K. M. Smith and R. Guilard, World Scientific Publishing, **2010**.
[111] A. Kay, M. Graetzel, *J. Phys. Chem.* **1993**, *97*, 6272–6277.
[112] T. Bessho, S. Zakeeruddin, C.-Y. Yeh, E.-G. Diau, M. Grätzel, *Angew. Chem. Int. Ed.* **2010**, *49*, 6646–6649.
[113] D. M. Guldi, *Chem. Soc. Rev.* **2001**, *31*, 22–36.
[114] G. Bottari, O. Trukhina, M. Ince, T. Torres, *Coord. Chem. Rev.* **2012**, *256*, 2453–2477.
[115] D. Kuciauskas, S. Lin, G. R. Seely, A. L. Moore, T. A. Moore, D. Gust, T. Drovetskaya, C. A. Reed, P. D. W. Boyd, *J. Phys. Chem.* **1996**, *100*, 15926–15932.
[116] A. Hirsch, *Nat. Mater.* **2010**, *9*, 868–871.
[117] H. R. Karfunkel, T. Dressler, *J. Am. Chem. Soc.* **1992**, *114*, 2285–2288.
[118] F. Diederich, Y. Rubin, *Angew. Chem. Int. Ed.* **1992**, *31*, 1101–1123.
[119] H. W. Kroto, J. R. Heath, S. C. O'Brien, R. F. Curl, R. E. Smalley, *Nature* **1985**, *318*, 162–163.
[120] S. Iijima, *Nature* **1991**, *354*, 56–58.
[121] K. S. Novoselov, *Science* **2004**, *306*, 666–669.
[122] R. Haddon, L. Brus, K. Raghavachari, *Chem. Phys. Lett.* **1986**, *125*, 459–464.
[123] S. H. Yang, C. L. Pettiette, J. Conceicao, O. Cheshnovsky, R. E. Smalley, *Chem. Phys. Lett.* **1987**, *139*, 233–238.
[124] D. Wróbel, A. Graja, *Coord. Chem. Rev.* **2011**, *255*, 2555–2577.

[125] L. Echegoyen, L. E. Echegoyen, *Acc. Chem. Res.* **1998**, *31*, 593–601.
[126] S. R. Wilson, D. I. Schuster, B. Nuber, M. S. Meier, M. Maggini, M. Prato, R. Taylor, Organic Chemistry of Fullerenes, in *Chemistry, Physics and Technology*, Ed. K. M. Kadish and R. S. Ruoff, Wiley-Interscience, **2000**.
[127] R. C. Haddon, K. Raghavachari, Electronic Structure of the Fullerenes: Carbon Allotropes of the Intermediate Hybridization, in *Buckminsterfullerenes*, Ed. W. E. Billups and M. A. Ciufolini, VCH Publishers, **1993**, New York.
[128] C. Bingel, *Chem. Ber.* **1993**, *126*, 1957–1959.
[129] X. Camps, A. Hirsch, *Perkin Trans.* **1997**, 1595–1596.
[130] M. Maggini, G. Scorrano, M. Prato, *J. Am. Chem. Soc.* **1993**, *115*, 9798–9799.
[131] Y. Sun, T. Drovetskaya, R. D. Bolskar, R. Bau, P. D. W. Boyd, C. A. Reed, *J. Org. Chem.* **1997**, *62*, 3642–3649.
[132] Q. Lu, D. I. Schuster, S. R. Wilson, *J. Org. Chem.* **1996**, *61*, 4764–4768.
[133] A. Hirsch, I. Lamparth, T. Groesser, H. R. Karfunkel, *J. Am. Chem. Soc.* **1994**, *116*, 9385–9386.
[134] D. M. Guldi, P. V. Kamat, Photophysical Properties of Pristine Fullerenes Functionalized Fullerenes, and Fullerene-Containing Donor-Bridge Acceptor Systems, in *Fullerenes: Chemistry, Physics and Technology*, Ed. K. M Kadish and R. S. Ruoff, Wiley-Interscience, **2000**.
[135] T. D. Ros, M. Prato, *Chem. Commun.* **1999**, 663–669.
[136] N. Tagmatarchis, H. Shinohara, *Mini-Rev. Med. Chem.* **2001**, *1*, 339–348.
[137] A. W. Jensen, S. R. Wilson, D. I. Schuster, *Bioorg. Med. Chem.* **1996**, *4*, 767–779.
[138] S. Bosi, T. D. Ros, G. Spalluto, M. Prato, *Eur. J. Med. Chem.* **2003**, *38*, 913–923.
[139] D. Jariwala, V. K. Sangwan, L. J. Lauhon, T. J. Marks, M. C. Hersam, *Chem. Soc. Rev.* **2013**, *42*, 2824–2860.
[140] S. S. Babu, H. Möhwald, T. Nakanishi, *Chem. Soc. Rev.* **2010**, *39*, 4021–4035.
[141] D. M. Guldi, S. Fukuzumi, The Small Reorganization Energy of Fullerenes, in *Fullerenes: From Synthesis to Optoelectronic Properties*, Ed. D. M. Guldi and N. Martín, Springer Netherlands, **2002**.
[142] I. Hiroshi, H. Kiyoshi, A. Tsuyoshi, A. Masanori, T. Seiji, O. Tadashi, S. Masahiro, S. Yoshiteru, *Chem. Phys. Lett.* **1996**, *263*, 545–550.
[143] C. Kang, Z. Lin, *J. Theor. Comput. Chem.* **2006**, *05*, 665–684.

[144] F. D'Souza, O. Ito, *Coord. Chem. Rev.* **2005**, *249*, 1410–1422.
[145] D. M. Guldi, G. M. A. Rahman, F. Zerbetto, M. Prato, *Acc. Chem. Res.* **2005**, *38*, 871–878.
[146] L. Isaacs, P. Seiler, F. Diederich, *Angew. Chem. Int. Ed.* **1995**, *34*, 1466–1469.
[147] M. Izquierdo, B. Platzer, A. J. Stasyuk, O. A. Stasyuk, A. A. Voityuk, S. Cuesta, M. Solà, D. M. Guldi, N. Martín, *Angew. Chem.* **2019**, *131*, 7006–7011.
[148] M. Wolf, D. Lungerich, S. Bauroth, M. Popp, B. Platzer, T. Clark, H. L. Anderson, N. Jux, D. M. Guldi, *Chem. Sci.* **2020**, *11*, 7123–7132.
[149] B. Liu, H. Fang, X. Li, W. Cai, L. Bao, M. Rudolf, F. Plass, L. Fan, X. Lu, D. M. Guldi, *Chem. Eur. J.* **2014**, *21*, 746–752.
[150] M. Rudolf, O. Trukhina, J. Perles, L. Feng, T. Akasaka, T. Torres, D. M. Guldi, *Chem. Sci.* **2015**, *6*, 4141–4147.
[151] J.-M. Lehn, *Chem. Soc. Rev.* **2007**, *36*, 151–160.
[152] D. E. Discher, R. D. Kamien, *Nature* **2004**, *430*, 519–520.
[153] X. Wang, P. Gao, Y. Yang, H. Guo, D. Wu, *Nat. Commun.* **2018**, *9*, 1–15.
[154] A. Whitty, *Nat. Chem. Biol.* **2008**, *4*, 435–439.
[155] D. Astruc, E. Boisselier, C. Ornelas, *Chem. Rev.* **2010**, *110*, 1857–1959.
[156] S. Collavini, J. L. Delgado, *Sustain. Energy Fuels* **2018**, *2*, 2480–2493.
[157] S. Kirner, M. Sekita, D. M. Guldi, *Adv. Mater.* **2014**, *26*, 1482–1493.
[158] A. Zieleniewska, F. Lodermeyer, A. Roth, D. M. Guldi, *Chem. Soc. Rev.* **2018**, *47*, 702–714.
[159] T. Fromherz, *Sol. Energy Mater. Sol. Cells* **2000**, *63*, 61–68.
[160] C.-H. Chiang, C.-G. Wu, *Nat. Photonics* **2016**, *10*, 196–200.
[161] D. M. Guldi, *Phys. Chem. Chem. Phys.* **2007**, *9*, 1400–1420.
[162] S. Albrecht, K. Vandewal, J. R. Tumbleston, F. S. U. Fischer, J. D. Douglas, J. M. J. Fréchet, S. Ludwigs, H. Ade, A. Salleo, D. Neher, *Adv. Mater.* **2014**, *26*, 2533–2539.
[163] J. Yan, B. R. Saunders, *RSC Adv.* **2014**, *4*, 43286–43314.
[164] Y. Wang, R. West, C. H. Yuan, *J. Am. Chem. Soc.* **1993**, *115*, 3844–3845.
[165] J. Gong, K. Sumathy, Q. Qiao, Z. Zhou, *Renew. Sustain. Energy Rev.* **2017**, *68*, 234–246.
[166] W. Shockley, H. J. Queisser, *J. Appl. Phys.* **1961**, *32*, 510–519.
[167] B. O'Regan, M. Grätzel, *Nature* **1991**, *353*, 737–740.
[168] F. Odobel, Y. Pellegrin, E. A. Gibson, A. Hagfeldt, A. L. Smeigh, L. Hammarström, *Coord. Chem. Rev.* **2012**, *256*, 2414–2423.

[169] E. Gibson, A. Smeigh, L. Le Pleux, J. Fortage, G. Boschloo, E. Blart, Y. Pellegrin, F. Odobel, A. Hagfeldt, L. Hammarström, *Angew. Chem. Int. Ed.* **2009**, *48*, 4402–4405.
[170] L. Li, E. A. Gibson, P. Qin, G. Boschloo, M. Gorlov, A. Hagfeldt, L. Sun, *Adv. Mater.* **2010**, *22*, 1759–1762.
[171] P. Qin, H. Zhu, T. Edvinsson, G. Boschloo, A. Hagfeldt, L. Sun, *J. Am. Chem. Soc.* **2008**, *130*, 8570–8571.
[172] J. He, H. Lindström, A. Hagfeldt, S.-E. Lindquist, *J. Phys. Chem. B.* **1999**, *103*, 8940–8943.
[173] H. P. R. Frederikse, Permittivity (Dielectric Constant) of Inorganic Solids, in *CRC Handbook of Chemistry and Physics, 97th Edition*, Ed. W. M. Haynes, David R. Lide and Thomas J. Bruno, CRC Press, **2016**.
[174] F. Odobel, L. Le Pleux, Y. Pellegrin, E. Blart, *Acc. Chem. Res.* **2010**, *43*, 1063–1071.
[175] P. A. M. Dirac, *Proc. R. Soc. Lond. A* **1926**, *112*, 661–677.
[176] A. Zannoni, *arXiv preprint cond-mat* **1999**, 1–6.
[177] S. M. Gupta, M. Tripathi, *Chin. Sci. Bull.* **2011**, *56*, 1639–1657.
[178] L. Wu, J. Zhang, W. Watanabe, *Adv. Drug Deliv. Rev.* **2011**, *63*, 456–469.
[179] X. Chen, S. S. Mao, *Chem. Rev.* **2007**, *107*, 2891–2959.
[180] X. Chen, Y. Cui, Introduction, in *Black TiO_2 Nanomaterials For Energy Applications*, Ed. X. Chen and Y. Cui, World Scientific Publishing Europe Ltd, **2017**.
[181] X. Chen, L. Liu, P. Y. Yu, S. S. Mao, *Science* **2011**, *331*, 746–750.
[182] X. Chen, L. Liu, F. Huang, *Chem. Soc. Rev.* **2015**, *44*, 1861–1885.
[183] A. Zaleska, *Recent Patents on Engineering* **2008**, *2*, 157–164.
[184] X. Yan, L. Tian and X. Chen, Synthesis and Properties of Hydrogenated Black TiO_2 Nanomaterials, in *Black TiO_2 Nanomaterials For Energy Applications*, Ed. X. Chen and Y. Cui, World Scientific Publishing Europe Ltd, **2017**.
[185] T. Leshuk, R. Parviz, P. Everett, H. Krishnakumar, R. A. Varin, F. Gu, *ACS Appl. Mater. Interfaces* **2013**, *5*, 1892–1895.
[186] C. Sun, Y. Jia, X.-H. Yang, H.-G. Yang, X. Yao, G. Q. M. Lu, A. Selloni, S. C. Smith, *J. Phys. Chem. C.* **2011**, *115*, 25590–25594.
[187] H. Lu, B. Zhao, R. Pan, J. Yao, J. Qiu, L. Luo, Y. Liu, *RSC Adv.* **2014**, *4*, 1128–1132.
[188] G. Wang, H. Wang, Y. Ling, Y. Tang, X. Yang, R. C. Fitzmorris, C. Wang, J. Z. Zhang, Y. Li, *Nano Lett.* **2011**, *11*, 3026–3033.
[189] J.-Y. Eom, S.-J. Lim, S.-M. Lee, W.-H. Ryu, H.-S. Kwon, *J. Mater. Chem. A* **2015**, *3*, 11183–11188.

[190] N. Liu, C. Schneider, D. Freitag, M. Hartmann, U. Venkatesan, J. Müller, E. Spiecker, P. Schmuki, *Nano Lett.* **2014**, *14*, 3309–3313.
[191] A. Naldoni, M. Allieta, S. Santangelo, M. Marelli, F. Fabbri, S. Cappelli, C. L. Bianchi, R. Psaro, V. Dal Santo, *J. Am. Chem. Soc.* **2012**, *134*, 7600–7603.
[192] Z. Wang, C. Yang, T. Lin, H. Yin, P. Chen, D. Wan, F. Xu, F. Huang, J. Lin, X. Xie, M. Jiang, *Adv. Funct. Mater.* **2013**, *23*, 5444–5450.
[193] R. Schaub, *Science* **2002**, *299*, 377–379.
[194] M. M. Khader, F. M. N. Kheiri, B. E. El-Anadouli, B. G. Ateya, *J. Phys. Chem.* **1993**, *97*, 6074–6077.
[195] X. Zhou, N. Liu, J. Schmidt, A. Kahnt, A. Osvet, S. Romeis, E. M. Zolnhofer, V. R. R. Marthala, D. M. Guldi, W. Peukert, M. Hartmann, K. Meyer, P. Schmuki, *Adv. Mater.* **2016**, *29*, 1604747.
[196] M. Ni, M. K. Leung, D. Y. Leung, K. Sumathy, *Renew. Sustain. Energy Rev.* **2007**, *11*, 401–425.
[197] A. H. Samuel, J. L. Magee, *J. Chem. Phys.* **1953**, *21*, 1080–1087.
[198] A. Mozumder, J. L. Magee, *J. Chem. Phys.* **1966**, *45*, 3332–3341.
[199] L. Monchick, J. L. Magee, A. H. Samuel, *J. Chem. Phys.* **1957**, *26*, 935–941.
[200] C. Ruckebusch, M. Sliwa, P. Pernot, A. de Juan, R. Tauler, *J. Photochem. Photobiol. C* **2012**, *13*, 1–27.
[201] J. J. Snellenburg, S. P. Laptenok, R. Seger, K. M. Mullen, I. H. M. van Stokkum, *J. Stat. Softw.* **2012**, *49*.
[202] K. M. Mullen, I. H. M. van Stokkum, *J. Stat. Softw.* **2007**, *18*.
[203] S. Laptenok, K. M. Mullen, J. W. Borst, I. H. M. van Stokkum, V. V. Apanasovich, A. J. W. G. Visser, *J. Stat. Softw.* **2007**, *18*.
[204] R. C. Team, R: A Language and Environment for Statistical Computing, R Foundation for Statistical Computing, **2014**, http://www.R-project.org/.
[205] A. A. Istratov, O. F. Vyvenko, *Rev. Sci. Instrum.* **1999**, *70*, 1233–1257.
[206] I. H. van Stokkum, D. S. Larsen, R. van Grondelle, *Biochim. Biophys. Acta – Bioenergetics* **2004**, *1657*, 82–104.
[207] G. H. Golub, C. F. V. Loan, *Matrix Computations (Johns Hopkins Studies in Mathematical Sciences) (3rd Edition)*, Johns Hopkins University Press, **1996**.
[208] R. M. Savic, D. M. Jonker, T. Kerbusch, M. O. Karlsson, *J. Pharmacokinet. Pharmacodyn.* **2007**, *34*, 711–726.
[209] J. Schüttler, H. Ihmsen, *Anesthesiology* **2000**, *92*, 727–738.
[210] K. Godfrey, *Compartmental Models and Their Application*, Academic Press, London, **1983**.

[211] C. Hippius, I. H. M. van Stokkum, E. Zangrando, R. M. Williams, F. Würthner, *J. Phys. Chem. C* **2007**, *111*, 13988–13996.
[212] L. Duan, J. Qiao, Y. Sun, Y. Qiu, *Adv. Mater.* **2011**, *23*, 1137–1144.
[213] C. Bizzarri, E. Spuling, D. M. Knoll, D. Volz, S. Bräse, *Coord. Chem. Rev.* **2018**, *373*, 49–82.
[214] D. Volz, M. Wallesch, C. Fléchon, M. Danz, A. Verma, J. M. Navarro, D. M. Zink, S. Bräse, T. Baumann, *Green Chem.* **2015**, *17*, 1988–2011.
[215] W.-Y. Wong, C.-L. Ho, *Coord. Chem. Rev.* **2009**, *253*, 1709–1758.
[216] X. Gong, J. C. Ostrowski, G. C. Bazan, D. Moses, A. J. Heeger, *Appl. Phys. Lett.* **2002**, *81*, 3711–3713.
[217] T. Tsuzuki, S. Tokito, *Adv. Mater.* **2007**, *19*, 276–280.
[218] G. M. Mudd, *Ore Geol. Rev.* **2012**, *46*, 106–117.
[219] H. Uoyama, K. Goushi, K. Shizu, H. Nomura, C. Adachi, *Nature* **2012**, *492*, 234–238.
[220] D. Di, A. S. Romanov, L. Yang, J. M. Richter, J. P. H. Rivett, S. Jones, T. H. Thomas, M. A. Jalebi, R. H. Friend, M. Linnolahti, M. Bochmann, D. Credgington, *Science* **2017**, *356*, 159–163.
[221] X. Ai, Y. Chen, Y. Feng, F. Li, *Angew. Chem. Int. Ed.* **2018**, *57*, 2869–2873.
[222] Z. Bin, L. Duan, Y. Qiu, *ACS Appl. Mater. Interfaces* **2015**, *7*, 6444–6450.
[223] J. Kido, Y. Iizumi, *Appl. Phys. Lett.* **1998**, *73*, 2721–2723.
[224] A. P. Kulkarni, P.-T. Wu, T. W. Kwon, S. A. Jenekhe, *J. Phys. Chem. B* **2005**, *109*, 19584–19594.
[225] P. T. Furuta, L. Deng, S. Garon, M. E. Thompson, J. M. J. Fréchet, *J. Am. Chem. Soc.* **2004**, *126*, 15388–15389.
[226] K. R. J. Thomas, J. T. Lin, Y.-T. Tao, C.-H. Chuen, *Chem. Mater.* **2002**, *14*, 3852–3859.
[227] W. Zhu, M. Hu, R. Yao, H. Tian, *J. Photochem. Photobiol. A* **2003**, *154*, 169–177.
[228] N. Tamoto, C. Adachi, K. Nagai, *Chem. Mater.* **1997**, *9*, 1077–1085.
[229] H. Antoniadis, M. Inbasekaran, E. P. Woo, *Appl. Phys. Lett.* **1998**, *73*, 3055–3057.
[230] H. B. Borate, A. S. Kudale, S. G. Agalave, *Org. Prep. Proced. Int.* **2012**, *44*, 467–521.
[231] P. Das, R. J. Butcher, C. Mukhopadhyay, *Green Chem.* **2012**, *14*, 1376–1387.
[232] J. Wang, Q. Li, C. Qi, Y. Liu, Z. Ge, R. Li, *Org. Biomol. Chem.* **2010**, *8*, 4240–4242.
[233] X. Xin, Y. Wang, W. Xu, Y. Lin, H. Duan, D. Dong, *Green Chem.* **2010**, *12*, 893–898.

[234] S.-L. Cui, X.-F. Lin, Y.-G. Wang, *J. Org. Chem.* **2005**, *70*, 2866–2869.
[235] L. Rong, H. Han, F. Yang, H. Yao, H. Jiang, S. Tu, *Synth. Commun.* **2007**, *37*, 3767–3772.
[236] J. Sepioł, P. Milart, *Tetrahedron* **1985**, *41*, 5261–5265.
[237] J. H. Baxendale, E. J. Rasburn, *J. Chem. Soc. Faraday Trans. 1* **1973**, *69*, 771–775.
[238] D. M. Guldi, H. Hungerbuehler, K.-D. Asmus, *J. Phys. Chem.* **1995**, *99*, 9380–9385.
[239] G. Porter, S. K. Dogra, R. O. Loutfy, S. E. Sugamori, R. W. Yip, *J. Chem. Soc. Faraday Trans. 1* **1973**, *69*, 1462–1474.
[240] P. Wardman, *J. Phys. Chem. Ref. Data* **1989**, *18*, 1637–1755.
[241] A. Ruff, E. Heyer, T. Roland, S. Haacke, R. Ziessel, S. Ludwigs, *Electrochim. Acta* **2015**, *173*, 847–859.
[242] G. Sforazzini, A. Kahnt, M. Wykes, J. K. Sprafke, S. Brovelli, D. Montarnal, F. Meinardi, F. Cacialli, D. Beljonne, B. Albinsson, H. L. Anderson, *J. Phys. Chem. C* **2014**, *118*, 4553–4566.
[243] B. Dereka, A. Rosspeintner, R. Stężycki, C. Ruckebusch, D. T. Gryko, E. Vauthey, *J. Phys. Chem. Lett.* **2017**, *8*, 6029–6034.
[244] E. Vauthey, *ChemPhysChem* **2012**, *13*, 2001–2011.
[245] J. T. Buck, R. W. Wilson, T. Mani, *J. Phys. Chem. Lett.* **2019**, *10*, 3080–3086.
[246] A. Maroz, R. Hermann, S. Naumov, O. Brede, *J. Phys. Chem. A* **2005**, *109*, 4690–4696.
[247] K. Karon, M. Lapkowski, A. Dabuliene, A. Tomkeviciene, N. Kostiv, J. V. Grazulevicius, *Electrochim. Acta* **2015**, *154*, 119–127.
[248] J.-M. Lehn, *Angew. Chem. Int. Ed.* **1988**, *27*, 89–112.
[249] G. E. Zervaki, E. Papastamatakis, P. A. Angaridis, V. Nikolaou, M. Singh, R. Kurchania, T. N. Kitsopoulos, G. D. Sharma, A. G. Coutsolelos, *Eur. J. Inorg. Chem.* **2014**, *2014*, 1020–1033.
[250] F. D'Souza, O. Ito, *Chem. Soc. Rev.* **2012**, *41*, 86–96.
[251] T. Lazarides, M. Delor, I. V. Sazanovich, T. M. McCormick, I. Georg akaki, G. Charalambidis, J. A. Weinstein, A. G. Coutsolelos, *Chem. Commun.* **2014**, *50*, 521–523.
[252] K. Ladomenou, M. Natali, E. Iengo, G. Charalampidis, F. Scandola, A. G. Coutsolelos, *Coord. Chem. Rev.* **2015**, *304-305*, 38–54.
[253] G. de la Torre, F. Giacalone, J. L. Segura, N. Martín, D. M. Guldi, *Chem. Eur. J.* **2005**, *11*, 1267–1280.
[254] F. Giacalone, J. L. Segura, N. Martín, D. M. Guldi, *J. Am. Chem. Soc.* **2004**, *126*, 5340–5341.
[255] W. B. Davis, W. A. Svec, M. A. Ratner, M. R. Wasielewski, *Nature* **1998**, *396*, 60–63.

[256] C. Schubert, J. T. Margraf, T. Clark, D. M. Guldi, *Chem. Soc. Rev.* **2015**, *44*, 988–998.
[257] F. J. M. Hoeben, P. Jonkheijm, E. W. Meijer, A. P. H. J. Schenning, *Chem. Rev.* **2005**, *105*, 1491–1546.
[258] S. Burattini, B. W. Greenland, D. H. Merino, W. Weng, J. Seppala, H. M. Colquhoun, W. Hayes, M. E. Mackay, I. W. Hamley, S. J. Rowan, *J. Am. Chem. Soc.* **2010**, *132*, 12051–12058.
[259] A. Bagaki, H. B. Gobeze, G. Charalambidis, A. Charisiadis, C. Stangel, V. Nikolaou, A. Stergiou, N. Tagmatarchis, F. D'Souza, A. G. Coutsolelos, *Inorg. Chem.* **2017**, *56*, 10268–10280.
[260] S. Vela, S. Bauroth, C. Atienza, A. Molina-Ontoria, D. M. Guldi, N. Martín, *Angew. Chem. Int. Ed.* **2016**, 55, 15076–15080.
[261] C. Stangel, A. Charisiadis, G. E. Zervaki, V. Nikolaou, G. Charalambidis, A. Kahnt, G. Rotas, N. Tagmatarchis, A. G. Coutsolelos, *J. Phys. Chem. C.* **2017**, *121*, 4850–4858.
[262] C. B. KC, K. Ohkubo, P. A. Karr, S. Fukuzumi, F. D'Souza, *Chem. Commun.* **2013**, *49*, 7614–7616.
[263] C. B. KC, G. N. Lim, P. A. Karr, F. D'Souza, *Chem. Eur. J.* **2014**, *20*, 7725–7735.
[264] C. Stangel, C. Schubert, S. Kuhri, G. Rotas, J. T. Margraf, E. Regulska, T. Clark, T. Torres, N. Tagmatarchis, A. G. Coutsolelos, D. M. Guldi, *Nanoscale* **2015**, *7*, 2597–2608.
[265] L. Lu, T. Zheng, Q. Wu, A. M. Schneider, D. Zhao, L. Yu, *Chem. Rev.* **2015**, *115*, 12666–12731.
[266] M. Scharber, D. Mühlbacher, M. Koppe, P. Denk, C. Waldauf, A. Heeger, C. Brabec, *Adv. Mater.* **2006**, *18*, 789–794.
[267] B. Qi, J. Wang, *J. Mater. Chem.* **2012**, *22*, 24315–24325.
[268] R. Tao, T. Umeyama, K. Kurotobi, H. Imahori, *ACS Appl. Mater. Interfaces* **2014**, *6*, 17313–17322.
[269] M. Lenes, G.-J. A. H. Wetzelaer, F. B. Kooistra, S. C. Veenstra, J. C. Hummelen, P. W. M. Blom, *Adv. Mater.* **2008**, *20*, 2116–2119.
[270] M. Lenes, S. W. Shelton, A. B. Sieval, D. F. Kronholm, J. C. (Kees) Hummelen, P. W. M. Blom, *Adv. Funct. Mater.* **2009**, *19*, 3002–3007.
[271] Y. He, G. Zhao, B. Peng, Y. Li, *Adv. Funct. Mater.* **2010**, *20*, 3383–3389.
[272] M.-H. Liao, Y.-Y. Lai, Y.-Y. Lai, Y.-T. Chen, C.-E. Tsai, W.-W. Liang, Y.-J. Cheng, *ACS Appl. Mater. Interfaces* **2013**, *6*, 996–1004.
[273] X. Meng, G. Zhao, Q. Xu, Z. Tan, Z. Zhang, L. Jiang, C. Shu, C. Wang, Y. Li, *Adv. Funct. Mater.* **2013**, *24*, 158–163.

[274] T. Umeyama, T. Miyata, A. C. Jakowetz, S. Shibata, K. Kurotobi, T. Higashino, T. Koganezawa, M. Tsujimoto, S. Gélinas, W. Matsuda, S. Seki, R. H. Friend, H. Imahori, *Chem. Sci.* **2017**, *8*, 181–188.
[275] D. A. Lukyanov, A. S. Konev, K. Amsharov, A. F. Khlebnikov, A. Hirsch, *J. Org. Chem.* **2018**, *83*, 14146–14151.
[276] IPCC, *Climate Change 2013: The Physical Science Basis. Contribution of Working Group I to the Fifth Assessment Report of the Intergovernmental Panel on Climate Change*, (Eds.: T. F. Stocker, D. Qin, G.-K. Plattner, M. Tignor, S. K. Allen, J. Boschung, A. Nauels, Y. Xia, V. Bex, P. M. Midgley), Cambridge University Press, Cambridge, United Kingdom and New York, NY, USA, **2013**.
[277] J.-P. Correa-Baena, A. Abate, M. Saliba, W. Tress, T. J. Jacobsson, M. Grätzel, A. Hagfeldt, *Energy Environ. Sci.* **2017**, *10*, 710–727.
[278] J. Khan, M. H. Arsalan, *Renew. Sustain. Energy Rev.* **2016**, *55*, 414–425.
[279] G. Yu, J. Gao, J. C. Hummelen, F. Wudl, A. J. Heeger, *Science* **1995**, *270*, 1789–1791.
[280] J. Hou, O. Inganäs, R. H. Friend, F. Gao, *Nat. Mater.* **2018**, *17*, 119–128.
[281] K. A. Click, D. R. Beauchamp, Z. Huang, W. Chen, Y. Wu, *J. Am. Chem. Soc.* **2016**, *138*, 1174–1179.
[282] M. A. Gross, C. E. Creissen, K. L. Orchard, E. Reisner, *Chem. Sci.* **2016**, *7*, 5537–5546.
[283] N. Kaeffer, J. Massin, C. Lebrun, O. Renault, M. Chavarot-Kerlidou, V. Artero, *J. Am. Chem. Soc.* **2016**, *138*, 12308–12311.
[284] G. Sahara, H. Kumagai, K. Maeda, N. Kaeffer, V. Artero, M. Higashi, R. Abe, O. Ishitani, *J. Am. Chem. Soc.* **2016**, *138*, 14152–14158.
[285] D. Dini, Y. Halpin, J. G. Vos, E. A. Gibson, *Coord. Chem. Rev.* **2015**, *304-305*, 179–201.
[286] Y. Farré, M. Raissi, A. Fihey, Y. Pellegrin, E. Blart, D. Jacquemin, F. Odobel, *ChemSusChem* **2017**, *10*, 2618–2625.
[287] A. Nattestad, A. J. Mozer, M. K. R. Fischer, Y.-B. Cheng, A. Mishra, P. Bäuerle, U. Bach, *Nat. Mater.* **2009**, *9*, 31–35.
[288] I. R. Perera, T. Daeneke, S. Makuta, Z. Yu, Y. Tachibana, A. Mishra, P. Bäuerle, C. A. Ohlin, U. Bach, L. Spiccia, *Angew. Chem. Int. Ed.* **2015**, *54*, 3758–3762.
[289] M. Borgström, E. Blart, G. Boschloo, E. Mukhtar, A. Hagfeldt, L. Hammarström, F. Odobel, *J. Phys. Chem. B.* **2005**, *109*, 22928–22934.
[290] B. Dhital, V. G. Rao, H. P. Lu, *Phys. Chem. Chem. Phys.* **2017**, *19*, 17216–17223.

[291] L. Zhang, L. Favereau, Y. Farre, A. Maufroy, Y. Pellegrin, E. Blart, M. Hissler, D. Jacquemin, F. Odobel, L. Hammarström, *RSC Adv.* **2016**, *6*, 77184–77194.
[292] E. A. Gibson, A. L. Smeigh, L. Le Pleux, J. Fortage, G. Boschloo, E. Blart, Y. Pellegrin, F. Odobel, A. Hagfeldt, L. Hammarström, *Angew. Chem.* **2009**, *48*, 4402–4405.
[293] L. Le Pleux, A. L. Smeigh, E. Gibson, Y. Pellegrin, E. Blart, G. Boschloo, A. Hagfeldt, L. Hammarström, F. Odobel, *Energy Environ. Sci.* **2011**, *4*, 2075–2084.
[294] A. Morandeira, J. Fortage, T. Edvinsson, L. Le Pleux, E. Blart, G. Boschloo, A. Hagfeldt, L. Hammarström, F. Odobel, *J. Phys. Chem. C.* **2008**, *112*, 1721–1728.
[295] G. de Miguel, M. Wielopolski, D. I. Schuster, M. A. Fazio, O. P. Lee, C. K. Haley, A. L. Ortiz, L. Echegoyen, T. Clark, D. M. Guldi, *J. Am. Chem. Soc.* **2011**, *133*, 13036–13054.
[296] M. Natali, M. Ravaglia, F. Scandola, J. Boixel, Y. Pellegrin, E. Blart, F. Odobel, *J. Phys. Chem. C.* **2013**, *117*, 19334–19345.
[297] K. Ladomenou, V. Nikolaou, G. Charalambidis, A. G. Coutsolelos, *Coord. Chem. Rev.* **2016**, *306*, 1–42.
[298] M. Pazoki, P. W. Lohse, N. Taghavinia, A. Hagfeldt, G. Boschloo, *Phys. Chem. Chem. Phys.* **2014**, *16*, 8503–8508.
[299] A. Maufroy, L. Favereau, F. B. Anne, Y. Pellegrin, E. Blart, M. Hissler, D. Jacquemin, F. Odobel, *J. Mater. Chem. A* **2015**, *3*, 3908–3917.
[300] H. Tian, J. Oscarsson, E. Gabrielsson, S. K. Eriksson, R. Lindblad, B. Xu, Y. Hao, G. Boschloo, E. M. J. Johansson, J. M. Gardner, A. Hagfeldt, H. Rensmo, L. Sun, *Sci. Rep.* **2014**, *4*, 4282.
[301] L. D'Amario, L. J. Antila, B. P. Rimgard, G. Boschloo, L. Hammarström, *J. Phys. Chem. Lett.* **2015**, *6*, 779–783.
[302] L. D'Amario, J. Föhlinger, G. Boschloo, L. Hammarström, *Chem. Sci.* **2018**, *9*, 223–230.
[303] J. C. Freys, J. M. Gardner, L. D'Amario, A. M. Brown, L. Hammarström, *Dalton Trans.* **2012**, *41*, 13105.
[304] A. Kudo, Y. Miseki, *Chem. Soc. Rev.* **2009**, *38*, 253–278.
[305] K. Domen, *J. Catal.* **1986**, *102*, 92–98.
[306] T. K. Townsend, N. D. Browning, F. E. Osterloh, *Energy Environ. Sci.* **2012**, *5*, 9543–9550.
[307] K. Sayama, A. Tanaka, K. Domen, K. Maruya, T. Onishi, *J. Phys. Chem.* **1991**, *95*, 1345–1348.
[308] A. Kudo, H. Kato, S. Nakagawa, *J. Phys. Chem. B* **2000**, *104*, 571–575.
[309] J. Kiwi, M. Graetzel, *J. Phys. Chem.* **1984**, *88*, 1302–1307.

[310] J. Liu, Y. Liu, N. Liu, Y. Han, X. Zhang, H. Huang, Y. Lifshitz, S.-T. Lee, J. Zhong, Z. Kang, *Science* **2015**, *347*, 970–974.
[311] Y. Nosaka, A. Y. Nosaka, *Chem. Rev.* **2017**, *117*, 11302–11336.
[312] N. Liu, X. Zhou, N. T. Nguyen, K. Peters, F. Zoller, I. Hwang, C. Schneider, M. E. Miehlich, D. Freitag, K. Meyer, D. Fattakhova-Rohlfing, P. Schmuki, *ChemSusChem* **2016**, *10*, 62–67.
[313] R. Li, Y. Weng, X. Zhou, X. Wang, Y. Mi, R. Chong, H. Han, C. Li, *Energy Environ. Sci.* **2015**, *8*, 2377–2382.
[314] D. Bahnemann, A. Henglein, J. Lilie, L. Spanhel, *J. Phys. Chem.* **1984**, *88*, 709–711.
[315] J. Schneider, M. Matsuoka, M. Takeuchi, J. Zhang, Y. Horiuchi, M. Anpo, D. W. Bahnemann, *Chem. Rev.* **2014**, *114*, 9919–9986.
[316] X. Han, Q. Kuang, M. Jin, Z. Xie, L. Zheng, *J. Am. Chem. Soc.* **2009**, *131*, 3152–3153.
[317] A. Stevanovic, J. T. Yates, *J. Phys. Chem. C* **2013**, *117*, 24189–24195.

Appendix

A Conference Contributions

Oral Conference Contributions

(1) 10th International Conference of Porphyrins & Phthalocyanines, Munich, Germany, July 1 - 6, 2018
(2) CECP 2020 Central European Conference on Photochemistry, Bad Hofgastein, Austria, February 9 - 13, 2020

Poster Contributions on Conferences

(1) 10th International Conference of Porphyrins & Phthalocyanines, Munich, Germany, July 1 - 6, 2018
(2) Gordon Research Seminar on Molecules and Materials for Photochemical Energy Conversion and Imaging, Easton, MA, USA, July 13 - 14, 2019
(3) Gordon Research Conference on Light-Driven Reactions, Materials and Devices, Easton, MA, USA, July 14 - 19, 2019
(4) 5th Erlangen Symposium on Synthetic Carbon Allotropes, Erlangen, Germany, September 29 - October 2, 2019

Awards and Fellowship

(1) Former Fellow of the German Academic Scholarship Foundation
(2) Price for the Best Oral Presentation at the 10th International Conference of Porphyrins & Phthalocyanines, Munich, Germany, July 1 - 6, 2018

B List of Publications

(1) Bin Liu,* Hongyun Fang,* Xiaofang Li, Wenting Cai, Lipiao Bao, Marc Rudolf, Fabian Plass, Louzhen Fan, Xing Lu, and Dirk M. Guldi, Synthesis and Photopyhsical Properties of a $Sc_3N@C_{80}$-Corrole Electron Donor-Acceptor Conjugate, *Chem. Eur. J.* **2014**, *21*, 746-752

(2) Christina Stangel,* Fabian Plass,* Asterios Charisiadis, Emmanouil Giannoudis, Georgios Charalambidis, Kostas Karikis, Georgios Rotas, Galateia E. Zervaki, Nektarios N. Lathiotakis, Nikos Tagmatarchis, Axel Kahnt, and Athanassios G. Coutsolelos, Interfacing Tetrapyridyl-C_{60} with Porphyrin Dimers via π-Conjugated Bridges: Artificial Photosynthetic Systems with Ultrafast Charge Separation, *Phys. Chem. Chem. Phys.* **2018**, *20*, 21269-21279

(3) Vasilis Nikolaou,* Fabian Plass,* Aurélien Planchat, Asterios Charisiadis, Georgios Charalambidis, Panagiotis A. Angaridis, Axel Kahnt, Fabrice Odobel, and Athanassios G. Coutsolelos, Effect of the Triazole Ring in Zinc Porphyrin-Fullerene Dyads on the Charge Transfer Processes in NiO-Based Devices, *Phys. Chem. Chem. Phys.* **2018**, *20*, 24477-24489

(4) Ning Liu,* Shiva Mohajernia,* Nhat T. Nguyen, Seyedsina Hejazi, Fabian Plass, Axel Kahnt, Tadahiro Yokosawa, Andres Osvet, Erdmann Spiecker, Dirk. M. Guldi, and Patrik Schmuki, Long-Living Holes in Grey Anatase TiO_2 Enable Noble-Metal-Free and Sacrificial-Agent-Free Water Splitting, *ChemSusChem* **2020**, *13*, 4937-4944

(5) Fabian Plass, Daniil A. Lukyanov, Alexander S. Konev, Axel Kahnt, Konstantin Y. Amsharov, Alexander F. Khlebnikov, and Dirk M. Guldi, Controlling the Charge Transfer Mechanism and Efficiency by Means of Different C_{70} Regioisomeric Adducts, *Small Struct.* **2020**, *1*, 2000012

(6) Fabian Plass,* Sebastian Bönisch,* Felix Held,* Tobias Ullrich, Florian E. J. Fischer, Anton Guryev, Andreas Görling, A. Kahnt, and Svetlana B. Tsogoeva, Controlling and Fine-Tuning Charge Transfer Emission in 2,6-Dicyanoaniline Multichromophores Prepared through Domino Reactions: Entry to a Potentially New Class of OLEDs, *J. Org. Chem.* **2021**, *86*, 6111-6125

(7) Ilias Papadopoulos,* Arjun Menon,* Fabian Plass, Desiré Molina, Christina Harreiß, Axel Kahnt, Ángela Sastre Santos, Erdmann Spiecker, and Dirk M. Guldi, Efficient Charge-Transfer from Diketo-pyrrolopyrroles to Single-Walled Carbon Nanotubes, *Nanoscale*, **2021**, *13*, 11544-11551

*These authors contributed equally to this work.

Sustainable solar energy conversion is one of the main tasks of younger human history to be able to herald a successful energy turnaround by using profitable and environmentally friendly energy sources and carriers.

The use of nanostructured architectures, such as the implementation of molecular electron donor-acceptor systems in opto-electronic applications, is a promising option. Various strategies can be pursued: On the one hand, the development of novel and promising carbon rich compounds, the fundamental characterization of those plays a major role in this PhD thesis, and, on the other hand, the development and optimization of already existing compounds of molecules and materials, whose enormous potential has perhaps not yet been fully exploited.

Moreover, the combination of solar fuels such as hydrogen, as well as the use of novel, economical solar cells, but also sustainable OLEDs, will be important elements to protect life as we know it today and will make it worth living for future generations.

ISBN 978-3-96147-481-3

FAU UNIVERSITY PRESS 2022